

# **TRANSPORT PROCESSES IN THE NORTH ALEUTIAN SHELF**

**by**

**James D. Schumacher**

**Pacific Marine Environmental Laboratory  
National Oceanic and Atmospheric Administration  
7600 Sand Point Way, N.E.  
Seattle, Washington 98115**

Final **Report**

**Outer Continental Shelf Environmental Assessment Program  
Research Unit 549**

**August 1982**

## ACKNOWLEDGMENTS

I acknowledge the aid of a large number of persons, not only in the preparation of this document but in carrying out the field work and processing which have led to its existence. Of these, special thanks must go to the complement of the research vessels *Discoverer*, *Surveyor*, and Thompson (R. B. Tripp, chief scientist) for laboring under less than ideal conditions to carry out field operations. Lynn Long, Sharon Wright, Gini May, Lt. Paul Moen, and Phyllis Hutchens of NOAA/PMEL are due thanks for their help in processing the data and preparing this document.

This study was supported in part by the Bureau of Land Management through interagency agreement with the National Oceanic and Atmospheric Administration, under which a multiyear program responding to needs of petroleum development of the Alaskan continental shelf has been managed by the Outer Continental Shelf Environmental Assessment Program (OCSEAP) Office, Juneau, Alaska.

TABLE OF CONTENTS

	<i>Page</i>
ACKNOWLEDGMENTS . . . . .	443
LIST OF FIGURES . . . . .	447
LIST OF TABLES . . . . .	451
1. INTRODUCTION . . . . .	453
2. SETTING. . . . .	453
2.1 Geography . . . . .	453
2.2 Physical Properties . . . . .	456
2.3 Circulation and Tides . . . . .	458
2.4 Climatology . . . . .	459
3. METHODS. . . . .	460
3.1 Current and Bottom Pressure Data . . . . .	460
3.2 Hydrographic Data . . . . .	462
3.3 Wind Observations . . . . .	463
4. RESULTS. . . . .	463
4.1 The Unimak Pass Experiment . . . . .	463
4.1.1 Introduction . . . . .	463
4.1.2 Low Frequency and Mean Current . . . . .	465
4.1.3 Time-Series Relations . . . . .	470
4.1.4 Property Distributions . . . . .	477
4.1.5 Baroclinic Geostrophic Currents . . . . .	483
4.1.6 Discussion . . . . .	485
4.2 The North Aleutian Shelf Transport Processes Experiment . . . . .	489
4.2.1 Long-Period Time-Dependence of Hydrographic Features . . . . .	489
4.2.2 Short-Period Time-Dependence of Hydrographic Features . . . . .	508
4.2.3 Current and Wind Observations . . . . .	517
4.2.4 Salinity-Time Series . . . . .	531
5. SUMMARY AND CONCLUSIONS . . . . .	535
6. REFERENCES CITED . . . . .	538
APPENDIX A. Data Inventory. . . . .	543
APPENDIX B. Dynamical Characteristics of Three Low-Frequency Current Regimes Over the Bering Sea Shelf . . . . .	551

## LIST OF FIGURES

<i>Figure</i>		<i>Page</i>
1	Geomorphology of the southeastern Bering Sea shelf, including the study area . . . . .	454
2	Average progression of ice extent during the growth season, based on 1972-79 ice extents. . . . .	457
3	Geographic setting showing the Gulf of Alaska and Bering Sea shelves and a detailed view of the Unimak Pass study area with some orographic features and the location of current meter and pressure gauge moorings and CTD stations . . . . .	464
4	Results from 35-hr filtered current data presented as scatter plots and progressive vector diagrams . . . . .	467
5	Current vector time-series of current, bottom pressure, bottom pressure difference between UP3 and UP1, alongshore geostrophic wind, and atmospheric pressure gradient . . . . .	469
6	Coherence between current in Unimak Pass and bottom pressure difference along the pass for spring and summer records . . . . .	475
7	Coherence between bottom pressure difference and geostrophic wind components during spring and summer records . . . . .	476
8	Hydrographic data from September 1980 presented as temperature, salinity, and sigma-t sections . . . . .	478
9	Hydrographic data collected during February 1981 along the same section as in Figure 6 . . . . .	480
10	Hydrographic data for May 1981 from stations normal to Unimak Island . . . . .	481
11	Hydrographic data for September 1981 presented as areal extent of waters with salinity $\geq 31.75$ g/kg in the upper 50 m, and dynamic topography with a 0.01 dyn m contour interval . . . . .	482
12	Location of current meter moorings . . . . .	490
13	Location of CTD stations for the North Aleutian Shelf study . . . . .	491
14	Surface temperature contours . . . . .	492
15	Bottom temperature contours . . . . .	495

LIST OF FIGURES (continued)

Figure	<i>Page</i>
16 Surface salinity contours . . . . .	497
17 Bottom salinity contours . . . . .	499
18 Mean salinity contours . . . . .	501
19 Bottom minus surface sigma-t contours . . . . .	504
20 <b>Dynamic topography, 0/25 db</b> . . . . .	506
21 <b>Dynamic topography, 0/50 db</b> . . . . .	507
22 North Aleutian Shelf study area, showing location of <b>hydrographic</b> data section and mooring TP3A . . . . .	510
23 Hydrographic and <b>light</b> attenuation sections, <b>19</b> August 1980 . . .	511
24 <b>Hydrographic</b> and light attenuation sections, 24 August 1980 . . .	512
25 Hydrographic and light attenuation sections, <b>31</b> August 1980 . . .	513
26 Alongshore wind speed, onshore and alongshore current at 5 and 39 m, and <b>25-hr</b> average tidal mixing from the 39-m depth current record. . . . .	515
27 Current roses and means for near-surface records between August <b>1980</b> and January <b>1981</b> . . . . .	518
28 Current roses and means for near-bottom records between August <b>1980</b> and January 1981 . . . . .	519
29 Current roses and means for near-surface records between January <b>1981</b> and <b>May 1981</b> . . . . .	520
30 Current roses and means for near-bottom records between January <b>and May</b> 1981. . . . .	521
31 Current records from TP3A presented as 6-hourly vectors . . . . .	525
32 Current records from <b>TP3B</b> presented as 6-hourly vectors . . . . .	526
33 <b>Profiles</b> of mean, <b>alongshore</b> , and cross-shelf speed and net current <b>from TP3A and B</b> . . . . .	527
34 Current speed at four depths from <b>2.9-hr</b> data . . . . .	529

LIST OF FIGURES (continued)

<i>Figure</i>		<i>Page</i>
<b>35</b>	Comparison of alongshore and cross-shelf components from surface and observed wind . . . . .	530
36	Coherence squared estimates between surface and observed wind components. . . . .	532
37	Wind roses for BC2 and TPI A. . . . .	533
38	Salinity time-series from <b>TP</b> moorings . . . . .	534

LIST OF TABLES

<i>Table</i>		<i>Page</i>
1	Current and wind during first (spring) and second (summer) halves of the observations. . . . .	471
2	Correlation matrix. . . . .	472
3	Dynamic relief and <b>baroclinic</b> speed . . . . .	484
4	Current characteristics from TP moorings . . . . .	523

## 1. INTRODUCTION

The **general objective of research unit 549, Transport Processes in the North** Aleutian Shelf, **is** to provide oceanographic data and interpretation of such in Unimak Pass and a portion of the southeastern Bering Sea shelf along the Alaska Peninsula (Figure 1). The results of this study provide input to oil trajectory modeling and **a** characterization of the physical **environment**. This, together with other studies, permits an estimation of fate and impact of petroleum resource development in the proposed north Aleutian Shelf lease area.

**In this** report, **we** first describe the regional setting, including a review of previous oceanographic studies. We then discuss **methods of observation and analysis**. **Results are discussed in Section 4**, where they are treated separately for Unimak Pass and the north Aleutian **Shelf**. The **major** features are summarized in Section 5, Summary and Conclusions.

## 2. SETTING

### 2.1 Geography

The Alaska Peninsula (Figure 1) extends about 700 km (**~157°W to 165°W**) from the mainland to Unimak Pass and is oriented southwestward. The northern coast contains several **major embayments; Bechevin Bay and Isanotski Strait** which separate Unimak Island from the peninsula; **Izembek/Moffet Lagoon** located north of Cold Bay; the Nelson Lagoon, Herendeen Bay, Port **Moller** complex and Port **Heiden**. These indentations in an otherwise relatively straight coastline are accompanied by passages across the peninsula which break the rugged orographic contours. Such features permit local winds to become down gradient rather than **geostrophic** and hence can dramatically modify local winds over length scales of up to **30** km offshore.

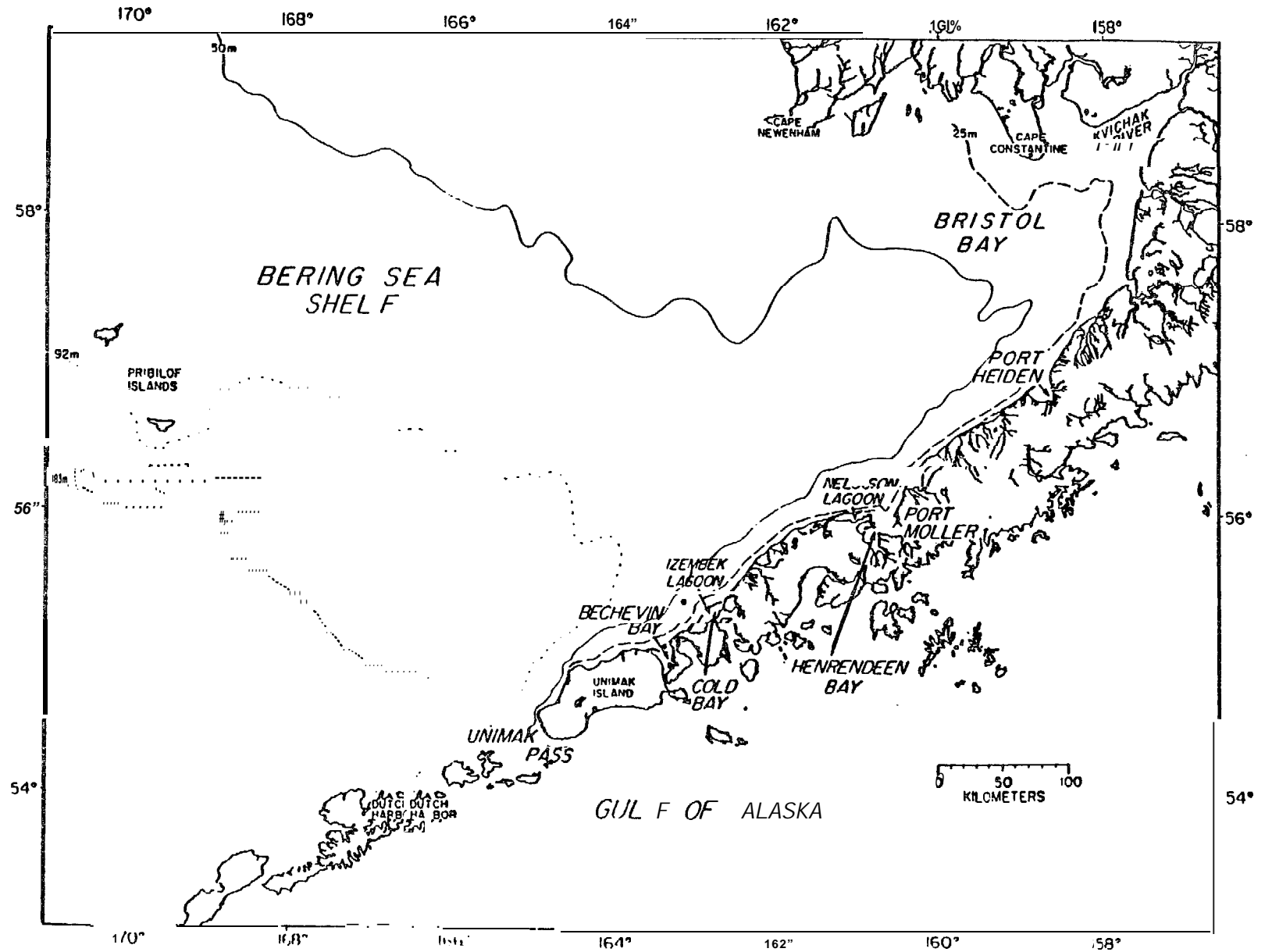


Figure 1. - Geomorphology of the southeastern Bering Sea shelf, including the study area.

Unimak Pass is the easternmost passage of significant cross-section ( $\sim 10^6 \text{ m}^2$ ) between the Bering Sea and the Gulf of Alaska. Complex orographic and bathymetric contours are typical in the vicinity of Unimak Pass. At the narrowest location (Scotch Cap to **Ugamak** Island) which we call the Pass proper, it is 19 **km wide** and has an average depth **of  $\sim 55$  m with** an along-pass **axis of  $285^\circ\text{T}$** . Complexity also exists due to the presence of the **Krenitzin** Islands southwest of Unimak Island and the passes between these islands and Unimak Pass proper. **On the Krenitzen** Islands, there are many peaks **in excess of 800 m** and elevations up to **2500 m** **exists** on the western end of Unimak Island.

Bathymetry along the remainder of the study area is less complex, the 50-m isobath generally trends **toward  $\sim 60^\circ\text{N}$**  from the northern coast of Unimak Island to about  **$159^\circ\text{W}$** , where it becomes **nearly orthogonal to the coastline**. The shelf **shoreward** of the 50-m isobath is generally 20 to 30 **km wide** west of Nelson Lagoon where it becomes  **$\sim 40$  km** in width and then is constricted to 20 km just east **of Port Moller**. From Port **Mollar** to Port Heiden, **the width of the coastal** region gradually broadens to 40 km. Seaward of the 50-111 isobath, depths increase monotonically to greater than 100 m off Unimak Island, however, the 92-m isobath becomes **nearly** orthogonal to the peninsula **east of** Cold Bay. **Isobaths** up to 80-m **parallel** the 50-m isobath and form a **trench-** like feature which extends into **Kvichak** Bay. This feature, which is most pronounced east of Port **Moller**, results in depths greater than 25 m to **just** east of Cape Constantine.

\*

## 2.2 Physical Properties

Kinder and Schumacher (1981a) characterized this region of the shelf in terms of hydrographic properties and structure; along most of the peninsula the germane domains are the coastal and the middle shelf. The coastal domain (away from the direct influence of freshwater addition) is typically well mixed and lies shoreward of the 50-m isobath. The middle shelf domain generally is two-layered and lies seaward of the 50 m isobath. Separating these domains is a structural front (Schumacher et al., 1979) where a transition between well-mixed and two-layered vertical structure occurs. A typical width of the front is about 5 to 10 km. Geopotential contours across the front suggest baroclinic flow into Bristol Bay with surface speeds-of  $0.02\text{-}0.05\text{ ms}^{-1}$ . During winter, waters in the middle shelf are mixed to the bottom so that structural differences between domains are slight; however, fresher water remains in the coastal domain and cross-shelf density gradients persist.

Sources of fresh or less saline water include ice melt, local addition from rivers and, as will be shown later, flow of Kenai Current water through Unimak Pass. Recent studies of sea ice climatology include Webster (1979), Overland and Pease (1981), and Pease, Schoenberg and Overland (1982). The average progression (50% probability) of ice extent during the growth season (Figure 2: from Pease, Schoenberg and Overland 1982) indicates that ice growth occurs in northern Bristol Bay by December and progresses to maximum extent by March with ice covering much of Bristol Bay and extending along the peninsula to about  $160^{\circ}\text{W}$ . However, during extreme ice years, e.g. winter 1975-76, ice covered most of the north Alutian shelf westward to Unimak Island. Local (rather than transported) ice production occurs along the northern shore of

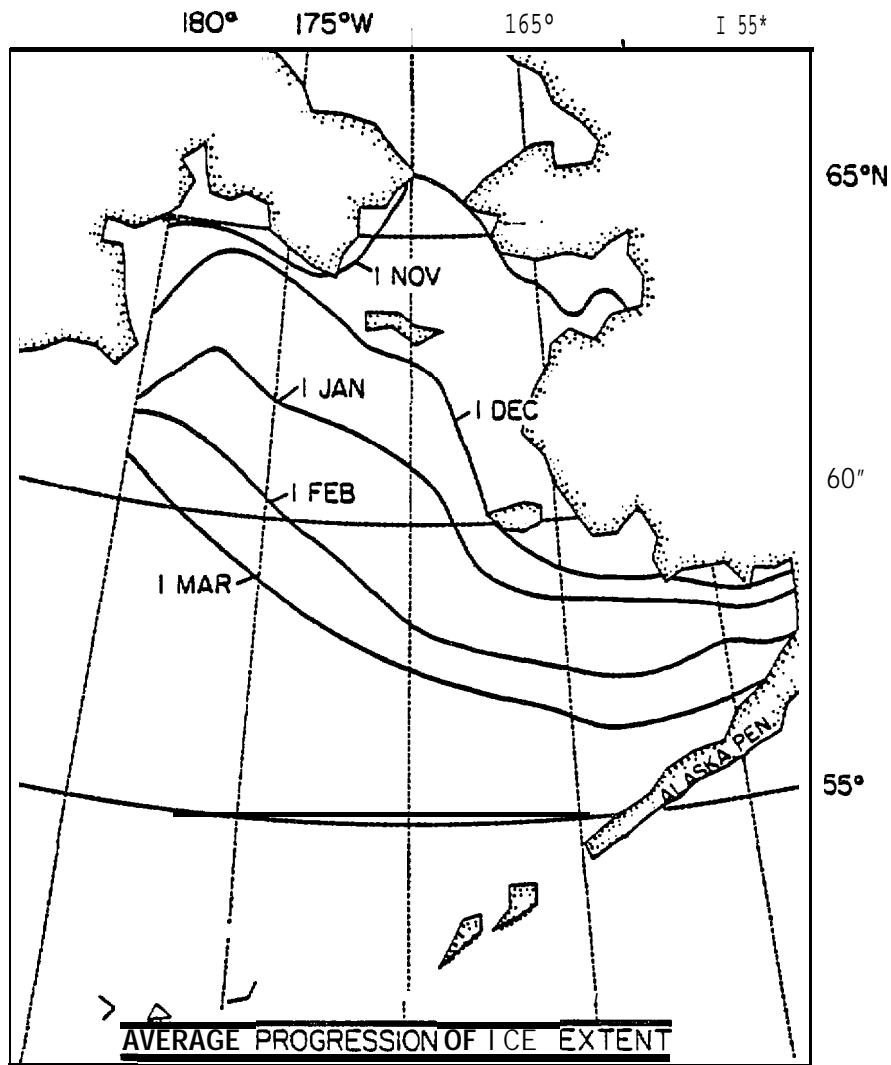


Figure 2. - Average progression (50% probability) of ice extent during the growth season, based on 1972-79 ice extents (from Pease et al., 1982).

Bristol Bay, and perhaps to a limited extent within the Port Moller system. Although there are no major rivers along the peninsula, rainfall is substantial. Brewer, et al. (1977) show a decrease from  $\sim 3.2$  m at  $\sim 158^\circ\text{W}$  to 0.8 m at  $162.5^\circ\text{W}$  (Cold Bay). Just north of the eastern end of the Peninsula, the Kvichack River enters Bristol Bay. Seifert and Kane (1977) indicate that this river has a basin area of  $16,800 \text{ km}^2$  and an average annual flow of  $1.84 \times 10^5 \text{ m}^3 \text{ s}^{-1}$ . Hydrography indicate that mean daily discharge can vary by a factor of three between wet and dry years and that the greatest monthly discharge occurs in October ( $1,700 \text{ m}^3 \text{ s}^{-1}$ ) with the minimum in April ( $\sim 283 \text{ m}^3 \text{ s}^{-1}$ ). However, a clear freeze cycle is not detectable, so that during winter discharge does not cease.

### 2.3 Circulation and tides

Since there are abundant fisheries (including Alaskan King Crab, Halibut, and Salmon) in the north Aleutian shelf region, much of the early (pre-1975) oceanography was in support of these resources. Although only a few, short-term ( $\sim 4$  days) current observations were made in the past (Reed, 1971), there exists the supposition that waters of the Gulf of Alaska enter the Bering Sea through Unimak Pass; general inflow vectors appear on large scale circulation schemes (e.g., Hughes, Coachman and Aagaard, 1974; Takenouti and Ohtani, 1974; and Favorite, Dodimead and Nasu, 1976). This belief is based on mariner's reports as given in The Coast Pilot, drift bottle studies (Thompson and Van Cleve, 1936; Favorite and Fisk, 1971) and on hydrographic data. The inflow of water through Unimak Pass has also been inferred in studies of lateral water mass interactions on the southeastern Bering Sea shelf (Coachman and Charnell, 1977; Coachman and Charnell?, 1979).

Circulation along the peninsula is less well known. Kinder and Schumacher (1981 b) present limited current meter data which suggests flow along the 50-m isobath into Bristol Bay. Schumacher and Pearson (1981) present drift card and radar tracked **drogue** data which support the inference of inflow in the vicinity of the **50-m** isobath.

Tides constitute more than 90% of the horizontal **kinetic** energy (Kinder and Schumacher, 1981a) and are important to mixing and through interaction with **bathymetry** and/or relative sea **level** changes versus mean depth, to the generation of residual flow. Pearson, **Mofjeld** and Tripp (1981) described the tides over the north Aleutian shelf. The tide enters the Bering Sea through the central and western Aleutian Island passes and progresses as a free wave to the shelf. Largest tidal amplitudes are found over the southeastern shelf region, especially along the **Alaska** Peninsula and interior Bristol Bay. Each **semidiurnal** tide propagates as a **Kelvin** wave along the Alaska Peninsula but appears to be converted on reflection in interior Bristol Bay to a **Sverdrup** wave. In general, tidal ellipses are oriented along **isobaths** and are nearly rectilinear.

#### 2.4 Climatology

A **major** influence of the general atmospheric circulation on the area is the region of low pressure normally located in the vicinity of the Aleutian chain, referred to as the Aleutian Low. On monthly mean pressure charts (e.g. Brewer, et al. 1977) this appears as a low-pressure cell normally oriented with the **major** axis in an east-west direction. This is a statistical low, indicating only that pressures are generally lower **along** the **major** axis as a **result** of the passage of low-pressure centers or storms. Storms are most frequent in this area and are more intense than in **adjacent** regions. The most

frequent trajectory of these storms **is** along the Aleutian Islands and into the Gulf of Alaska in winter, and **along** the same general path in the west but curving northward into the Bering Sea in summer (Overland, **1981**). The monthly frequency of low-pressure centers **in** the southern Bering Sea is slightly higher **in** winter (generally four to five) than in summer (three to four), with winter storms being more **i**ntense. Climatology of the southern Bering Sea **can** be characterized **by** a progression of storms rather than fixed weather types (Overland, 1981) and the presence of mountain passes will further complicate **local** wind characteristics.

### 3. METHODS

#### 3.1 Current and **Bottom Pressure**

**Most of** our measurements were made using RCM-4 **Aanderaa** recording current **meters on taut-wire moorings**. **Typical instrument placement was 20 m** below the surface and **10 m** above the bottom. Where water depths were less than **35 m**, a single **RCM-4** was located at 10 m above the bottom. The subsurface flotation was usually at 18 m depth, and exerted about 1000 lb (1 lb = **4.45N**) buoyancy. Sampling interval was 30 minutes. **Aanderaa RCM-4** current meters record speed by summing the number of rotor turns for (in our case) 15, or **30-min** intervals. Direction is **recorded at the time of sampling by measuring compass and vane orientation**. **Therefore**, speed recorded at time  $t_n$  is integrated over  $\Delta t = t_n - t_{n-1}$ , while direction is instantaneous at time  $t_n$ . Speed at  $t_n$  and  $t_{n-1}$  were averaged before converting to east and north components of velocity at time  $t_n$ . These components were then low-pass filtered (filter half-amplitude response was at a period **of 2.9 hr**) and a second-order polynomial was used to

interpolate the observations to whole hours. We estimate that directions were accurate to  $\pm 5^\circ$  and speeds to  $\pm 1$  cm/see, exclusive of rotor pumping mooring motion, or fouling. A summary of meter location, depth and obstruction period is given in Appendix A. Note that on **most of** the Transport Processes (TP) moorings, one of the **RCM-4's** was fitted with a transmissometer.

It is well known that mechanical current meters such as the **RCM-4** may give erroneous speeds because of effects from either mooring motion or high frequency water **motion** (e.g. **Quadfasel** and **Schott**, 1979, give several references). **Pearson**, **Schumacher**, and **Muench** (1981) have examined the performances of moorings like ours on the Alaskan shelves, and they found speed differences **at** tidal frequencies of  $\leq 10\%$  when windy and calm seasons were compared, however, during storms erroneous speeds do occur. Extrapolating their results to **lower** frequencies, we believe that the effects of mooring motion and rotor pumping were minor and that errors were probably limited to a few percent increase of the speeds of low frequency flows (which were usually strongest during windy periods).

At some locations along the Alaska Peninsula, Neil Brown acoustical (**ACM**) current meters were used because biological fouling was a problem for mechanical rotors (**Schumacher** and **Pearson**, **1980**). The **ACM'S** emit continuous high frequency acoustic signals which are phase advanced or delayed as they travel with or against the current. The relative phase is converted to a voltage which **i**s directly proportional to the water velocity. Currents are measured along two right angle horizontal paths. At a pre-determined interval, in this case one minute, the component velocities are averaged and recorded. Ten minute segments of the original one minute sample interval data were averaged.

In order to characterize the bottom pressure field and to estimate sea level changes, Aanderaa TG-2 or TG-3 pressure gauges were deployed on all of moorings. These instruments were located in a cage welded to the anchor, thereby eliminating any possible noise due to mooring motion. Sampling intervals varied between 15 and 30 minutes.

Data from the current meters and pressure gauges are processed in a similar manner. The original series are converted to engineering units, and time base is checked by comparing field logs to the number of records. Excessive values are removed by determining the standard deviation ( $\sigma$ ) of consecutive one-thousand record segments and eliminating values greater than six  $\sigma$  from the segment mean. A tidal analysis is then performed on the edited data set to check consistency of tidal amplitudes and phases.

Two sets of time-series are produced from edited current and pressure observations using a Lanczos filter [cf. Charnel and Krancus, 1976]. The first set is filtered so that over 99% of the amplitude was passed at periods greater than 5 hr, 50% at 2.9 hr, and less than 0.5% at 2.0 hr. These sets are used to determine tidal constituents and spectral estimates. The second sets are filtered to remove most of the tidal energy; the filter passed 99% of the amplitude at periods greater than 55 hr, 50% at 35 hr, and less than 0.5% at periods less than 25 hr. These sets are resampled at 6 hr intervals for use in examining subtidal current and pressure.

### 3.2 Hydrographic Data

Conductivity and temperature versus depth (CTD) data were obtained during three cruises conducted by NOAA's Pacific Marine Environmental Laboratory and

one "ship of opportunity" cruise (Appendix A). The CTD systems sampled five times per second during the down-cast (lowering rate of 30 m/min). Nansen bottle samples were taken at most stations to provide temperature and salinity calibration. Data from monotonically increasing depth were "despiked" to eliminate excessive values and were averaged over 1-m intervals to produce temperature and salinity values from which density and geopotential anomaly were computed.

### 3.3 Wind Observations

Because orography can effect large-scale geostrophic winds (Livingston and Royer, 1980), a meteorological station was established near Lagoon Point and was maintained throughout the current meter observation period. The wind sensor was located about 7 m above ground level. The ensuing parameters are recorded like the Aanderaa RCM4 and are processed similarly. We also have surface wind time series over the mooring period which were computed by Fleet Numerical Weather Central from 6 hr synoptic surface pressure maps, using a 3° grid mesh and interpolated at 57°N, 163.5°W. The surface winds were estimated by rotating computed geostrophic wind by 15° to the left and reducing it in magnitude by 30% (Bakun, 1973). Climatological data from Brewer, et al. (1977) was also used.

## 4. RESULTS

### 4.1. The Unimak Pass Experiment

Three current meter/pressure gauge moorings (Figure 3) were deployed in and on either end of Unimak Pass to describe currents and evaluate forcing

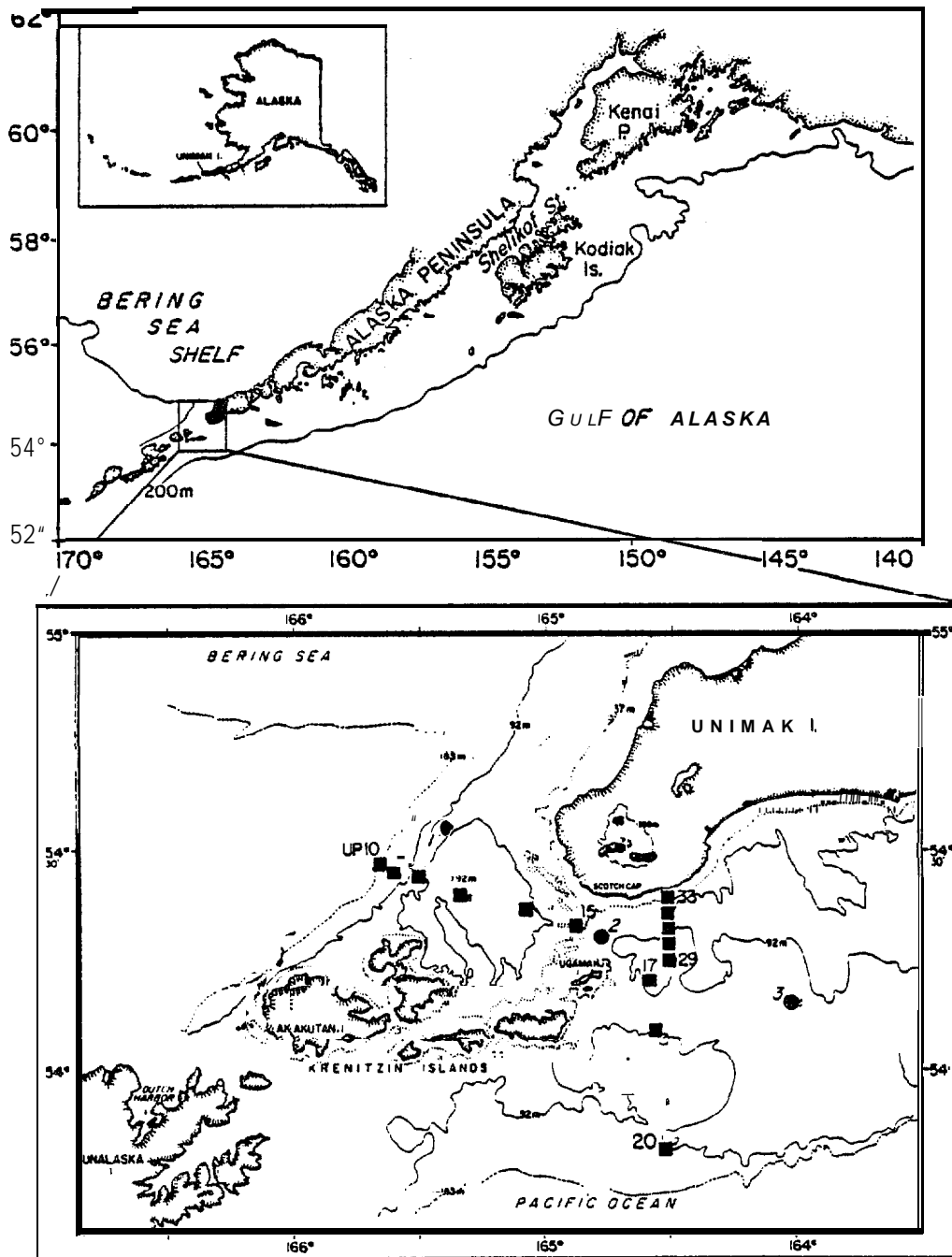


Figure 3. - Geographic setting showing (a) the Gulf of Alaska and Bering Sea shelves and (b) a detailed view of the Unimak Pass study area with some orographic features and the location of current meter and pressure gauge moorings (dots) and CTD stations (squares). Depth contours (given in meters) were constructed from the 20 (dotted line), 50, and 100 fathom **isobaths**.

mechanisms. Each mooring consisted of two **Aanderaa RCM-4** current meters separated by  $\sim 1$  m and located 20 m above the bottom and an Aanderaa TG-3 pressure gauge. Such redundancy of **current** meters increases the probability of recovering at least one data set per mooring (one meter did fail).

From 11 March **1980** to 15 August **1980**, the atmospheric pressure gradient across Unimak Pass was determined using the National Meteorological **Center's** **twice** daily sea level pressure analyses for the Northern Hemisphere. Each map was quality checked for station accuracy and pressure analysis, and then a pressure gradient vector was determined for  $54^{\circ}\text{N}$ ,  **$165^{\circ}\text{W}$**  and recorded **in** terms of direction from true north and magnitude in  $\text{rob}/10$  latitude. Wind time series over the mooring period were computed by Fleet Numerical Weather Central from 6 h synoptic surface pressure maps, using a  $3^{\circ}$  grid mesh and interpolated at  $54^{\circ}\text{N}$ ,  **$163^{\circ}\text{W}$** .

#### 4.1.1. Introduction

Straits or passes which connect large bodies of water are a *common* geographical feature throughout the world and water transported through the straits can have a profound impact on oceanographic characteristics in the surrounding bodies of water. **In his** review of currents in a strait, **Defant (1961)** discusses the oceanography of several well-known examples and notes that the dynamic cause of currents in these straits lies in the density difference between the **adjacent** bodies of water. While mean flow generally may **be** driven by such differences, shorter period (two **to** ten days) fluctuations are **driven** by **barotropic** sea level differences along the strait. These, in turn, can **be** produced by **large-scale** meteorological forcing which

results **in** sea level changes at the coast. Examples of passages where such forcing was observed include the English Channel (Bowden, 1956), the Bering Strait (Coachman and **Aagaard**, 1981) and the Strait of Belle Isle (Garrett and **Toulany**, 1981; Garrett and **Petrie**, 1981).

We present results from current, bottom pressure and **hydrographic** data which support the supposition of inflow to the Bering Sea, however, the waters are from the **shelf** of the Gulf of Alaska and not the Alaska Stream. Further, both driving mechanisms noted above are operative; the mean flow was related **to** a **baroclinic** coastal current along the southern side of the Alaska **Peninsula** and fluctuations were related to an along pass bottom pressure difference generated by sea level changes mainly over the Gulf of Alaska shelf.

#### 4.1.2 Low Frequency and Mean Current

The **35 hr** filtered current meter data are shown as scatter diagrams (Figure 4A) and progressive vector diagrams (**PVD's**, **Figure 4B**). The scatter diagrams depict the distribution of the 6-hourly current vectors and thus provide a visualization of variance about axes, while **PVD's** emphasize the time-dependent nature of the low frequency flow. In the Bering Sea (**UP1**) about 50% of the vectors were in the northwest quadrant with a mean speed of about 15 **cm/s**. There were, however pulses toward the south with magnitudes of **15** to 20 **cm/s**. Currents at UP2 tended to parallel the **isobaths** in the pass and about 75% of the observations indicated **flow** from the **Gulf** of Alaska shelf into the Bering Sea. Maximum pulses (60 to 75 **cm/s**) prevailed over **tidal** current reversals. On the Gulf **shelf (UP3)**, flow was highly variable in direction with a slight westward tendency. The strongest flows were **15** to

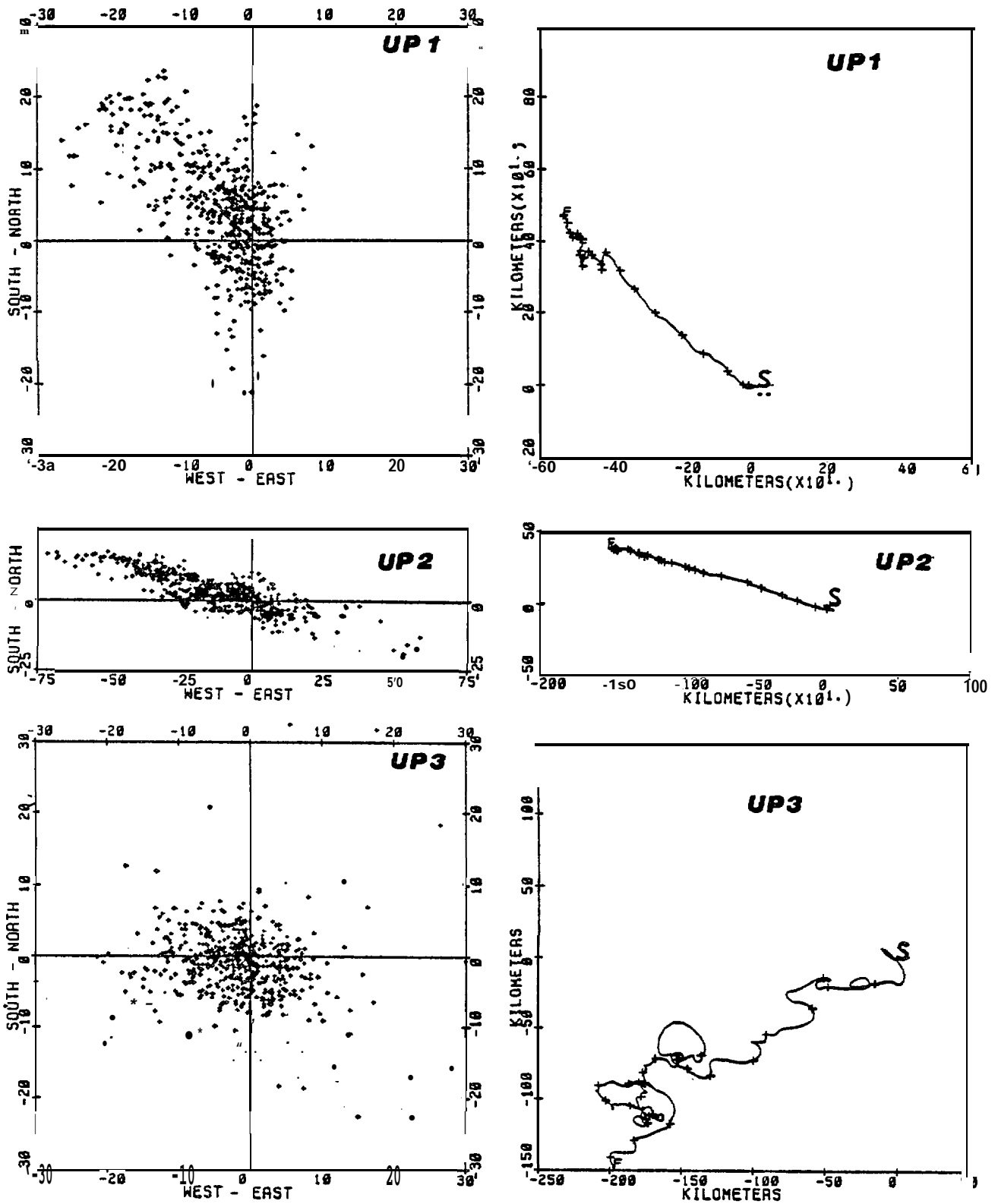


Figure 4. - Results from 35-hr filtered current data presented as scatter plots and progressive vector diagrams (S represents the start of the record, and the crosses are at 5-day intervals). Note the different speed and length scales.

30 **cm/s** toward **the** southeast. The **PVD's** (Figure 4B) show similar flow features, however, the 5-day time ticks *suggest* that **two** distinct **levels of** current magnitude occurred during the observation period: the strongest flow existed during approximately the first seventy days while flow was markedly less during the last half of the current records.

In Figure 5, we present plots of the 35 **hr** filtered currents and bottom pressure for each of the mornings, the **UP3-UP1** bottom pressure difference ( **$\Delta P$** ), the atmospheric pressure gradient, and the **geostrophic (Bakun) winds**. The currents are resolved along the axis of greatest variance (defined by the principal **eigenvector** of the orthogonal velocity component **covariance** matrix computed for the entire record) which also corresponds to flow through the pass. The atmospheric pressure gradient is resolved along an axis of **165°T** approximately normal to the Gulf of Alaska coastline. The winds are resolved **along** 255°, parallel to the Alaska Peninsula.

A characteristic common among **all** the time-series was a transition from a period of large fluctuations to one of lesser variance which occurred **about** halfway through the records. Analysis of the atmospheric pressure gradient series showed that while the direction of the principal axis remained constant toward 336°T (i.e. higher pressure over the **Gulf** of Alaska), magnitude increased during the second half by **a** factor of two and variance decreased. A dramatic change also occurred in winds with **alongshore** magnitude increasing from -1.7 m/s in the first period to -3.5 m/s in the later period. This suggests a four-fold increase in wind *stress* and enhanced coastal divergence **along** the Gulf side of the Alaska Peninsula. These results are consistent with the establishment of high pressure over the north Pacific Ocean which is a summer **climatological** feature (Brewer, ***et. al.***, 1977). **Thus**, that component

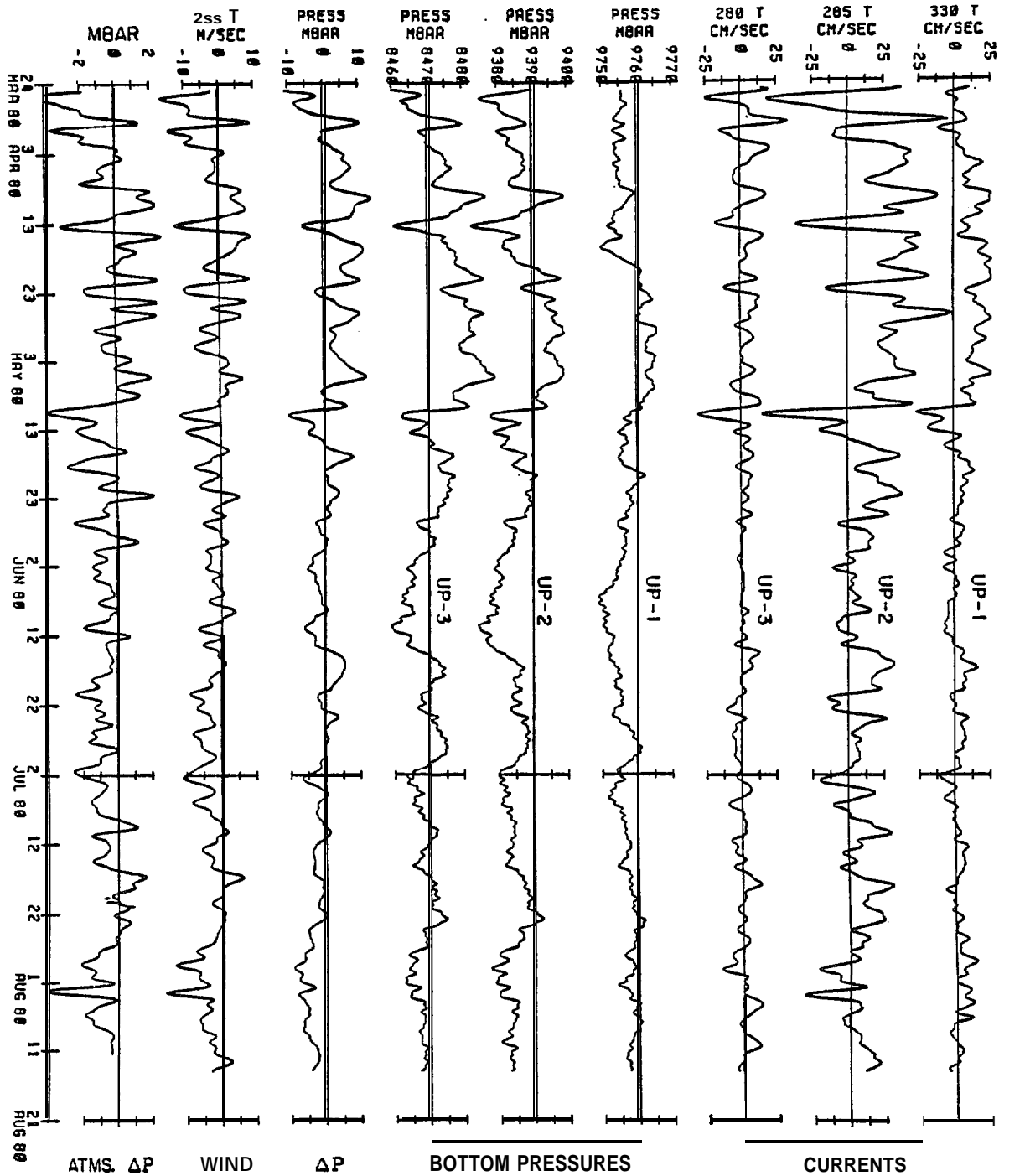


Figure 5. - Current vector time-series (35-hr filtered data) of current, bottom pressure, bottom pressure difference between UP3 and UP1 ( $\Delta P$ ), alongshore geostrophic wind, and atmospheric pressure gradient (ATMS AP in mbar/°lat.).

of current **which** is **a local** response to meteorological forcing **will** also undergo a seasonal change.

A seasonal signal exhibiting less energy during **summer** was evident in current and wind time-series from both the northwest (Schumacher **and** Reed, 1980) and northeast **Gulf** of Alaska (**Lagerloef, Muench,** and Schumacher, 1981) and from the southeastern Bering Sea (Kinder and Schumacher, 1981a). As will be discussed later, an important aspect of flow through Unimak Pass is a non-locally generated coastal current which has a seasonal signal linked **to** fresh water discharge (**Royer, 1981**). Although our records are too short to unequivocally define the amplitude and phase of a seasonal signal **in** flow through the pass, we clearly have observed a marked change between first and second halves of **the** records. The impact of this difference on mean current is given in **TABLE 1**. The first **half** of the records (**26 March to 3 June 1980**) is called spring and the second half summer because the derived winds during this time were very similar to **climatological** mean winds and hence reflect a seasonal signal.

Within Unimak Pass vector mean speed decreased by a **factor** of three between first and second halves, while direction remained **nearly** constant. The error estimate is a measure of statistical significance for the vector **mean; the values in TABLE 3 are twice the RMS error estimate and thus are analogous to a 95% confidence interval**. Using this measure, mean flow in the pass was **always** significant while on the shelves **adjacent** to the pass there was significant mean flow only during spring.

#### 4.1.3 Time-Series Relations:

We consider the correlations given in **TABLE 2** in the context of a simple conceptual model of low frequency currents as follows: **1)** currents in Unimak

Table 1. - Current and wind during first (spring) and second (summer) halves of the observations.

Record	Observation Period	Vector Mean Speed (cm/s: °T)	Error Estimate <sup>1</sup> (cm/s)	Variance (cm <sup>2</sup> /s <sup>2</sup> )
UP1	spring	9.8 : 306	± 6.6	14.1
	summer	2.2 : 334	* 2.2	8.9
UP2	spring	19.3 : 285	± 9.2	37.4
	summer	6.0 : 282	± 4.6	13.1
UP3	spring	3.2 : 240	± 2.4	41.0
	summer	1.0 : 198	± 1.2	1.2.4
Geostrophic Wind	spring	2.3 x 10 <sup>2</sup> : 030	± 2.6	18.1 x 10 <sup>4</sup>
	summer	3.8 x 10 <sup>2</sup> : 048	± 1.6	11.6 X 10 <sup>4</sup>

<sup>1</sup> Estimate of Error =  $2\sigma/(\ell/\tau)^{1/2}$ , where  $\sigma$  is the standard deviation along the vector mean speed axis,  $\ell$  is the record length and  $\tau$  is the integral time scale or area under the auto-correlation function (Allen and Kundu, 1978).

Pass are driven by the pressure difference on either side of the pass, 2) the pressure difference is produced by sea level changes which can occur along the coast on both sides of the pass, and 3) currents observed on the adjacent shelves represent a barotropic response to pressure gradients rather than an Ekman layer response. All of the observed currents were collected at least 47 m below the surface. As noted by Winant (1980), conventional estimates of the thickness of the Ekman layer are about 40 m and Royer, Hansen and Pashinski (1979) suggested that the stratified Ekman layer depth in the northern Gulf of Alaska is probably less than 35 m.

Table 2. - Correlation matrix.

	UPPER.			BOTTOM PRESSURE			WIND		BOTTOM PRESSURE DIFFERENCE ( $\Delta P$ )	ATMOSPHERIC PRESSURE GRAD
	UP1	UP2	UP3	UP1	UP2	UP3	ALONG SHORE	CROSS SHELF		
UP1	1.0	.67	.34	.47(4)	.49	.47(4)	.40(1)	.44(4)	.69(1)	.47(2)
UP2		1.0			.69	.9			.8	.6
UP3	--	--	1.0	*	.38	.41	.57(1)	.24(6)	.50(1)	.55(1)
U				0	.8			.5		
UP2					0	.9	.6	.5	.65	
UP3	--	--	--	--	--	1.0	.54( )	.38(6)	.50(1)	.58(2)
ALONG SHORE	--	--	--	--	--	--	1.0	*	.45(1)	.58(2)
CROSS SHELF	--	--	--	--	--	--	--	1.0	.2(6)	.29( )
BOTTOM PRESSURE DIF	--	--	--	--	--	--	--	--	1.0	.40( )

Note: rows lag columns and numbers in parentheses are multiples of 6 hr.

The linear relation between pressure difference and current at UP2 accounted for 76% of the current variance (85% in spring and 50% in summer). When **alongshore** winds increased, bottom pressure at UP3 decreased, however response at **UP1** was not significantly correlated **with alongshore** wind. Further, the variance in the bottom pressure record from **UP1** was only one-third of that estimated in the record at UP3. Thus, changes in the bottom pressure difference were primarily a result of forcing on **the Gulf** shelf with a large fraction, **42%** (50% in spring and 25% in summer) accounted for by the relation with **alongshore** wind. To address the question why there was more energy in current and bottom pressure records from the Gulf shelf than from the Bering **Sea** at meteorological frequencies we use **climatological** data (Brewer, **et al.**, 1977) and principal storm track data from March through August 1980 (Mariner's Weather Log, **1981**). We divided data from a **10°** by 10° region (50° to 60°: 150° to 170°) into a Bering Sea area north of 55° and a Gulf of Alaska area south of that latitude. There were seven principal storm tracks located in the Gulf and three in the Bering Sea. During our observations in 1980, there were eleven principal and eight secondary storm tracks south of the Peninsula **while** over the Bering Sea there were only six principal and three secondary storm tracks. In general, we expect to find greater meteorologically induced activity over the Gulf shelf.

It appeared that cross-shelf wind also contributed to the pressure difference, **with** significant correlation to bottom pressure on both shelves. The strength of **these** relations only accounts **for ~6%** (12% in spring, not significant in summer) and 14% (28% in spring, not significant in summer) of the variance at **UP1** and UP3 respectively. Hayes (1979) noted the importance of cross-shelf wind **to** pressure gradient and estimated correlation coefficients of similar **magnitude over the northeast Gulf of Alaska shelf. Chao and Pietrafesa (1980)**

noted that a larger contribution from cross-shelf wind forcing usually results in a **phase lag** of sea **level** fluctuation response, and **the** results in **TABLE 2** are consistent with their results. In general, our conceptual model **of** interaction between wind, bottom pressure and current in Unimak Pass accounts for much of the observed current fluctuations.

In order **to** examine relations between pressure difference and both Unimak Pass current and **geostrophic** wind as a function of frequency, we present coherence squared estimates in Figures 6 and 7. Current in the pass was coherent at **all** frequencies with the pressure difference series **during both spring** and summer with the largest coherence squared (**~0.70 to 0.96**) at periods **of** about **3 to 10** days. **During** both record segments coherence decreased at the longest period resolved (**~23** days). In order to present **coherence** results as a single, **phase** independent measure, we use the following technique. At each frequency where coherence squared was significant **at the 95% level**, the product **of** the dependent variable (**i.e.** current) variance times **the** coherence squared was determined. Summing **this** product over all frequencies and dividing **by** the **total** record variance, we determined that **89% and 66% of** the current fluctuations were accounted for **by** fluctuations in **the** pressure difference series during spring and summer, respectively.

Coherence squared estimates between the pressure difference and **geostrophic** wind components (Figure **7**) were greatest **during** spring: **70% and 26%** of the fluctuations in bottom pressure difference were accounted for by relations with **alongshore** and cross-shelf winds, respectively. **During** summer, the percent of variance **explained was** only **9% and 7%** respectively. **If** the variance at periods longer than **10** days was neglected (the **series** were **not** coherent at these periods), then the values were **43% and 33%**. **It** appears that **at** periods longer than **~10** days, the bottom pressure **field** was **responding** to

# UP2 CURRENT vs BOTTOM PRESSURE DIFFERENCE

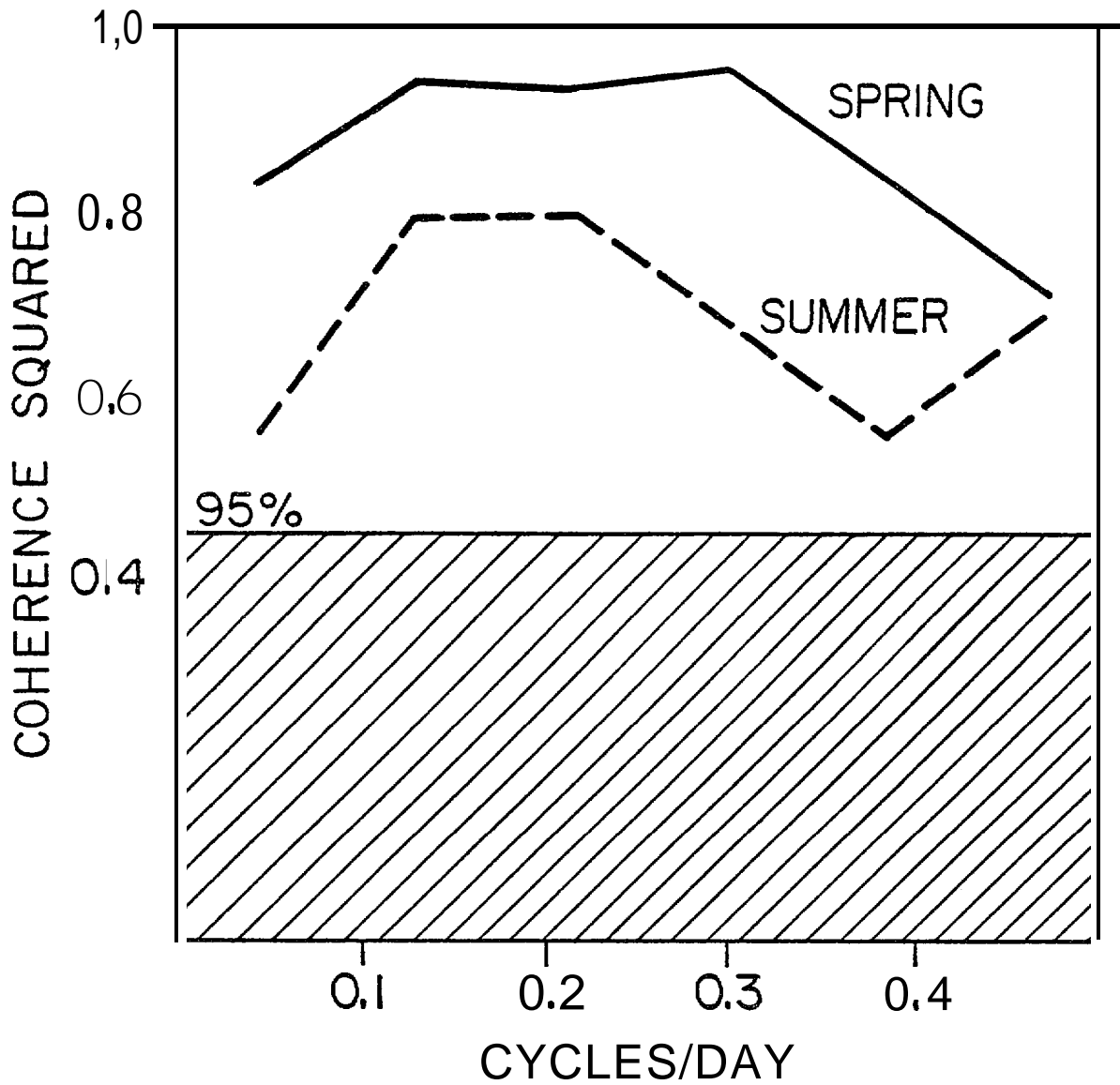


Figure 6. - Coherence between current in Unimak Pass (UP2) and bottom pressure difference along the pass for spring (solid line) and summer (dashed line) record segments.

---

BOI OM PRESSURE DIFFERENCE vs WIND

---

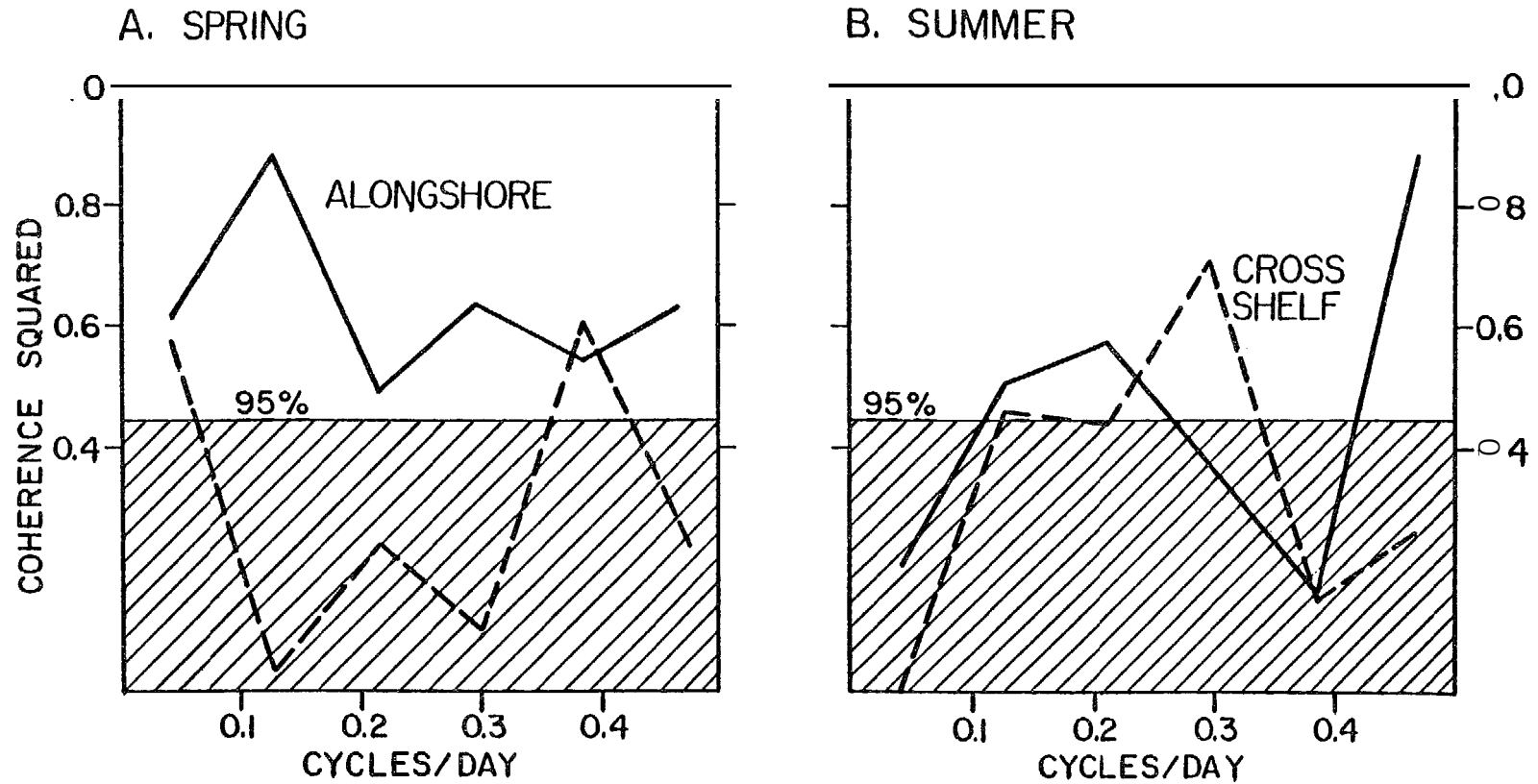


Figure 7. - Coherence between bottom pressure difference and geostrophic wind components during (a) spring and (b) summer record segments. The coherence with alongshore wind component is shown as a solid line and with the cross-shelf component as a dashed line.

forcing other than wind induced pressure gradients. It is most likely that changes **of** density were the cause; Reed and Schumacher (1981) noted that insolation is important to monthly mean sea level anomalies as early as June at Dutch Harbor.

The current time-series indicated that flow was generally from the Gulf of Alaska to the Bering Sea **shelf** and both mean and fluctuating currents were significantly greater during spring. Relations between the various series suggest that large scale atmospheric pressure fields, hence **geostrophic** winds, were responsible for the 3 to 10 day fluctuations. The mode of interaction was **mainly perturbation in** sea level along the Gulf of Alaska coast. The **longer period wind** stress was **alongshore** (northeastward) which would generate a **barotropic** component of current **alongshore** (towards the northeast), rather than the observed negative **alongshore** or westward mean flow through the Pass. So, we now examine **hydrographic** data to describe property distributions and to elucidate the role of mass distribution in generating long-term mean flow through Unimak Pass.

#### 4.1.4 Property Distributions

Vertical sections of temperature, salinity and sigma-t for 4 to 5 September 1980 are shown in Figures 8A, B and C, **respectively. Across the** bottom of each panel the magnitude **of** the surface minus the bottom value of each parameter is also shown. Over the Gulf of Alaska shelf (stations 17 **to 20**) thermal stratification exceeded **4.0°C** and the upper 50 m were considerably warmer than over the Bering Sea shelf (stations 14 to 10). Although tides and thus tidal mixing are more energetic within Unimak Pass proper (station 15), thermal stratification **in** the pass (**~2.5°C**) was greater than thermal stratification (**~0.9 to 1.5°C**) observed in Bering shelf waters. A similar distribution

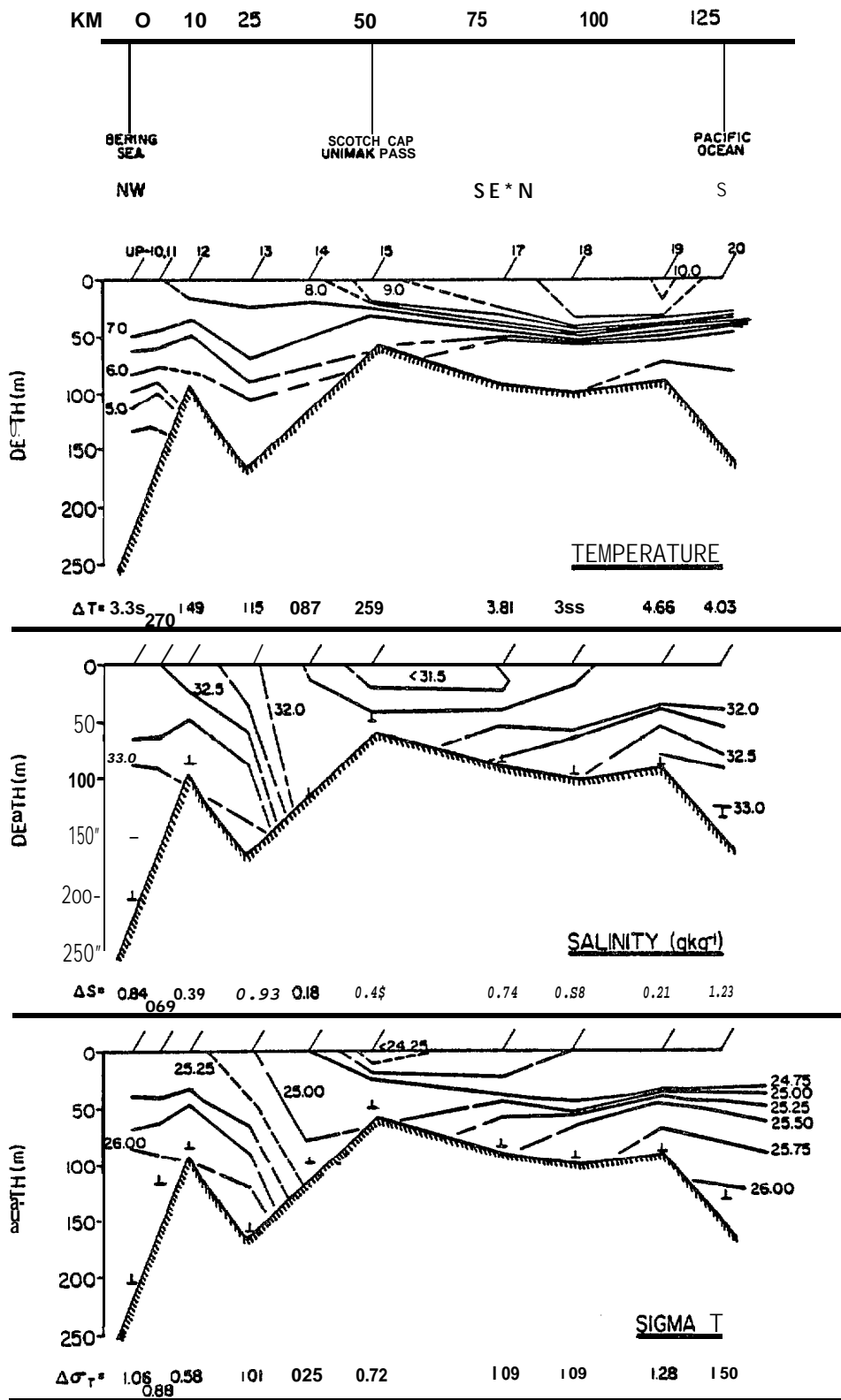


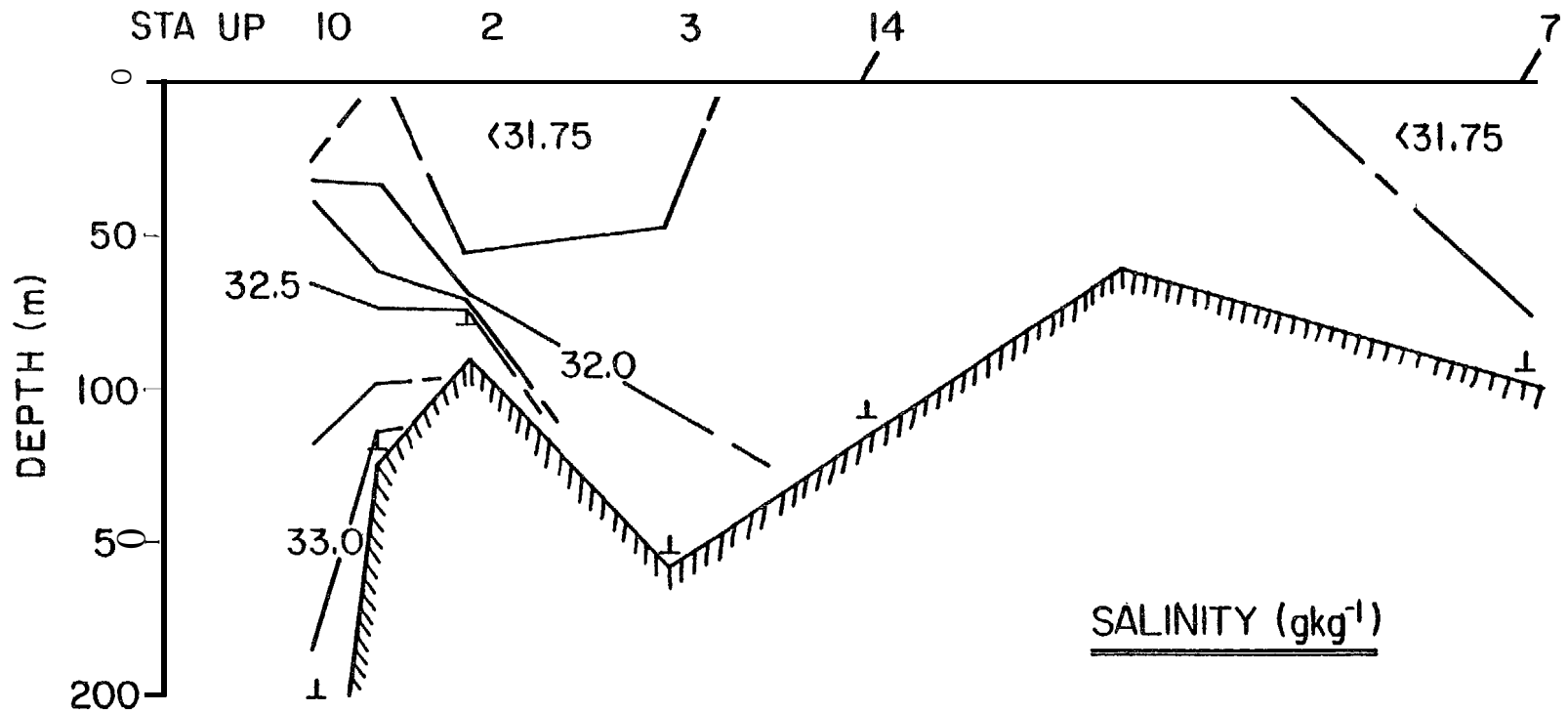
Figure 8. - Hydrographic data from September 1980 presented as temperature ( $^{\circ}\text{C}$ ), salinity, and sigma-t sections. The  $\Delta$  values are the magnitude of surface minus bottom 1 m averaged values. See Figure 1 for station locations.

existed in salt content; AS values were greatest over the Gulf shelf, persisted within the pass and were least west of the pass proper. We note a region of low salinity ( $\leq 31.75$  g/n/kg) existed within  $\sim 25$  km of Unimak Island. The impact of temperature and salinity upon density is shown in the bottom panel of Figure 8. As expected, the distribution of density bears a marked resemblance to salinity. When water temperatures are less than  $10^\circ\text{C}$ , the equation of state for seawater dictates that variations of salinity contribute more than those of temperature to changes in density (Gebhart and Mollendorf, 1977).

A second hydrographic section through Unimak Pass was occupied on 17 February 1981 and we present the vertical section of salinity with the AT and  $\Delta\sigma_t$  values across the bottom (Figure 9) for comparison to conditions observed in September 1980. Surface temperatures (not shown) were  $\sim 3.5$  to  $4.0^\circ\text{C}$  and increased less than  $1.0^\circ\text{C}$  with depth so there was little structure in thermal field. Isohalines again indicated regions of low salinity ( $\leq 31.75$  g/n/kg), however, the only substantial stratification ( $\Delta\sigma_t \geq 0.5$ ) existed over the Bering Sea shelf. As was observed in September 1980, the strongest vertical and horizontal salinity gradients were found over the Bering Sea shelf. A five-station hydrographic section normal to Unimak Island was occupied on 13 May and again 2 June 1981. Both sections showed low salinity ( $\leq 31.75$  g/n/kg) water within  $\sim 20$  km of Unimak Island (cf., Figure 10) and little thermal structure.

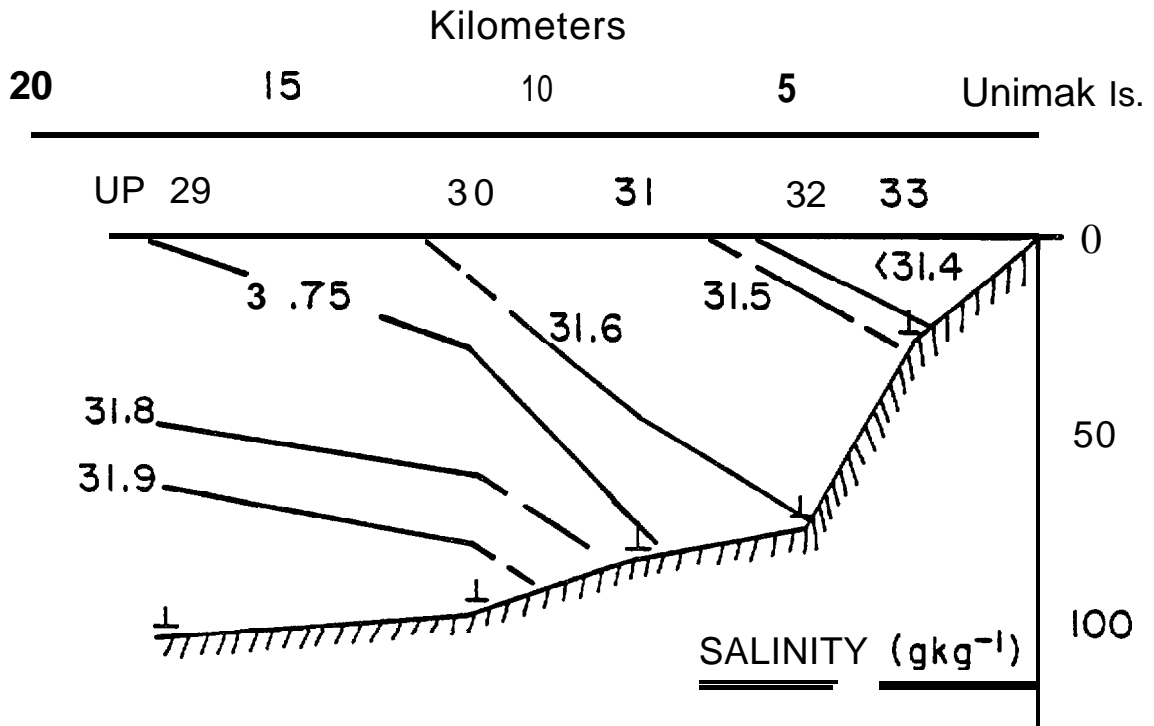
The most extensive spatial coverage was attained on a cruise conducted between 2 and 3 September 1981. Hydrographic data are presented as the areal extent of waters with salinity less than  $31.75$  g/n/kg in the upper 50 m (or to the bottom, Figure 11A) and as dynamic topography (0/50 db) in Figure 11B. West of the pass proper, the bulk of less saline water was in a band within  $\sim 10$  km of the coast, while south of Unimak Island the band extended  $\sim 20$  km

480



$\Delta\sigma_T =$	0.95	0.82	0.30	0.01	0.03
$\Delta T =$	-0.91	-0.68	-0.28	-0.08	-0.34
$\Delta S =$	1.46	1.12	0.30	0.04	0.12
	1.30				

Figure 9. - Hydrographic data collected during February 1981 along the same section as in Figure 6. The  $\Delta$  values are the magnitude of surface minus bottom 1 m averaged values.



$\Delta\sigma_T = 0,23$	<b>0,35</b>	<b>0.18</b>	<b>0,36</b>	<b>0,09</b>
AT = 0.80	<b>0.70</b>	<b>0030</b>	<b>0.91</b>	<b>0*33</b>
AS = 0.21	<b>0034</b>	<b>0.21</b>	<b>0,33</b>	<b>0,14</b>

Figure 10. - Hydrographic data for May 1981 from stations normal to Unimak Island. The **A** values are the magnitude of surface minus bottom 1 m averaged values.

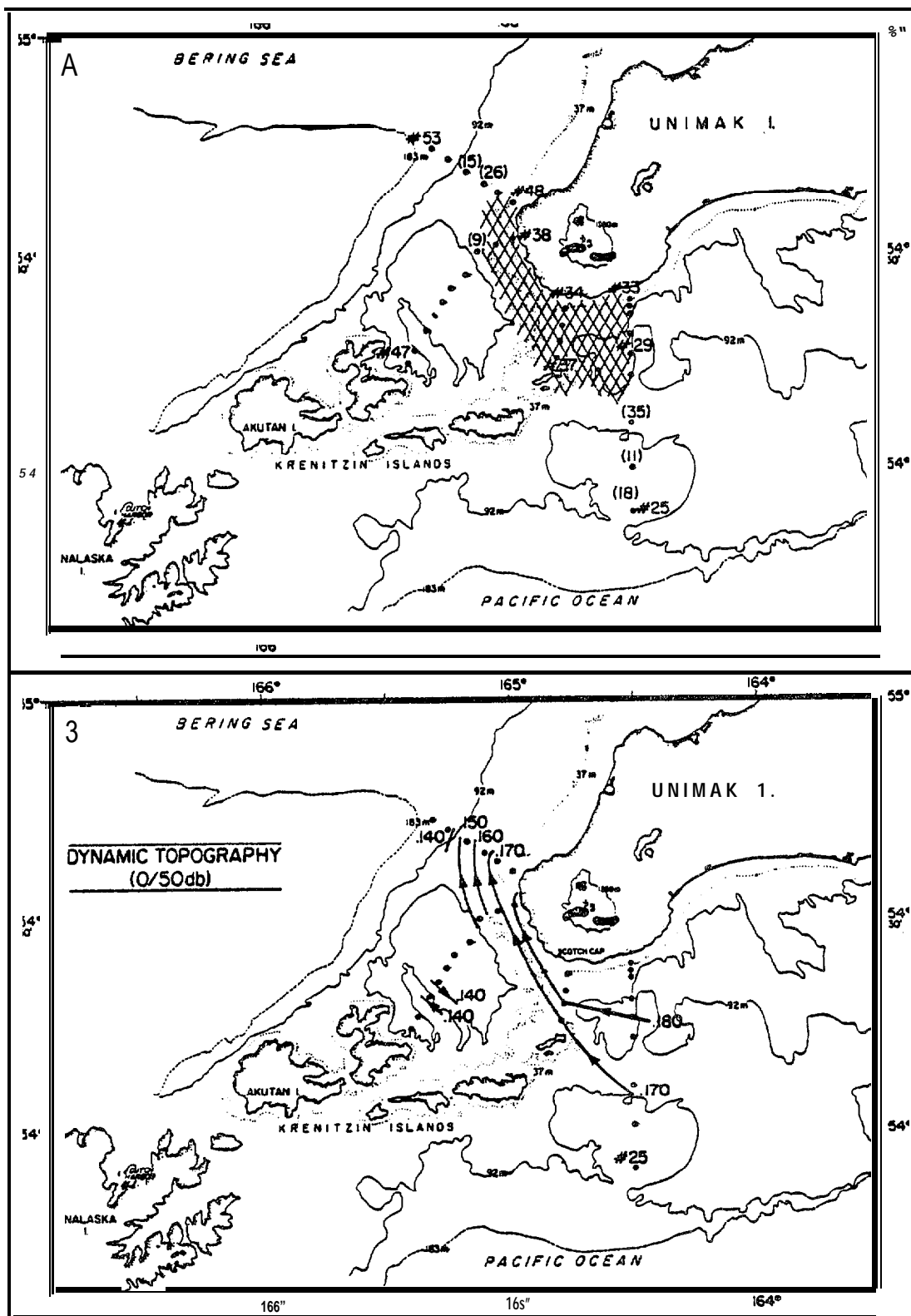


Figure 11. - Hydrographic data for September 1981 presented as (a) areal extent of waters with salinity  $\geq 31.75$  g/kg in the upper 50 m (or bottom) where the numbers in parentheses are depths of the low-salinity band for  $>50$ m, and (b) dynamic topography (0/50 db) with a 0.01 dyn m contour interval. CTD station numbers are indicated by the number sign (#).

offshore and less saline waters existed in a thin layer at least 60 km offshore. The dynamic topography (0/50 db) reflects the narrowing trend of **the** low salinity band, with relief increasing from 0.008" **dyn.m.** between stations 32 and 29 south of Unimak Island to 0.025 **dyn.m.** between stations 48 and 51 northwest of the island. The steep relief between stations 51 and 52 resulted from the presence of saline (>32.50 gln/kg) water over the Bering Sea shelf. These waters **also** resulted in lower relief west of station 40. The suggested curvature of **geopotential** contours indicates that relative **vorticity** generated either by changes in depth or a horizontal velocity gradient in the pass proper may be important to flow dynamics west of the pass.

#### 4.1.5 Baroclinic Geostrophic Currents

A persistent feature of the mass distribution in the five data sets was the presence of low salinity water along the coast of Unimak Island. Other **hydrographic** surveys (Kinder et al., 1978; Wright, 1980) have also shown less saline waters exist off Unimak Island and south of the Alaska Peninsula. We estimate the impact of the observed mass distribution on the velocity field by assuming a **geostrophic** balance. While this method neglects such factors as **wind** stress, bottom friction and **barotropic** pressure gradients, over the Bering Sea shelf (Kinder and Schumacher, 1981a) and along the Gulf of Alaska coast (**Royer, Hansen and Pashinski, 1979; Schumacher and Reed, 1980**) good agreement was shown between **baroclinic geostrophic** flow and both **Eulerian** and **Lagrangian** current observations.

In the TABLE 3, we present **baroclinic** currents of the surface relative to 50 db for **each set of station pairs** where the dynamic **relief was  $\geq 0.01$  dyn.m.:**

Table 3. - Dynamic relief and **baroclinic** speed

<b>Observation</b> Date	Station Pair	0/50 db Dynamic Relief (dyn. m. )	Speed (cm/s)	Direction (°T)
4 to 5 Sept. 1980	<b>12/13</b>	<b>0.014</b>	<b>9</b>	NE
	13/14	0.015	<b>10</b>	NNE
	14/15	0.011	<b>7</b>	<b>NE</b>
	<b>18/19</b>	0.012	<b>5</b>	w
<b>17 Feb. 1981</b>	<b>11/12</b>	<b>0.011</b>	13	NE
13 May <b>1981</b>	32/29	0.011	12	w
2 June <b>1981</b>	32/29	0.010	7	w
2 to 3 Sept. <b>1981</b>	36/37	<b>0.010</b>	17	w
	38/39	0.012	20	N
	39/40	0.013	22	N
	49/50	0.012	<b>19</b>	NE
	50/51	0.014	33	NE
	51/52	0.020	30	<b>NE</b>
	27/26	<b>0.010</b>	7	w

The inferred flow **from the** first three station pairs in September 1980 and **the** first four pairs in September 1981 together with set **11/12** suggests moderate flow (7 to 22 cm/s) through Unimak Pass. This is consistent with **our** current observations and compares favorably with dynamic topographies presented by Coachman and **Charnell (1977)** from March 1976 **CTD** data collected north and west of the **pass**. **Relief** across the remaining station pairs suggests a weaker westward flowing current (5 to **12** cm/s) **along** the **Gulf** side of the Alaska Peninsula **and** a stronger current (**19** to 33 cm/s) northwest of the pass.

Since 1975, sixty-one **CTD** stations were occupied within **about 50 km of** Unimak Pass proper. Separating these data into two sets, Gulf side (**N=29**) and Bering Sea side (**N=32**) of the pass we can strengthen our hypothesis that water east of the pass is generally less dense (due to lower salinity) than water **west of the pass**. We note that only data sets with casts on both sides during a given cruise were used to avoid **aliasing** the results. East of the pass, the mean dynamic **height** (0/50 db) and standard deviation was **0.162±0.016 dyn.m.** **and 0.136±0.016 dyn. m west of the pass**. Thus, including **CTD** data from all seasons, we find that water along the Gulf side of Unimak Island was generally about 3 **dyn.cm** greater in height (over 50 db) than waters west of Unimak Pass.

#### 4.1.6 Discussion

The results presented thus far have defined the behavior of current in Unimak Pass and the forcing for such flow: water is generally transported from the Gulf of Alaska onto the Bering Sea shelf. While subtidal flow with periods of 3 to 10 days was shown to be **mainly** driven by a wind-induced pressure difference along the pass, longer period (on the order of months) flow appeared to be driven by a coastal current existing along the Alaska Peninsula. Two important questions evolve from our results: what is the source of the coastal current and what is the impact of transport through Unimak Pass?

A recent study (Schumacher and Reed, 1980) has described and defined the **Kenai** Current, a strong coastal current which flows westward along the Gulf of Alaska coast from about **145°W** to the southwest end of **Shelikof Strait (~156°N)**. Royer (1981) has indicated that this feature is a component of the more extensive Alaska Coastal Current which is the consequence of the accumulation of runoff beginning along the British Columbia coast. He estimates transport

in **the** northeast Gulf of Alaska to be  $0.12 \pm 0.05 \times 10^6 \text{ m}^3/\text{s}$  and Reed, Schumacher and Wright (1981) show that **the** dynamic relief (0/90 db) is typically  $\sim 4$  dyn. cm. in this portion of the Alaskan Coastal Current. To the west, along the **Kenai** Peninsula, there is an increase in dynamic relief (4 to 20 dyn. cm) and transport (0.10 to  $1.2 \times 10^6 \text{ m}^3/\text{s}$ ) both varying with season. The behavior of the Kenai Current **west of Shelikof** Strait is not well known, however, Wright (1980) indicates relatively low **salinity water exists along the Alaska Peninsula as far west as Unimak Pass. Further, it is unlikely that the freshwater signal near Unimak Pass was of local origin since rainfall (Brewer, et al. 1977) undergoes a four-fold reduction (323 to 84 cm) from  $\sim 158^\circ\text{W}$  (Chignik) westward to  $162.5^\circ\text{W}$  (Cold Bay) and there are no gaged rivers. Current records from  $\sim 156^\circ\text{W}$  and  $158^\circ\text{W}$  (Muench and Schumacher, 1980) indicate a substantial mean flow ( $\sim 15$  cm/s) westward along the coast. These results, together with the hydrographic data presented above indicate that some fraction of the Kenai Current continues along the peninsula and flows through Unimak Pass.**

Using CTD data collected south of Unimak Island between stations 33 and 29 in May, June and September 1981, we estimate that **baroclinic** transport (computed to the greatest common depth) was  $\sim 6, 5$  and  $7 \times 10^4 \text{ m}^3/\text{s}$  respectively with **maximum surface** speeds of 12, 8 and 5 cm/s and dynamic relief (0/60 db) of  $\sim 2$  dyn. cm. For all estimates, the largest fraction of the transport (**>40%**) occurred between the two most seaward stations. Thus total **alongshore** transport may be substantially greater; during September 1981 transport between stations 33 and 26 (see Figure 9A) was  $\sim 24 \times 10^4 \text{ m}^3/\text{s}$ . Transport too far offshore to flow through the pass was **also** indicated in August 1980 data (see set 18/19 in **TABLE 4**). CTD data collected on a line normal to the Peninsula about 150 km east of Unimak Pass (at  $\sim 159^\circ\text{W}$ ) indicated **alongshore** transport of about

$\sim 24 \times 10^4 \text{ m}^3/\text{s}$  in conjunction with a band of low salinity water of similar cross shelf extent to that observed south of Unimak Island. Transport estimates between stations 38/42 and 48/52 (see figure 9A) were about 12 and  $16 \times 10^4 \text{ m}^3/\text{s}$  respectively. The hydrographic data suggest a baroclinic current south of the Peninsula with a large fraction flowing westward through Unimak Pass and continuing along the northwest coast of Unimak Island. Caution is necessary in estimating transport through Unimak Pass from a single current record. Assuming that the measured mean flow was representative over most of the cross-section (there were no reversals in baroclinic speed and vertical shear was moderate), we estimate  $\sim 6$  to  $20 \times 10^4 \text{ m}^3/\text{s}$  were transported through Unimak Pass which is consistent with the baroclinic estimates.

The dearth of CTD data precludes establishment of a seasonal signal near Unimak Pass, however, off the Kenai Peninsula baroclinic transport varied by an order of magnitude with a maximum observed in October (Schumacher and Reed, 1980). Using an annual curve fitting technique on six years of data, Royer, (1981) suggested a maximum occurred in December. If continuity exists along the current, then maximum baroclinic transport through Unimak Pass should occur during sometime during the first three months of the year. This is consistent with the observed current in Unimak Pass and the increase in sea level anomaly observed during December and January at Dutch Harbor (Reed and Schumacher, 1981). While baroclinic spin-up may account for increased speeds for one to two months, wind induced coastal convergence was of equal magnitude along the Kenai Peninsula; during January through March 1978, vector mean speed was  $\sim 25$  cm/s at a depth of 75 m in Shelikof Strait. Although there is uncertainty regarding phase and amplitude due to limited data, the nature of forcing suggests that changes in mean flow through Unimak Pass appear related to seasonal behavior of the Kenai Current, and not to local forcing.

We now consider the impact that transport through Unimak Pass has on water mass properties and on the water budget of the Bering Sea shelf. The **CTD** data presented above indicate a region of enhanced horizontal salinity gradient about 50 to 75 km west of Unimak Pass proper (figure 6, vicinity of station 13; figure 9, vicinity of stations 40/41 and 51/52). This feature can be compared to the 'middle front' which exists over the southeastern Bering Sea shelf (Coachman and Charnell, 1979; Coachman, et al., 1980; Kinder and Schumacher, 1981b) and has a profound influence on that region's productivity and nutrient fluxes (Iverson, et al., 1980; Coachman and Walsh, 1981). In these papers, the middle front, as determined from **CTD** data collected about 100 km northwest of Unimak Island, was characterized in terms of a vertical salinity gradient,  $\Delta S/\Delta z$ , and the horizontal gradient of the mean salinity,  $\Delta \bar{S}/\Delta x$ . Hydrographic data collected during 1980 and 1981 west of Unimak Pass indicated the following gradients existed:  $\Delta \bar{S}/\Delta z \sim 9 \times 10^{-5} \text{ gkg}^{-1} \text{ cm}^{-1}$ , and  $\Delta S/\Delta x \sim 45 \times 10^{-3} \text{ gkg}^{-1} \text{ km}^{-1}$  with a slight enhancement in the bottom 50 m. Thus, the vertical gradient was  $\sim$  fifty times stronger while the horizontal gradient of mean salinity was about five hundred times greater than that observed over the shelf to the northwest. The data indicate that the two fronts may be different dynamically and it is not known if they are contiguous, however, transport of less saline water from south of the Alaska Peninsula results in a strong salinity front west of Unimak Pass proper. Hattori and Goering (1981) note the role played by water flowing through Unimak Pass on the fertility of the region. Although these authors identify the water as being "Alaskan Stream," their temperature and salinity data suggest it was water of the coastal current. Upwelling along the Gulf side of Unimak Island, induced during summer by the mean alongshore (northeastward) wind-stress, may have provided the relatively high concentrations of nitrate and ammonium which they observed. Further, the

less saline waters may contribute substantially to the **baroclinic** coastal **flow** observed along the Bering Sea side of the Alaska **Peninsula** (Kinder and Schumacher, **1981 b**).

Recently, annual mean water transport through Bering Strait (from the Bering Sea into the Arctic Ocean) was reevaluated to be  $0.8 \pm 0.2 \times 10^6 \text{ m}^3/\text{s}$  (Coachman and Aagaard, 1981). The apparent source of most of this transport was flow along the Siberian coast (Coachman, Aagaard and Tripp, 1975; Kinder and Coachman, 1978). We note that our **estimates of transport** through Unimak Pass are five to ten times **greater than gauged freshwater addition along the Alaska** coast of the **Bering Sea and may account** for up to one-fourth the mean annual transport northward through Bering Strait.

#### 4.2 The North Aleutian Shelf Transport Processes Experiment

In order to characterize currents and hydrography over the North Aleutian shelf, ten moorings (figure 12) were deployed between August 1980 and May 1981 and a seventy-two station **CTD** grid was designed (figure 13). The ensuing observations **permit a description of currents and inferences to be made regarding the 50-m front.**

##### 4.2.1. Long-period Time-Dependence of **Hydrographic** Features

In this section, we present **CTD** data by cruise, **where we** selected the most synoptic period (about six days) set of casts. These data are presented as area distributions and both spatial and between-cruise changes are discussed.

Temperature: **In August 1980**, surface temperatures (figure 14A) varied **along** the peninsula **from  $\sim 11.5^\circ\text{C}$**  in inner Bristol Bay to  **$< 8.0^\circ\text{C}$**  north of Unimak Island. Across the shelf, the strongest difference ( **$\sim 2.0^\circ\text{C}$** ) was in the vicinity

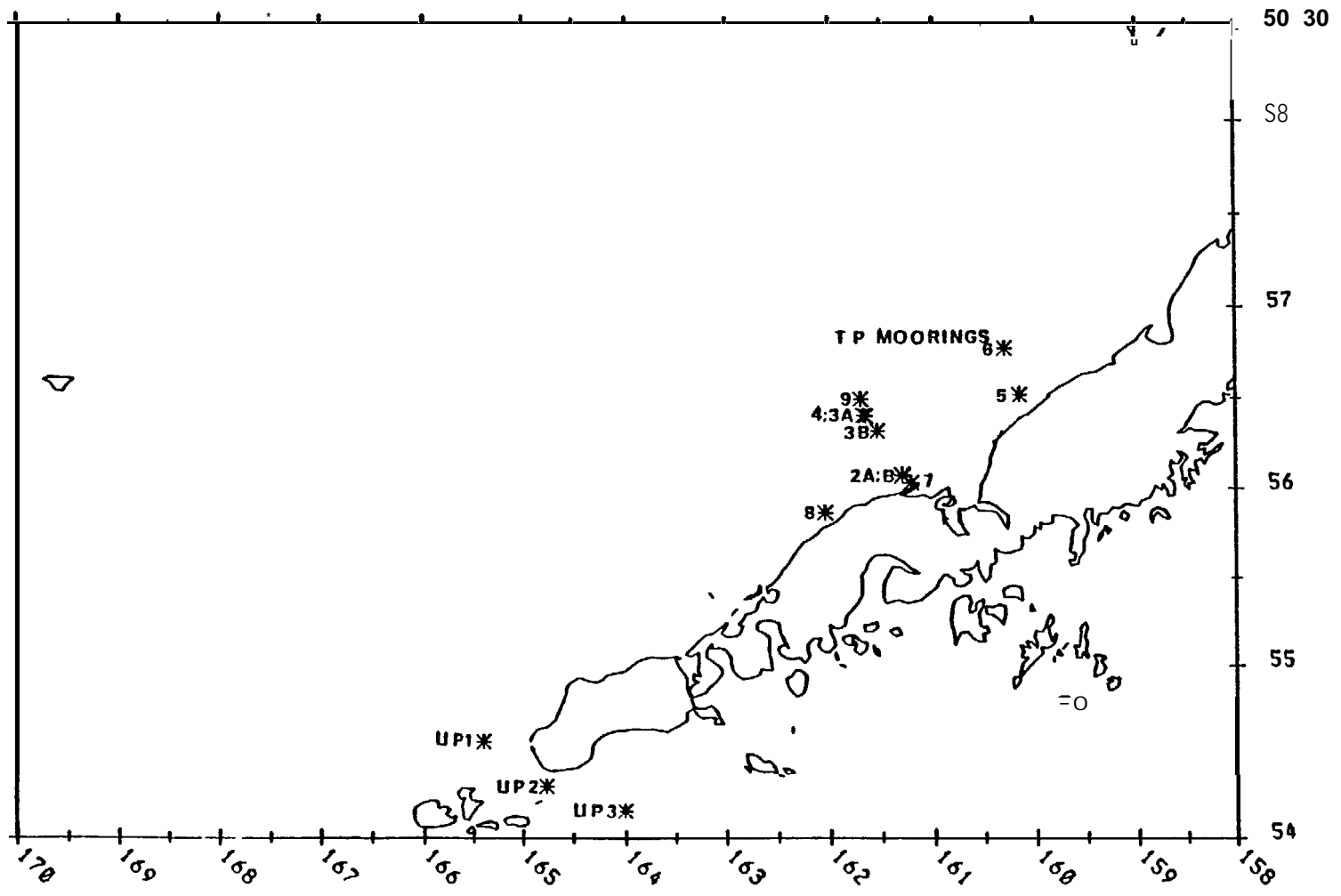


Figure 12. - Location of current meter moorings.

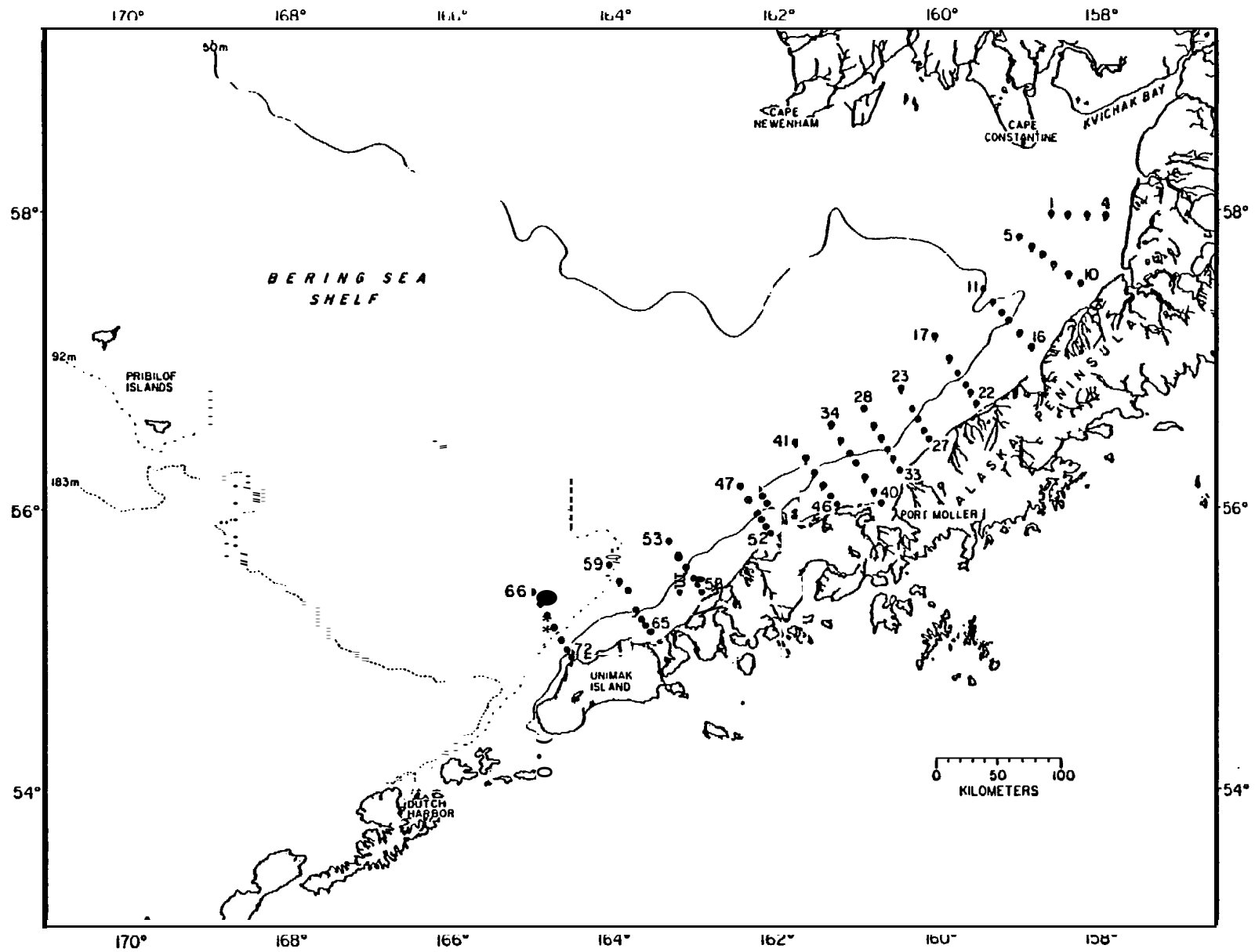


Figure 13. - Location of CTD stations (NA 1 to 72) for the North Aleutian Shelf study.

# SURFACE TEMPERATURE ("C)

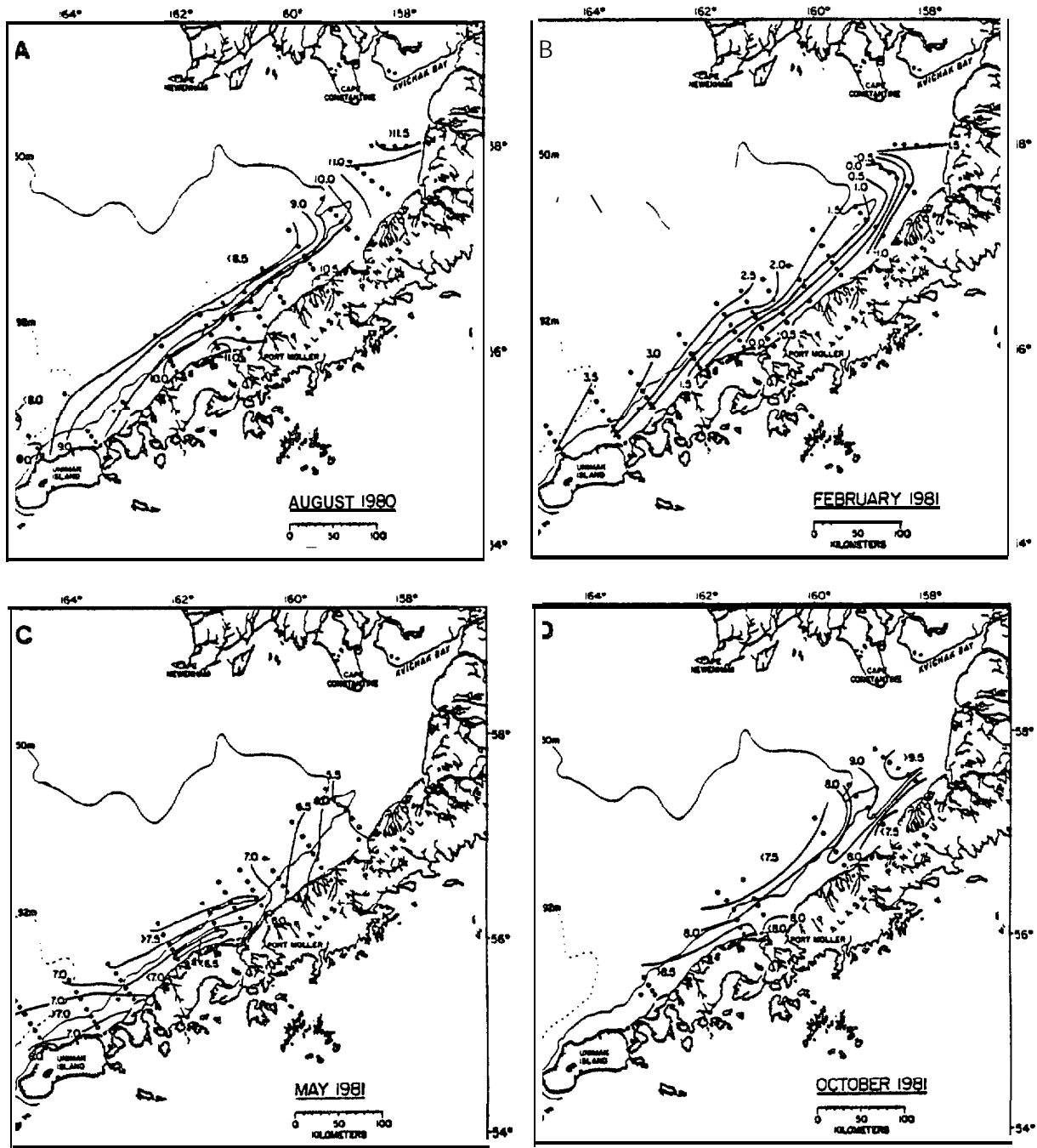


Figure 14. - Surface temperature ("C) contours.

of the 50-m isobath. This difference decreased and became perpendicular to the peninsula off Port Heiden as it followed the 50-111 isobath toward the northwest. West of Port **Moller**, the cross-shelf temperature difference decreased **to  $<1.0^{\circ}\text{C}$**  north of Unimak Island.

By February 1981, surface temperatures (figure 148) were close to the freezing point in inner Bristol Bay and the  **$0^{\circ}\text{C}$**  contour extended westward to Port **Heiden**. Temperatures  **$<0.5^{\circ}\text{C}$**  were also observed in Port **Moller**. Isotherms and the cross-shelf temperature difference ( **$\sim 2.5^{\circ}\text{C}$** ) followed a pattern similar to that observed in August, **paralleling** the trend of the 50-m isobath and decreasing west of Port **Moller**. Off Unimak Island, maximum surface temperatures ( **$>3.5^{\circ}\text{C}$** ) were observed over the corner of the outer shelf domain and the cross-shelf temperature difference was minimal ( **$<1.0^{\circ}\text{C}$** ) again.

In May, surface temperatures (figure 14C) increased **from  $\sim 5.5^{\circ}\text{C}$**  off Port Heiden **to  $\sim 8^{\circ}\text{C}$**  near Port **Moller**. West of Port **Moller**, surface temperatures were rather constant (with an average value of  **$7.0^{\circ}\text{C}$** ) and displayed a tendency to be aligned with the 50-m isobath, although the cross-shelf gradient was weak and had a banded structure. This distribution suggested the establishment of nominal middle shelf characteristics, i.e., two-layered as a result of solar insulation.

Surface temperatures (figure 140) were generally warmer by October. However, since waters over the middle shelf domain were 1 to  **$2^{\circ}\text{C}$**  cooler than **those inshore, the peak in thermal stratification had apparently passed and cooling was operative. Surface temperatures in the coastal domain were greatest** in regions where stratification from freshwater addition was observed. Although surface cooling had affected contours, there was a tendency for isotherms to parallel the 50-m isobath as noted before.

**Bottom** (nominally 5m above the bottom) temperatures during August 1980 (figure 15A) varied from **>11.5°C** in inner Bristol Bay to **<6.0°C** off Port Moller with a **minimum (~3.7°C** at NA59) in the corner of the outer shelf domain north of Unimak Island. Shoreward of the 50-m isobath and between Port Moller and Port Heiden, bottom temperatures were **~10°C** and they decreased to **<8°C** west of Port Moller. A strong (**>3°C**) difference existed from Port Heiden westward along the peninsula with a divergence of **this** trend off Port Moller. In general, the region of highest **bottom temperature** difference paralleled the **50-m isobath**. **Comparison with surface temperatures** indicated that the coastal domain was well mixed thermally and both the middle shelf and outer shelf domains were stratified.

Near freezing temperatures (**<1.5°C**) were observed on the bottom in inner Bristol Bay in February 1981 (figure 15B), and temperatures **<0°C** were present westward to Port Heiden and in Port Moller. An **~2.5°C** difference was located normal to the peninsula off Port Heiden. A similar difference paralleled the 50-m isobath to the vicinity of Port Moller. West of **this** area bottom temperatures increased to **>4.0°C** off Unimak Island. In general, there was **negligible** thermal stratification except over the outer shelf domain where bottom temperatures were **~0.5°C** greater than surface values.

In May, bottom temperatures (figure 15C) varied from **<4°C** seaward of the 50-m isobath to **>7°C** in Port Moller and isotherms paralleled the entire peninsula. Between Port Heiden and Izembeck Lagoon, and within **~20km** of the coast, thermal stratification was generally slight (**<1°C**), but seaward of the 50-m isobath thermal stratification was generally **>3°C** along the entire peninsula.

**Bottom** temperatures during October (figure 15D) had warmed from May by at least **1°C** over the middle shelf and values **>9.5°C** were present in inner Bristol

# BOTTOM TEMPERATURE ("C)

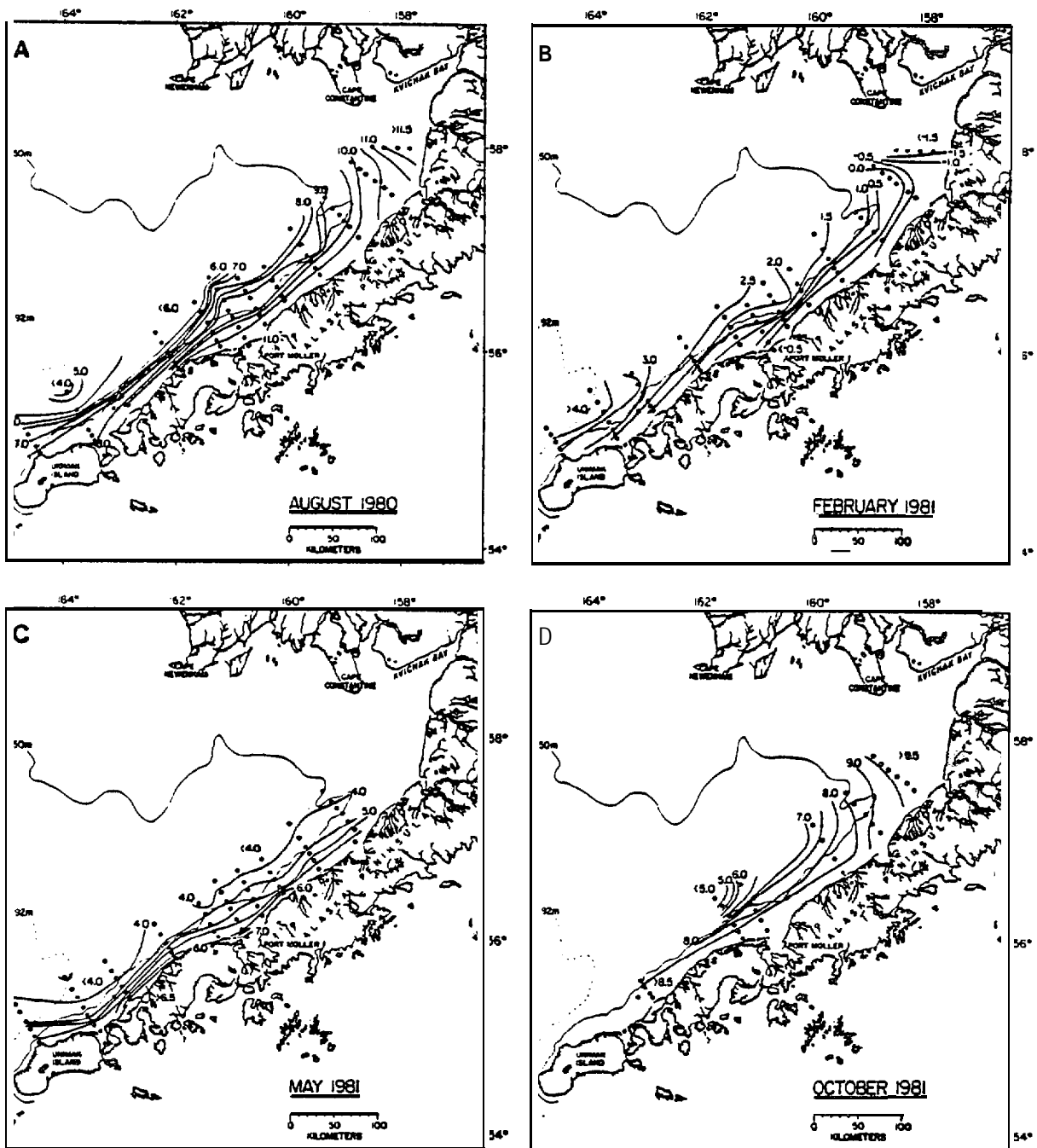


Figure 15. - Bottom temperature ("C) contours.

Bay. Isotherms again paralleled **bathymetry** and indicated a cross-shelf gradient of  $\sim 3.5^{\circ}\text{C}$ . Comparison with surface temperatures indicated isothermal water in Bristol Bay extending westward to near Port Heiden. Coastal waters west of Port Heiden indicated cooling, with surface temperatures as much as  $2^{\circ}\text{C}$  cooler than bottom waters. Middle shelf waters were stratified with surface to bottom temperature differences  $\geq 2^{\circ}\text{C}$ .

**Salinity:** In August, surface salinities (figure 16A) ranged from  $< 24.5 \text{ g kg}^{-1}$  in inner Bristol Bay to  $> 32 \text{ g kg}^{-1}$  over the outer shelf domain north of Unimak Island. A strong ( $25 \text{ g kg}^{-1}$ ) difference existed normal to the peninsula (between the 50 and 25-m **isobaths**) in inner Bristol Bay. In **the coastal domain** between Port Heiden and Unimak Island, salinities increased by about  $1 \text{ g kg}^{-1}$ . Salinities over the middle **shelf** were  $\geq 31.5 \text{ g kg}^{-1}$  and relatively constant.

By February 1981, the impact of Kvichak River runoff had diminished in inner Bristol Bay and surface salinities (figure 16B) were  $\sim 31 \text{ g kg}^{-1}$ . There was a remnant of the difference normal to the peninsula, but its magnitude was only  $\sim 0.5 \text{ g kg}^{-1}$ . Salinities over the middle shelf were  $> 32 \text{ g kg}^{-1}$  while **values** in Port Moller were  $< 30.5 \text{ g kg}^{-1}$ . This cross-shelf difference **diminished** to less than  $0.5 \text{ g kg}^{-1}$  off Unimak Island. The region of coastal water west of Port Moller with salinity  $< 31.5 \text{ g kg}^{-1}$  was substantially greater than in August.

In May, surface salinities (figure 16C) were more uniform throughout the study area; values were  $< 31 \text{ g kg}^{-1}$  in Port Heiden and Port Moller with values  $> 31.75 \text{ g kg}^{-1}$  over the middle shelf domain between these ports. The **cross-shelf** difference varied from  $\sim 1 \text{ g kg}^{-1}$  off Port Moller to  $< 0.5 \text{ g kg}^{-1}$  north of Unimak Island where an intrusion of more **saline** water ( $> 31.8 \text{ g kg}^{-1}$ ) was observed over the **outer** shelf domain.

# SURFACE SALINITY (g/kg)

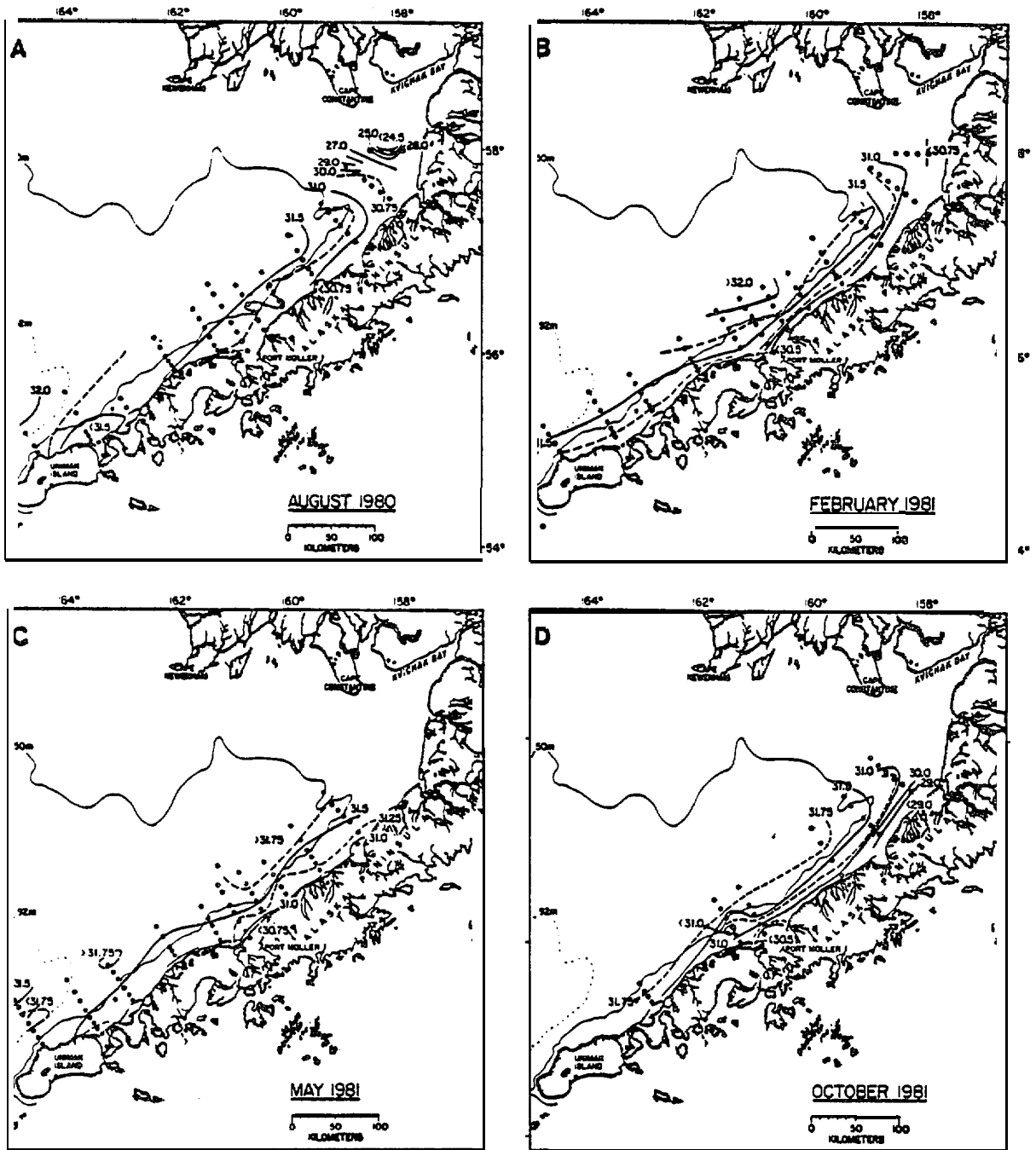


Figure 16. - Surface salinity (g/kg) contours.

By October, surface salinities (figure 16D) showed that the cross-shelf difference between Ports Heiden and Moller had increased to  $>2 \text{ g kg}^{-1}$  and  $1.25 \text{ g kg}^{-1}$  respectively off the two ports. These data suggest **substantial** addition of freshwater along the peninsula as **far** west as Port Moller; however, farther west, surface salinities were greater than in May.

In August, bottom salinities (figure 17A) along the peninsula varied *front*  $<29 \text{ g kg}^{-1}$  in inner Bristol Bay to  $>32.5 \text{ g kg}^{-1}$  over the outer shelf north of Unimak Island. An **alongshore** gradient was concentrated between inner Bristol Bay and Port Heiden where it was normal to the peninsula. The cross-shelf difference was generally weak ( $<0.5 \text{ g kg}^{-1}$ ). Comparison with surface values showed the greatest stratification in inner Bristol Bay with values of  $\sim 5 \text{ g kg}^{-1}$ . Over most of **the** coastal and middle shelf domains **stratification** was weak ( $<0.2 \text{ g kg}^{-1}$ ) but over the outer shelf **region** moderate ( $0.5$  to  $1.0 \text{ g kg}^{-1}$ ) stratification was observed.

By February, bottom salinities (figure 176) indicated that the **along-**shelf gradient **had diminished** with values ranging from  $<30.75 \text{ g kg}^{-1}$  in inner Bristol Bay to  $>32. \text{ g kg}^{-1}$  off Unimak Island. However, the **cross-shelf** difference was stronger ( $\sim 1.5 \text{ g kg}^{-1}$ ) and more closely **aligned** with the bathymetric trend. Although **waters over the outer shelf were less saline than** observed on any other **cruise**, they were more saline in the middle shelf off Port Moller. As was observed in surface salinity, the area of encompassed by the  $31.5 \text{ g kg}^{-1}$  **isohaline** was extensive (particularly west of Port Moller). Throughout most of **the** coastal and middle shelf domains, stratification was weak ( $<0.25 \text{ g kg}^{-1}$ ), whereas moderate values obtained over the outer shelf domain.

In May, bottom salinities (figure 17C) showed that coastal and **outer** shelf **domain** waters were generally **more saline than in February**, while middle shelf waters were less saline. Given the station coverage, the **alongshore**

# BOTTOM SALINITY (g/kg)

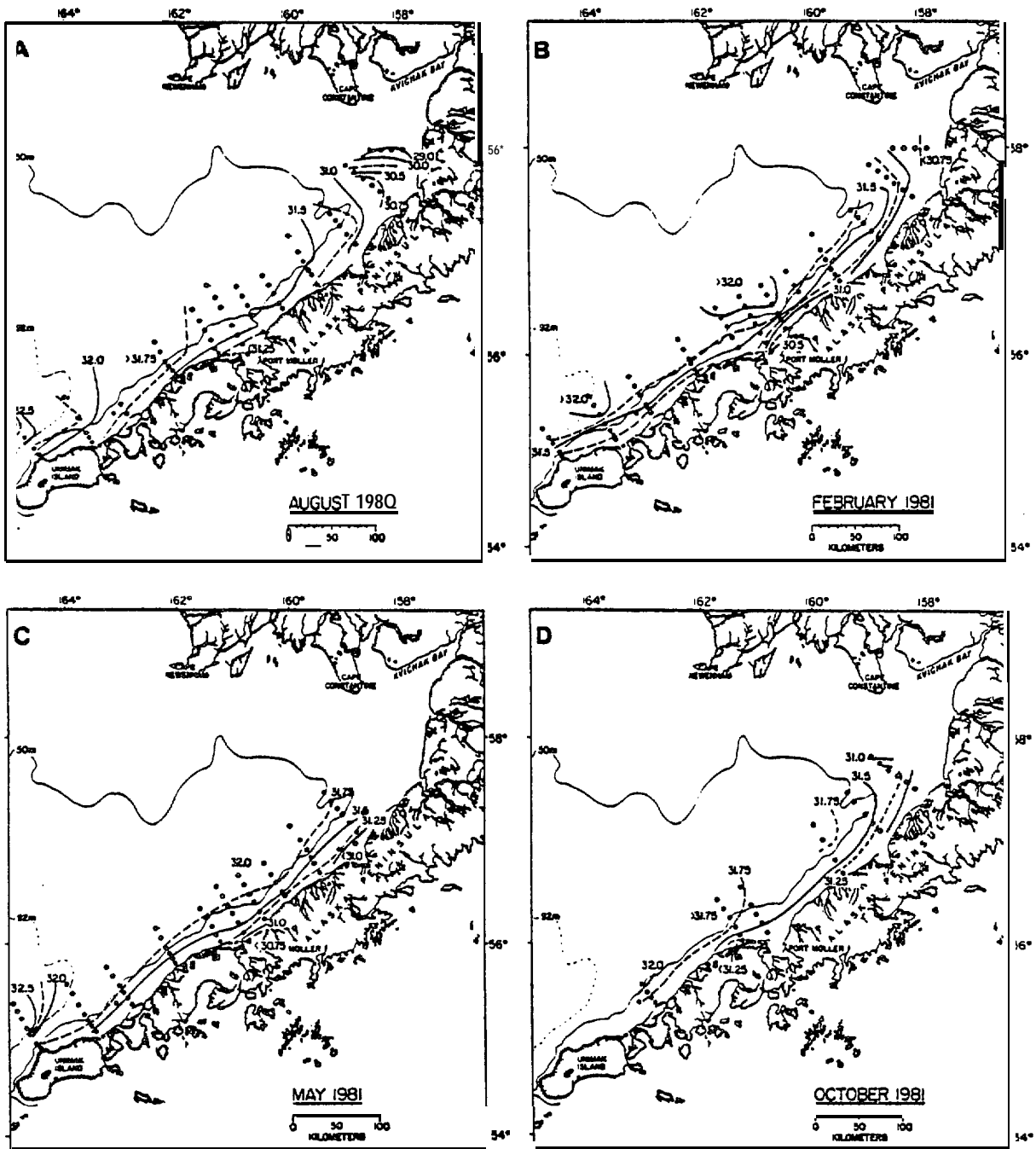


Figure 17. - Bottom salinity (g/kg) contours.

gradient did **not** exist and cross-shelf differences were weaker than in February, **but** still followed the bathymetric **trend. Shoreward of the 50-m isobath, stratification was generally  $<0.25 \text{ g kg}^{-1}$ , with slightly greater values over the middle shelf.** As was noted for the previous data sets, stratification was moderate over the outer shelf domain.

Bottom salinities in October (figure 17D) indicated a slightly stronger alongshore gradient, ranging from  $<31 \text{ g kg}^{-1}$  in Bristol Bay **to  $>32 \text{ g kg}^{-1}$  off Izembeck Lagoon,** however, the cross-shelf difference was weaker than in May. The strong cross-shelf difference of surface salinity along the coast between Ports **Heiden** and **Moller** was riot as strong across the bottom. This resulted in a band of stratification ( $\sim 0.5 \text{ g kg}^{-1}$ ) along the coast east of Port Heiden which graded off to  $<0.1 \text{ g kg}^{-1}$  over the middle shelf east of Port **Moller.** West of here, stratification was  $0.25$  to  $0.7 \text{ g kg}^{-1}$  except for the stations less than **50 m** deep off **Izembeck Lagoon.**

We present surface to bottom mean salinity,  $\bar{s}$ , (Figure 18A to D) to further elucidate the impact of the various sources of fresh or less saline water. The lowest  $\bar{s}$  ( $<27.75 \text{ g kg}^{-1}$ ) was observed in August and reflected the direct influence of the **Kvichak River.** Comparison with  $\bar{s}$  from **the** three other cruises suggested that **Kvichak River** water had a controlling influence on salinity as far west as station line NA5 to 10, or  $\sim 100$  km east of Port **Heiden.** By February, the mean salinity had increased **by  $\sim 3 \text{ g kg}^{-1}$**  in this region while the values from October were similar to those in August.

Values of  $\bar{s}$  from the middle shelf domain showed much less variability, minimum values were observed in August ( $>31.5 \text{ g kg}^{-1}$ ) with maximums **in** February (up to  $32.1 \text{ g kg}^{-1}$ ) while values in May and October were intermediate ( $\sim 31.75 \text{ g kg}^{-1}$ ). Mean salinity over the outer shelf domain north of **Unimak Island** showed similar magnitude of variability, but phasing was different; maximums occurred in **August** and minimums in February.

MEAN SALINITY (g/kg)

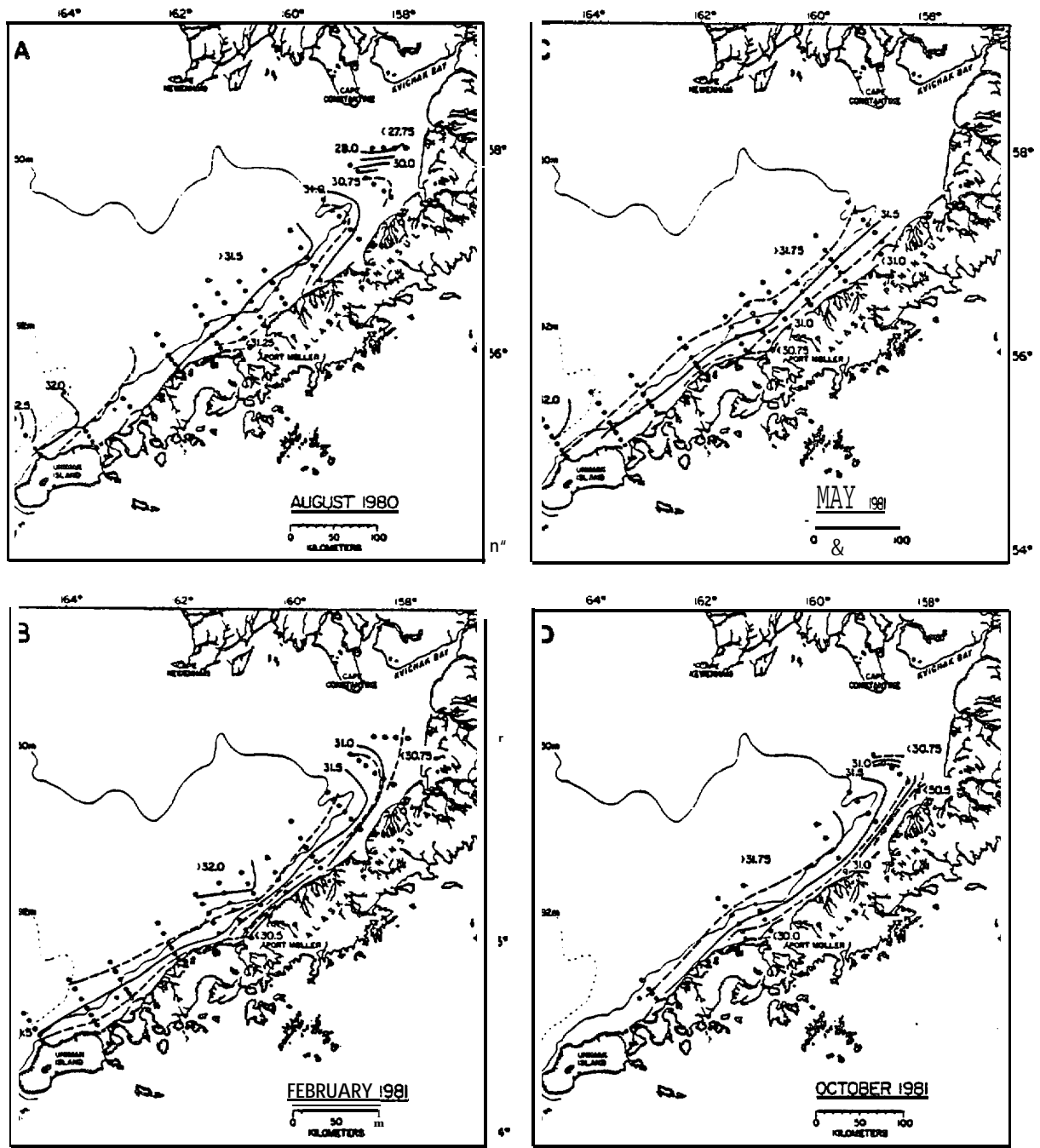


Figure 18. - Mean salinity (g/kg) contours.

In the coastal domain between Port **Moller** and **Unimak** Island, the range of  $\bar{s}$  was again moderate ( $\sim 0.5 \text{ g kg}^{-1}$ ), however there was a substantial change in the area encompassed by the  $31.5 \text{ g kg}^{-1}$  mean isohaline. This area was most saline in August and only slightly less so in October, with the lowest values observed in February and these increased slightly by May. The **Kenai** Current has a **baroclinic** maxima in October followed by a **barotropic** maxima between January and April (Schumacher and Reed, 1980) and some manifestation of these maxima were observed in Unimak Pass and persisted into May (Schumacher, Pearson and Overland, 1982). We suggest that less saline water from the **Kenai** Current was the cause for the observed reduction of mean salinity west of Port **Moller** (Particularly in February). Within Port **Moller**, the lowest mean salinity also occurred in February, and ice was observed to be a local feature (but offshore surface temperatures were  $>2.0^{\circ}\text{C}$ ). We suggest that ice is formed within the Port **Moller** complex and it melts when advected seaward; however, such local formation would not affect mean salinity over the vast region west of Port **Moller**. Ice formation along the shore of **Kuskokwin** Bay and the north coast of **Bristol Bay** may be advected (by wind) to this region of the coastal domain and provide a freshwater flux, but this process would generally occur between late February through March (see, figure 2).

Finally, we note that in the vicinity of Port **Heiden**, and to a lesser extent west of Port **Moller**, the mean salinity in a band along the coast was lowest in October. This region is more than 200 km from the **Kvichak** River, west of the region where river runoff is clearly identifiable in the data. Although there are no gaged rivers on the peninsula, there is substantial rainfall. An estimate of drainage area between Ports **Moller** and **Heiden** is about the same as that for the **Kvichak** River. Thus, the maximum freshwater flux should occur in October and be of similar magnitude to the **Kvichak** River. We suggest that it was this source that resulted in lower salinities in the

coastal domain west of the Kvichak River influence and extending westward to the vicinity of Port **Moller**.

Stratification: Bottom-surface sigma-t values ( $\Delta\sigma_t$ ) are a measure of stratification which combines the effects of both salinity and temperature. In general, coastal domain waters are well mixed, except in the presence of freshwater addition; middle shelf waters are two-layered during periods of positive **bouyancy** (insolation and ice melt) input and well mixed otherwise, and outer shelf domain waters are **usually layered (Kinder and Schumacher, 1981a)**.

Area plots of  $\Delta\sigma_t$  are shown in Figure 19 A to O. The **strongest  $\Delta\sigma_t$**  ( $> 3.5$ ) was observed in August in inner Bristol Bay and was primarily caused by salinity stratification resulting from **Kvichak** River discharge. Just south of this area, coastal domain waters westward to Port Heiden were mixed ( $\Delta\sigma_t < 0.1$ ). In the vicinity of Port **Moller**, a complex distribution of  $\Delta\sigma_t$  existed, with values ranging from 0 nearshore, to  $>0.25$  over the adjacent portion of the middle shelf. **As will** be shown later (Section 4.2.6), this distribution was a result of storm mixing and cross-shelf **advection**. Between Port **Moller** and **Izembeck** Lagoon,  $\Delta\sigma_t$  was generally  $<0.25$ , while near the 50-m isobath values were  $>0.5$  and over the outer shelf domain they exceeded 0.75.

By February, **most** of the water column from inner Bristol Bay to west of Port **Moller** was mixed. Exceptions occurred near Ports **Heiden** and **Moller**, where  $Au_t \sim 0.25$  and again was related mainly to salinity stratification. A likely source of less saline surface water was melting of **local** or regional ice. West of Port **Moller**, the coastal and middle shelf domains were mixed, while over the outer shelf moderate (up to 0.4) stratification existed.

$\Delta$  SIGMA-T

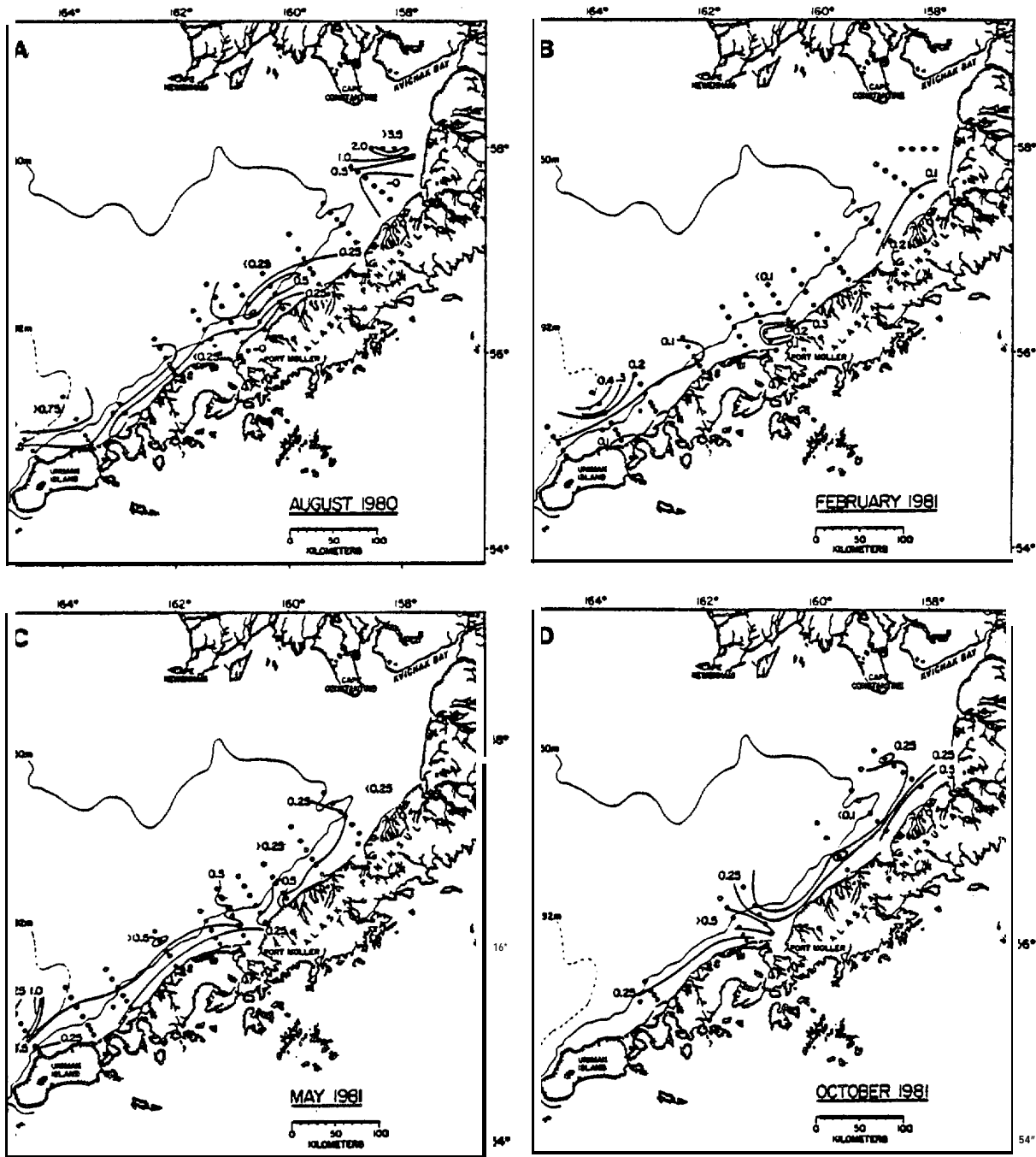


Figure 19. - Bottom minus surface sigma-t contours.

The effect of increasing insolation was evident in May; waters over the middle shelf were moderately stratified ( $Au_t > 0.25$ ), although temperatures had increased from February by  $\sim 7^\circ\text{C}$ , temperature differences and  $\Delta\sigma_t$  were weak in the coastal domain. (an exception was near Port **Moller** where a lens of fresher water had not yet been mixed with more saline bottom water). Over the outer shelf, strong stratification existed as a result of low salinity surface water well offshore. The presence of a low salinity band in the vicinity of the middle front is a common feature and has been attributed to the southwest extent of the regional ice field [Kinder and Schumacher, 1981b).

Surface heat loss was evident by October, and coupled with weak haline stratification resulted in a mixed water column over most of the middle shelf domain. Along the coast east of Port **Heiden** and just west of Port **Moller**,  $\Delta\sigma_t$ 's exceeded 0.5 due to the presence of less saline surface waters. As noted above, this was likely due to freshwater addition not associated with the Kvi chak River, but with local freshwater addition.

Dynamic Topography: The combined effect of temperature and salinity on the horizontal pressure field and hence the computed **geostrophic** flow is shown in Figure 20A to D and 21A to 0. While caution is necessary in inferring currents in this manner, particularly to shallow reference levels, good agreement historically between **Eulerian** and **Lagrangian** measurement and **geostrophic** flow exists over this shelf (Schumacher and Kinder, 1983: see Appendix B). Both the 0/25 and 0/50 dbar dynamic topography showed that relief of  $\geq 1.0$  dyn cm was a persistent feature of the **baroclinic** pressure field across the shelf. Contours typically aligned with the bathymetry and

# DYNAMIC TOPOGRAPHY (0/25 db)

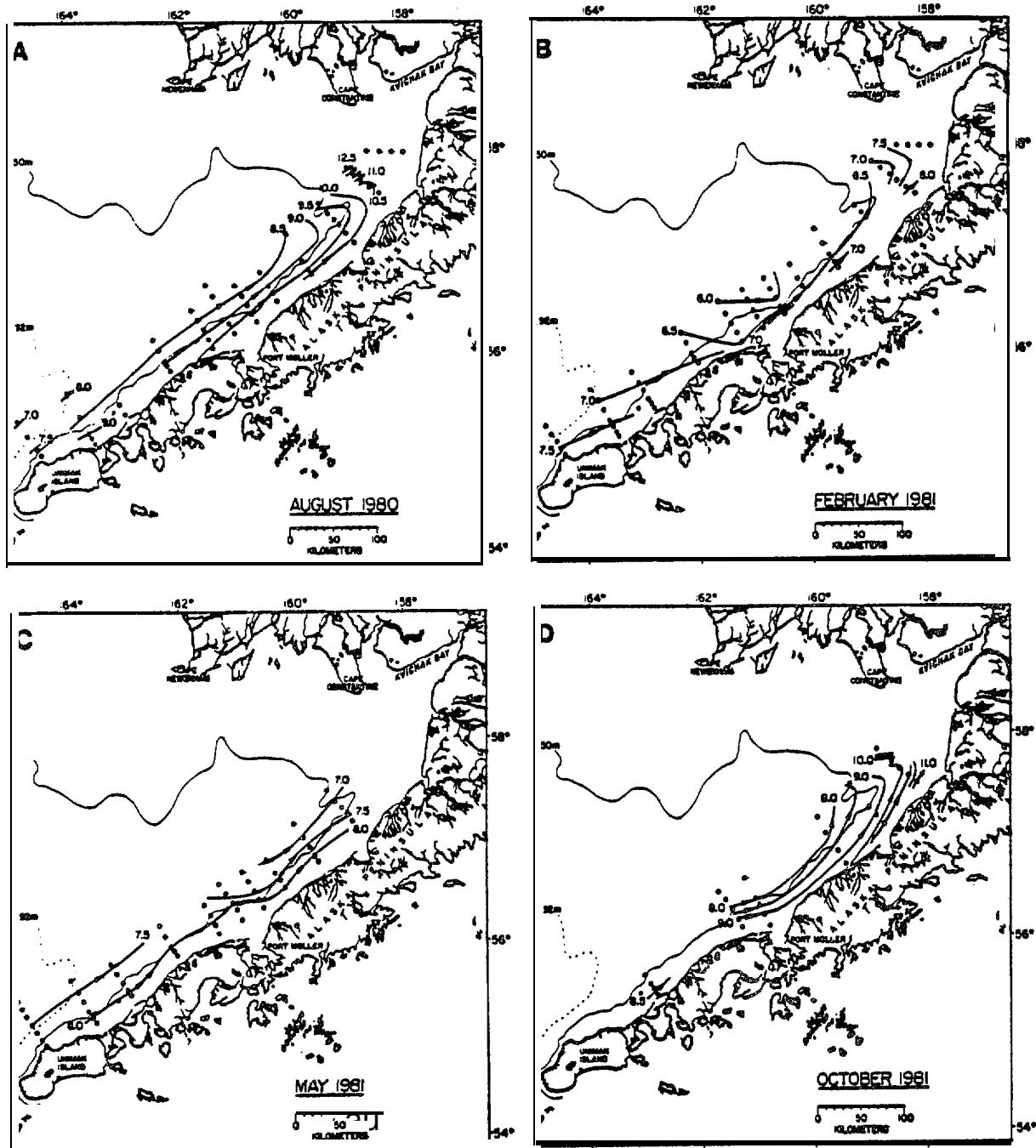


Figure 20. - Dynamic topography, 0/25 db.

# DYNAMIC TOPOGRAPHY (0/50db)

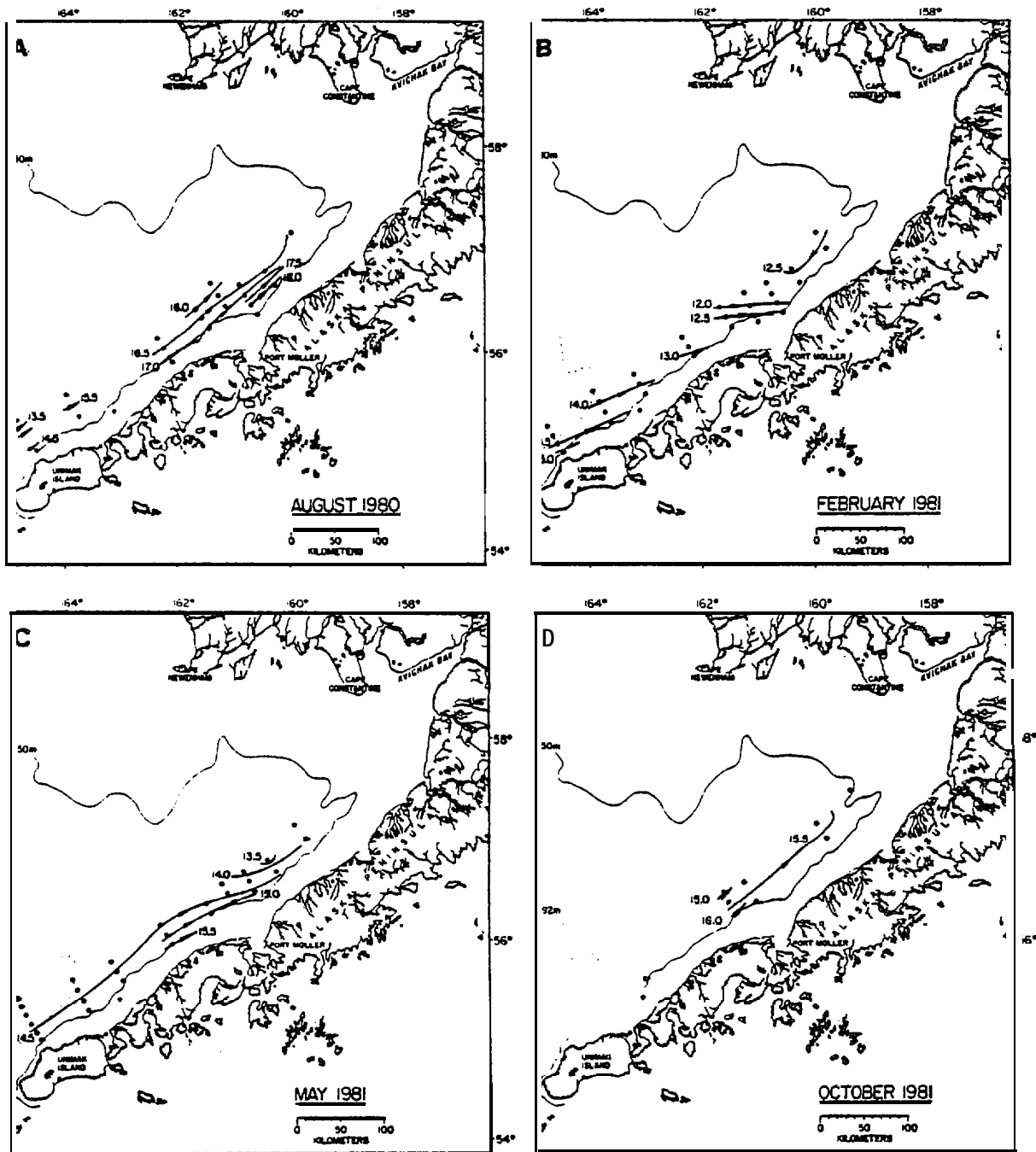


Figure 21. - Dynamic topography, 0/50 db.

the 0/25 dbar contours paralleled the offshore trend of the 50-m isobath north of Port Heiden. The impact of freshwater addition from the Kvichak River (figure 20A) and along the peninsula westward to Port Heiden (figure 200) was evident in the increased relief. Maximum surface speeds relative to 25 dbar were  $\sim 7$  cm  $s^{-1}$  off Port Moller in August and  $\sim 11$  cm  $s^{-1}$  in inner Bristol Bay during October. Maximum values (0/50 dbar) also occurred off Port Moller in August. In general, regardless of time of year, the cross-shelf density distribution was such that baroclinic geostrophic surface currents of 2 to 7 cm  $s^{-1}$  existed with inferred flow into Bristol Bay parallel to isobaths.

#### 4.2.2 Short-Period Time-Dependence of Hydrographic Features

In the previous Section we showed that some processes (e.g. runoff, ice, change in insolation, etc.) result in changes of hydrographic characteristics on time scales from  $\sim$  a month to seasonal. We present hydrographic, suspended particulate matter (SPM) wind and current data collected along the Alaska Peninsula (figure 22) during a 14-day period in August 1980. These data show that a storm significantly altered mean hydrographic conditions, vertically mixing middle shelf domain waters. Further, Ekman fluxes (coastal divergence and convergence) with time-scales of 2 to 5 days appeared to play an important role in reestablishment of stratification and together with enhanced tidal mixing (using the mean of the speed cubed as a measure of mixing energy) resulted in a return to nominal coastal and middle shelf domain conditions within 14 days.

Hydrography and Light Attenuation The line of **CTD** stations **normal** to the peninsula (**figure 22**) was occupied on **19, 24 and 31 August 1980**.

The time **to** complete a line was about six hours. About one day prior to **running the first** section, the remnants of typhoon **Marge** passed eastward through the study area. This storm resulted in winds up to 30 ins-l and 6 to 8 **m waves**. The turbulence associated with this storm mixed the water column **at** least 50 km seaward of the coast i.e., into the middle shelf domain (figure 23). Suspended particulate matter was also **well** mixed within 10 km of the shore and seaward of station 45 **isopleths** exhibited weak monotonically increasing vertical gradients.

During the second occupation of this section (figure 24), the entire shelf region was **themally** stratified, with surface **minus bottom temperature difference** (AT) from 0.6 to 2.7°C. Colder bottom waters intruded onshore, with a displacement of the **8.5°C-isotherm** of about 10 km. A similar change from mixed to stratified structure was observed in **isohalines** with the strongest difference ( $\Delta S = 0.13 \text{ g kg}^{-1}$ ) over the normally mixed **coastal domain**. **Again, the data suggested an onshore** flux, e.g. at station 42 bottom salinity increased by  $0.05 \text{ g kg}^{-1}$ , **while** upper layer salinities decreased. Light attenuation values indicated a 50% reduction in **nearshore** concentration of **SPM, while** over the middle shelf domain a subsurface minimum layer was established.

**Hydrographic** conditions **observed** on 31 August (figure **25**) showed a return to more typical stratification; **middle** shelf waters were stratified with  $\Delta \sigma_t \geq 0.43$  and coastal domain waters were vertically well mixed. We note that stratification was now stronger than that observed on May 31 (inset, figure 22) by about a factor of three. **SPM profiles** also indicated mixed conditions **in** the coastal domain and a minimum **layer** was clearly established near or below the **pycnocline**.

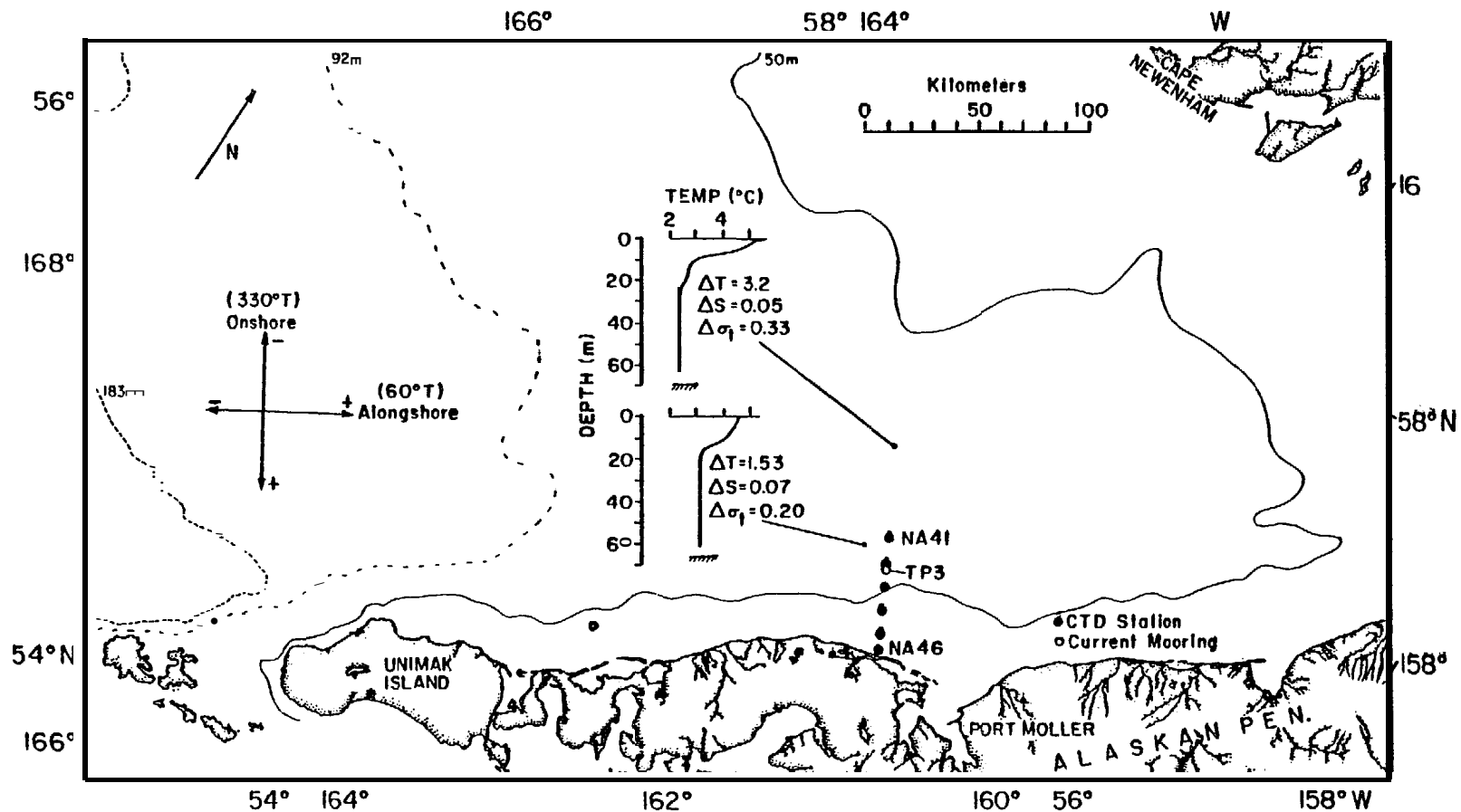


Figure 22. - North Aleutian Shelf study area, showing location of hydrographic data section (NA41 to NA 46) and mooring TP3A. Also shown are CTD data from 31 May 1980 and axes used for current and wind data.

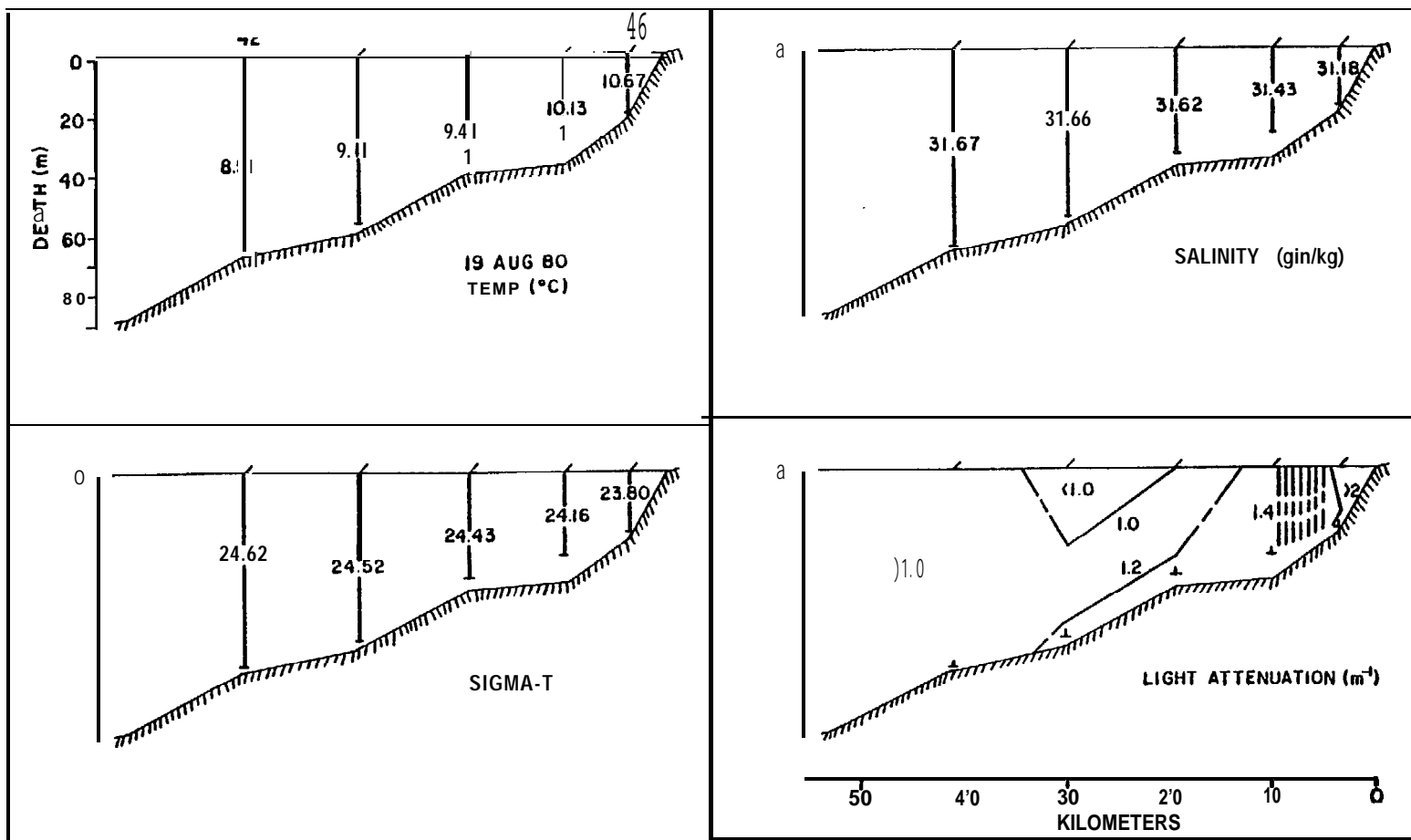


Figure 23. - Hydrographic and light attenuation sections from 19 August 1980. Note the location of the 8.5 °C isotherm.

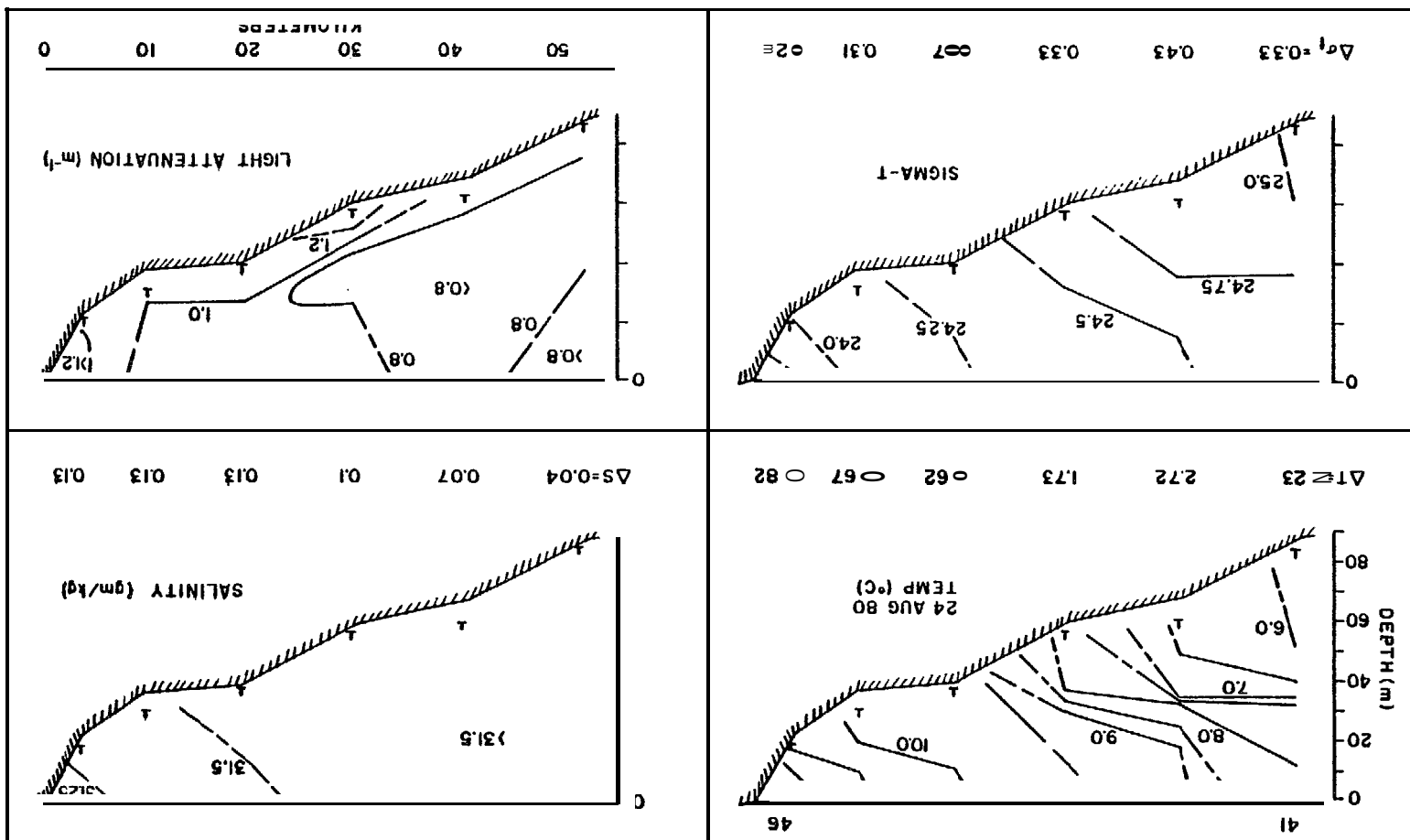


Figure 24. - Hydrographic and light attenuation sections from 24 August 1980. Contour intervals are 0.5 °C, 0.25 g/kg, 0.25 sigma-t units, and 0.2 m<sup>-1</sup> for light attenuation. Magnitude of upper minus lowest 1 m average parameter is presented under a given station as a Δ. Note, lowest 1 m average salinity at station 42 was 31.71 g/kg.

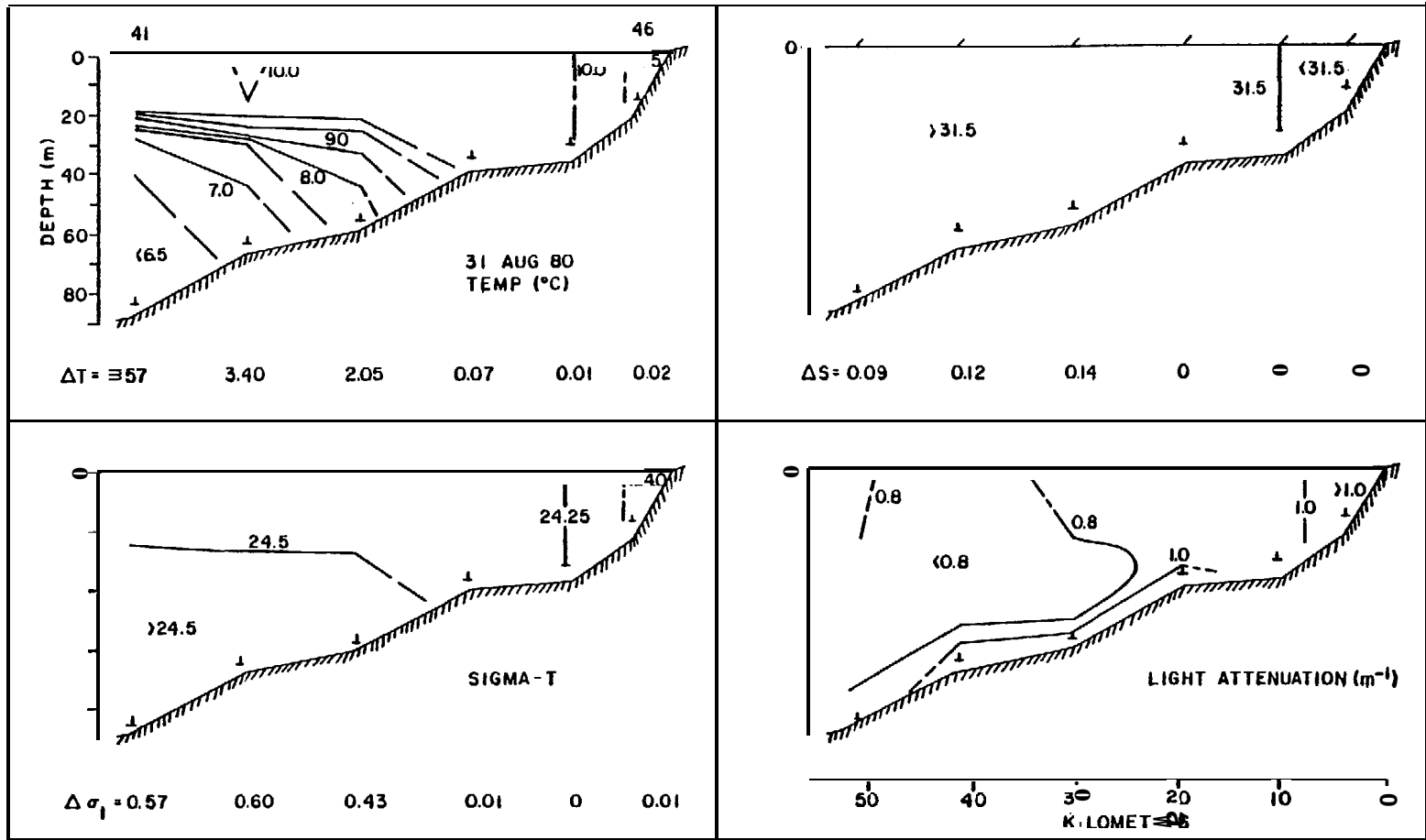


Figure 25. - Hydrographic and light attenuation sections from 31 August 1980.

**Winds and Currents Alongshore** (v positive  $60^\circ\text{T}$ , see figure 22) **winds** measured from the NOAA ship Surveyor are shown in Figure 26. The **passage of the** storm resulted in maximum **alongshore** wind speeds of about  $25 \text{ m s}^{-1}$ . About 3.5 days after the storm's peak speeds, a period of relatively steady **alongshore** winds existed for about 3 days with a mean speed of  $5.5 \text{ m s}^{-1}$ . We note that **with the** exception of the **storm** winds and those on 24 August, onshore wind speeds (not shown) were only about  $1 \text{ m s}^{-1}$ .

Currents at 5 and 39 m below the surface at TP3A are shown in the next **two panels of figure 26**, where the **alongshore** axis is the same as for the wind and the onshore axis is u positive  $150^\circ\text{T}$ . Near-surface currents reversed from onshore to offshore concomitant with the wind reversal and this initial offshore pulse lasted for about 3 days. While near surface currents were offshore those at 39 m were onshore for the same time period. The visual correlation between wind and near-surface current did not extend to currents at 39 m depth. The **alongshore** current appeared to be similar at the two depths.

In the bottom panel of Figure 26, we present 25-average  $S^{-3}$  values. The flux of turbulent energy generated at the seafloor,  $E_t$ , was estimated by assuming that the mean rate of work of tidal currents against bottom stress ( $\tau = \rho_0 C_D u u$ ) is  $\bar{\tau} \cdot \bar{u}$  where  $u$  is the mean flow velocity near the bottom (Fearnhead, 1975). Here we have used hourly values of current speed from the 39 m depth current record, **and** have not included either a drag coefficient or density (including these parameters yields dimensions of tidal power, but  $S^{-3}$  gives a relative measure of this quantity). By the third occupation of the **CTD** section, tidal mixing power had increased by about a factor of three.

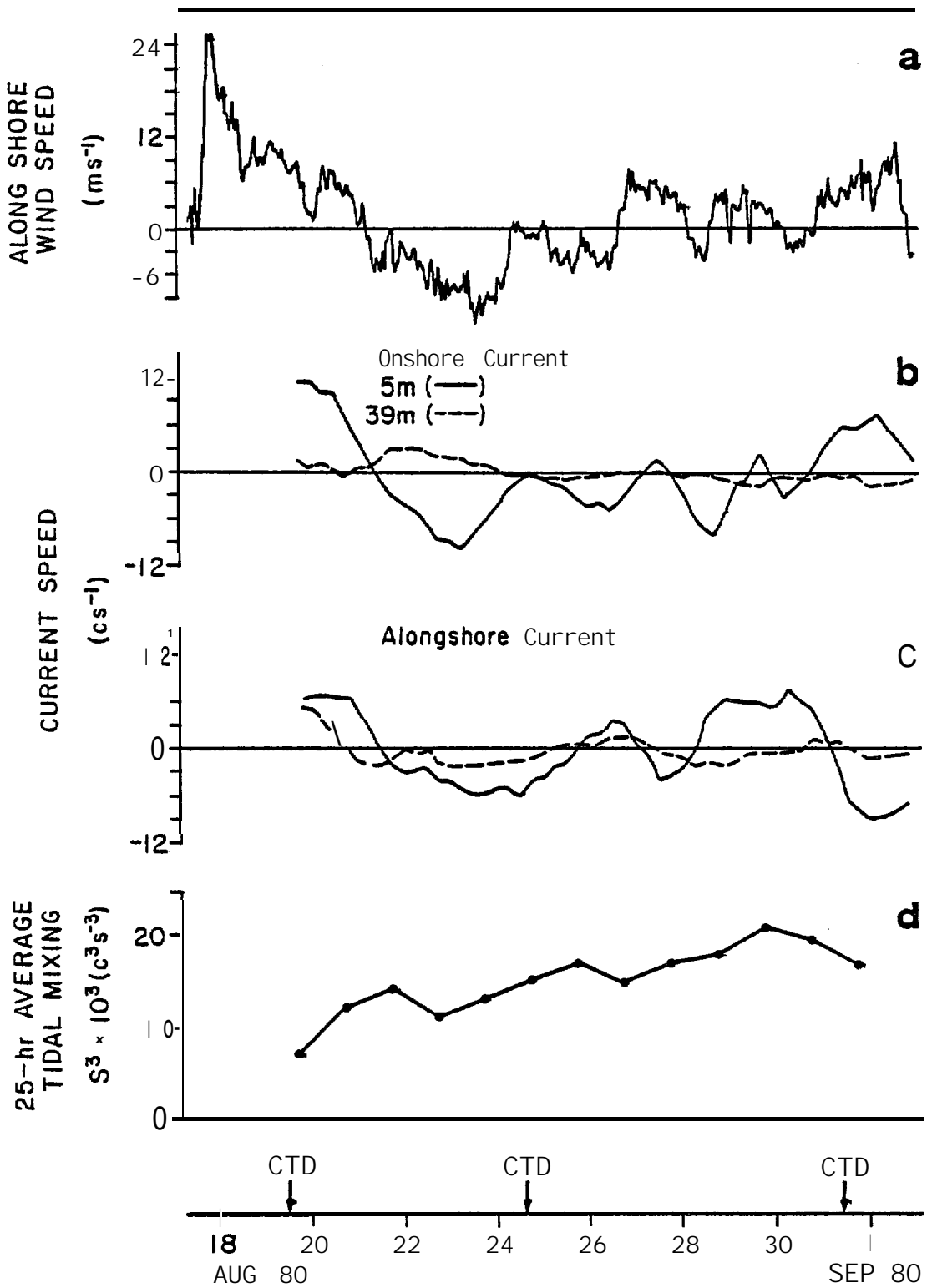


Figure 26. - Alongshore wind speed, onshore and alongshore current at 5 and 39 m, and 25-hr average tidal mixing from the 39-m depth current record.

**Discussion** The destruction and subsequent **reestablishment** of typical summer middle shelf and coastal **domain hydrographic characteristics was related to** winds and tides. The initial vertical mixing **of** the water **column** resulted **from** a combination of wind-wave and current shear turbulence which destroyed vertical structure **to** at least 50 km, or twice **the** usual distance, from the shore. **Longshore** winds then reversed and generated an offshore **Ekman** flux in the near surface waters and a continuity preserving onshore **flux** at depth. The offshore flux transported warmer less saline surface water offshore, while the onshore flux at depth provided colder more saline waters; the net result was stratification **across** the entire study area. **As** tidal mixing power increased, coastal **domain waters became vertically** mixed and middle shelf domain waters **returned** to a two-layered configuration.

**Near-surface** current spectra (not shown) indicated that of the total fluctuating horizontal kinetic energy ( $KE = \frac{1}{2}[u'^2 + v'^2]$ ) per unit mass, **subtidal** energy was **31.6 cm<sup>2</sup> S<sup>-2</sup>** or about 6%. This is consistent with previous studies (Kinder and Schumacher, **1981 b**). We note that 50% of the subtidal **KE** was contained in the 2 to 5 day period bands. The wind spectrum contained little energy (**1.3 m<sup>2</sup> s<sup>-2</sup>** or about 10% of the total  $KE_w$ ) at **tidal or higher** frequencies, however, 25% of the  $KE_w$  was contained in 2 to 5 day periods with the remainder at periods  $\geq 7$  days.

The visual correlation between longshore winds and onshore currents, **suggesting Ekman dynamics, was substantiated by a linear correlation coefficient** between the two low-pass filtered time-series of **r=0.83** at 0 lag. **In** frequency, the maximum coherence between **hourly** wind and current components was at a period **of 2.9 days** with a coherence squared of 0.995 or about 99% of the variance. A **second** maximum occurred **at 4.8** days with a coherence squared of 0.91 (for both estimates the **95%** level of significance was **0.78**). Onshore

currents and **alongshelf winds** were correlated to a lesser extent at lower depths, with correlations decreasing (**0.57**, 0.53, and **0.42**) and lags increasing (0, 6 and 60 hours) at 10, **15** and 29 m respectively. The current record from 39m depth had a negative correlation (**r = -0.68** at 48 hours) with **alongshore** winds. These results suggest that longshore winds generated off/onshore **Ekman** fluxes in an upper layer with, at times (e.g. 21 to 24 August), a compensating flow lower **in** the water column. During this particular event, coastal divergence would result in a **barotropic** pressure gradient toward shore. If **this** were **geostrophically** balanced, then an **alongshore** current (in this reference frame a negative value) would be generated. The observations indicated **such** flow during both 21 to 24 August and 30 August to 1 September wind events. An empirical estimate of 5m onshore current response to **alongshore** wind was  $10^{-2}$  to 1, or a **10ins-L** wind generated a  $10 \text{ cm s}^{-1}$  current.

#### 4.2.3. Current and Wind Observations

In this Section we describe current characteristics from records collected at nine locations along the Alaska Peninsula and wind characteristics from observations near Port **Moller** (figure **12**). Mooring information and editing procedures are given in Appendix A. **In** the following analysis, we have used the 35-h filtered data unless otherwise noted.

##### Mean and Low-Frequency Flow:

We present the current data as roses (where the direction was partitioned into twelve **30°** sectors) and vector means with one standard deviation (along and orthogonal to the principal axis, or axis with the **greatest variance**) in Figures 27 and 28 for the first deployment period (August 1980-January 1981)

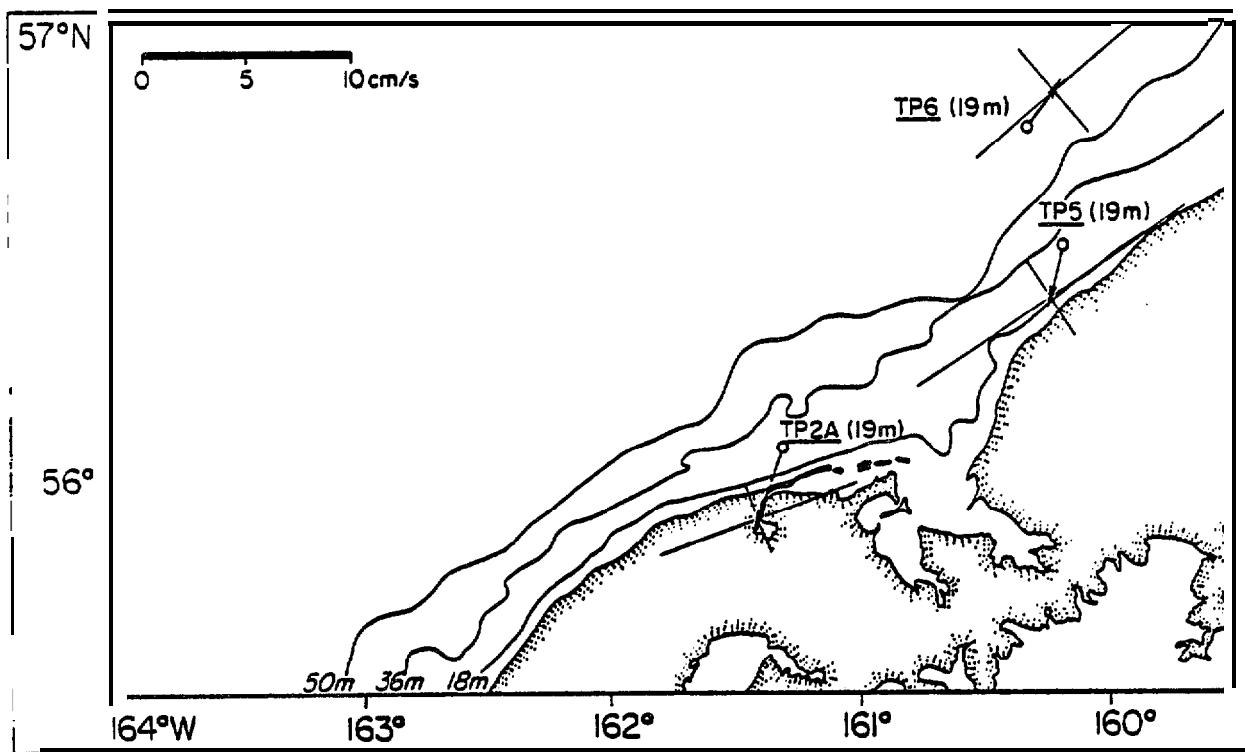
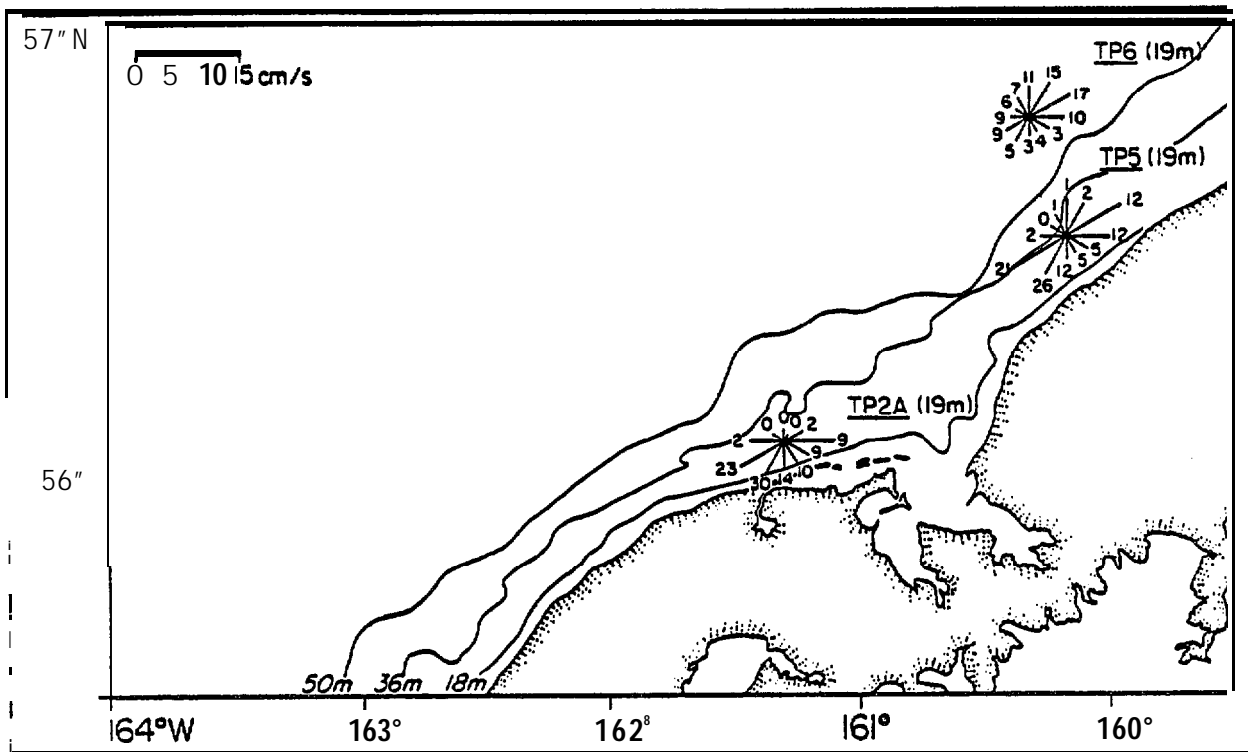


**Figure 27.** - Current roses and means for near-surface records between August 1980 and January 1981. The cross at the end of the current vector is the standard deviation along and across the principal axis. (Instrument depths are given in parentheses.)

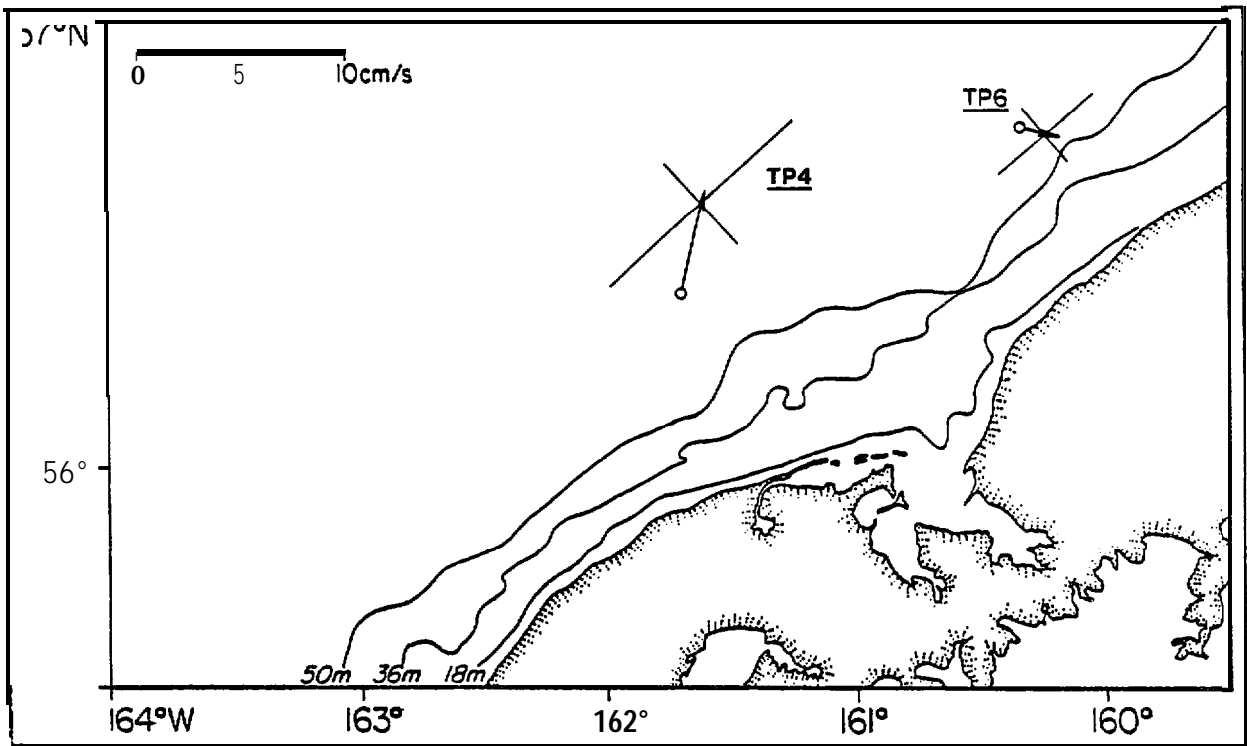
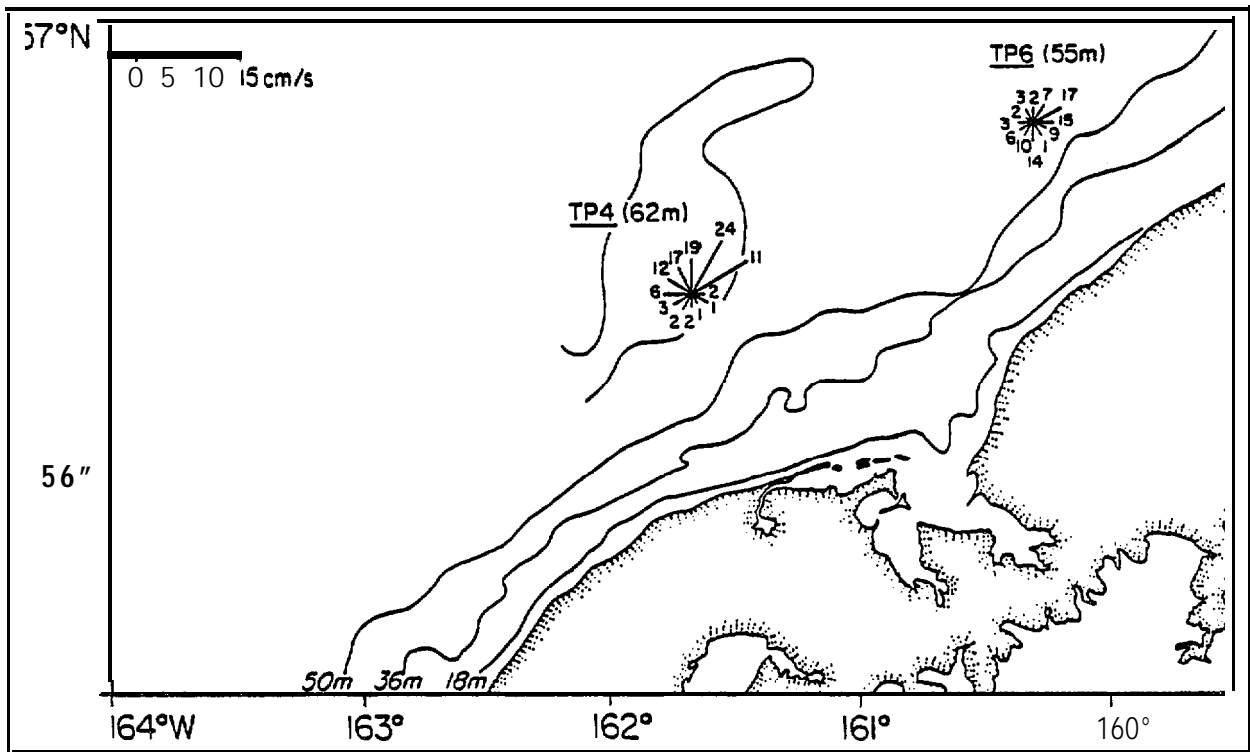


Figure 28. - Current roses and means for near-bottom records between August 1980 and January 1981.

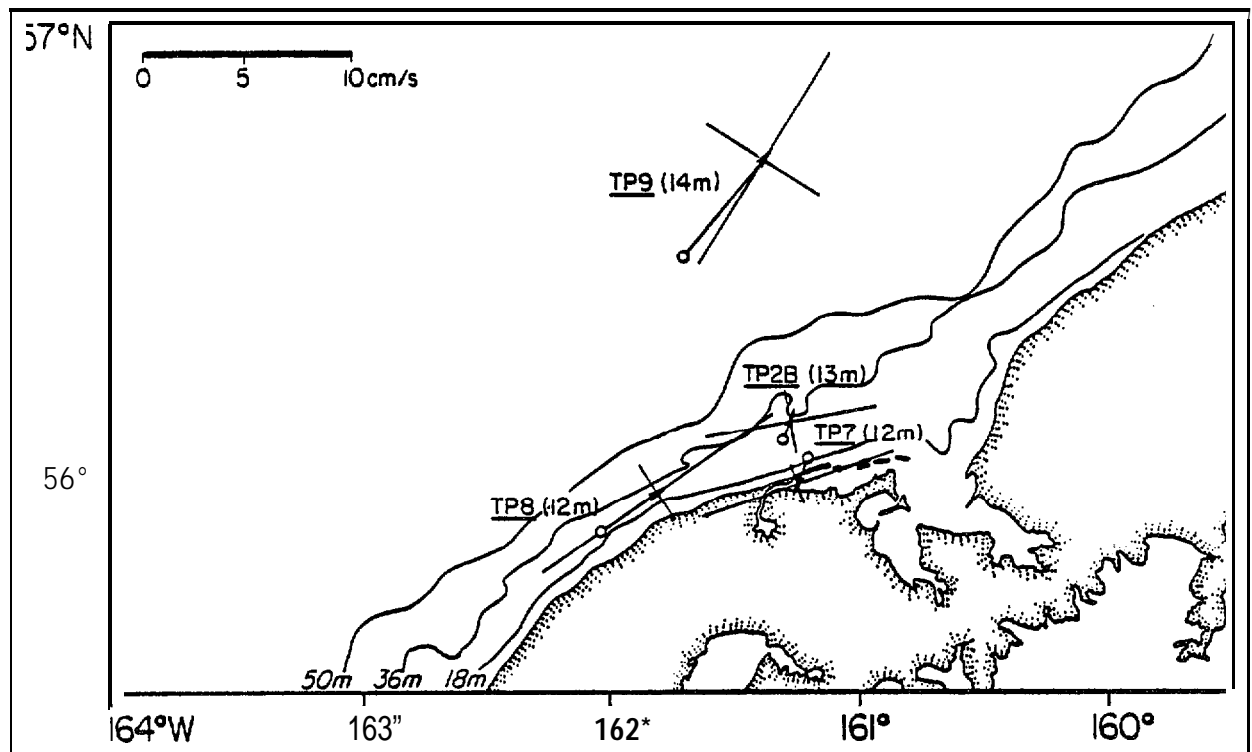
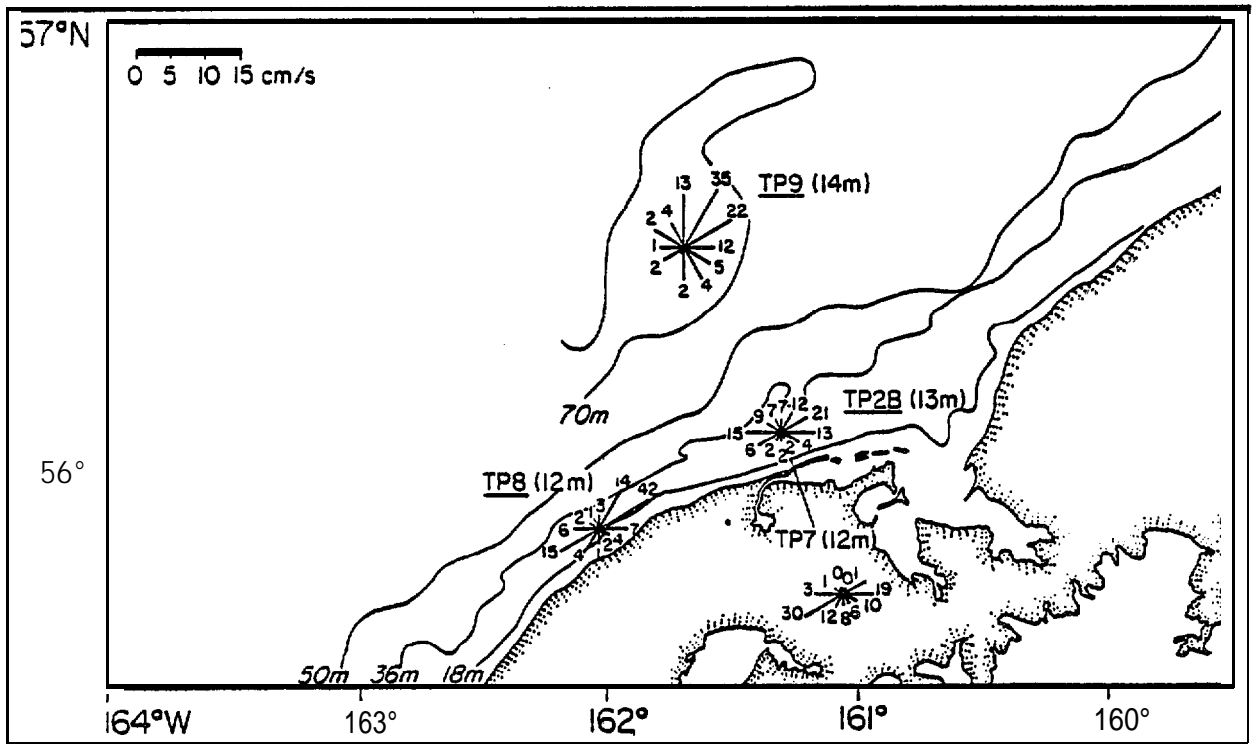


Figure 29. - Current roses and means for near-surface records between January 1981 and May 1981.

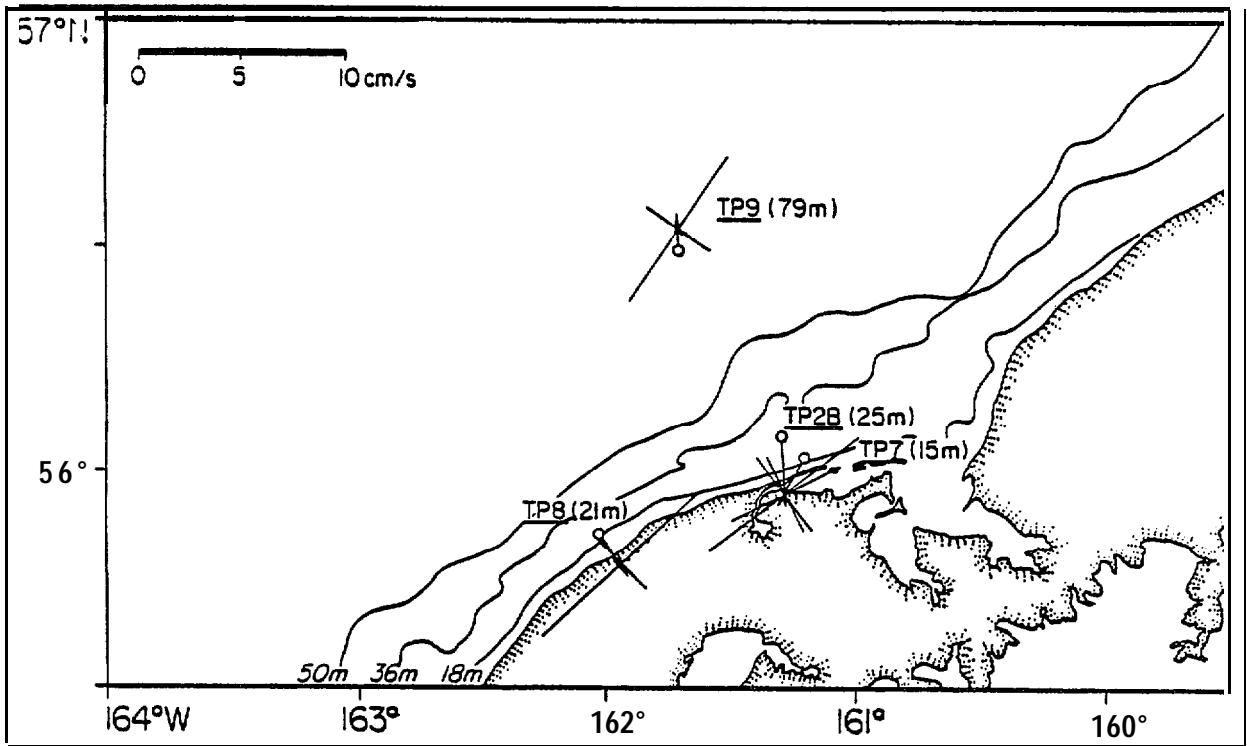
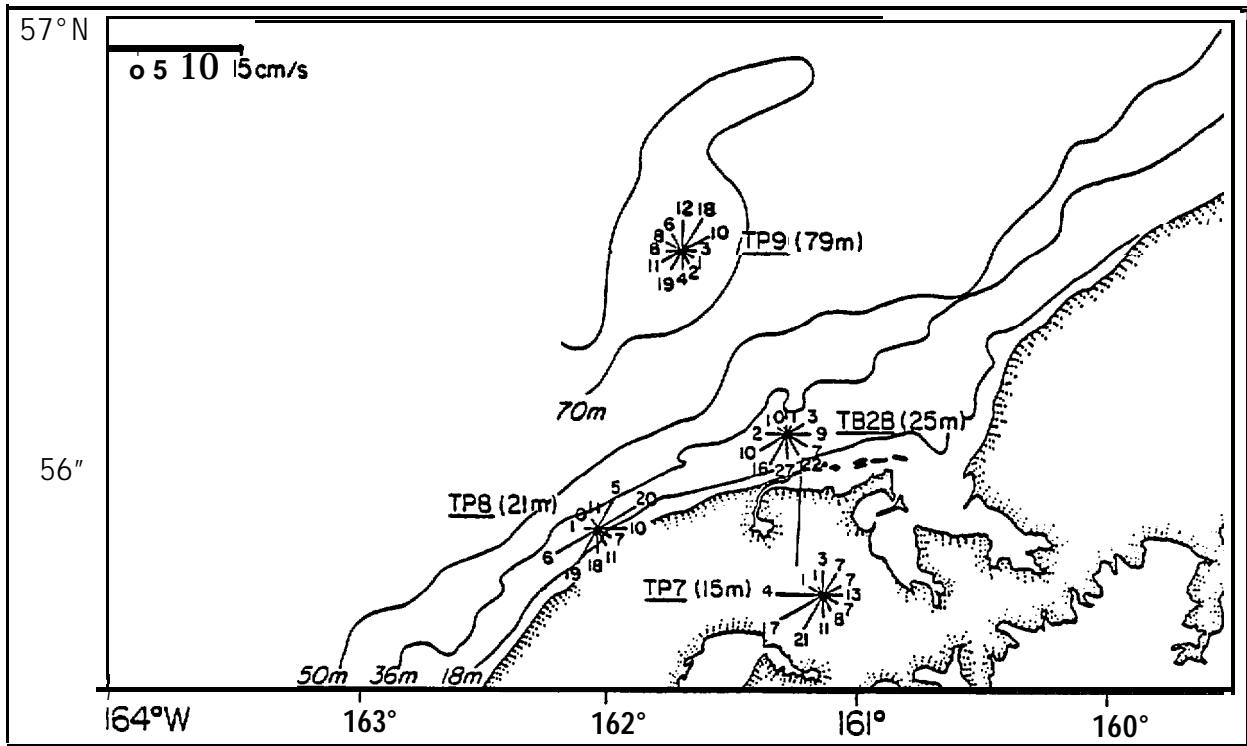


Figure 30. - Current roses and means for near-bottom records between January and May 1981.

and in Figures 29 and 30 for the second observation period (January-May 1981). A feature common to **all** records was that the majority of observations and the principal axes tended to be **along** the **local bathymetry**. Vector mean flow, however, was not consistently along **bathymetry** except seaward of the 50-m isobath. **Shoreward** of the 50-m isobath and in the vicinity of Port **Moller** (i. e. **TP2A/B**, **TP7** and **TP5**), mean flow had a cross-isobath component.

To establish the statistical significance of the vector mean speeds, we employed a method similar to Allen and **Kundu** (1978). An independent time scale,  $\tau$ , was defined as the area under the **autocorrelation function** for a particular record. This time scale was then used to provide a root mean square error estimate,  $E$ , given by

$$E = \pm 2\sigma / (t/\tau)^{1/2}$$

where  $t$  is the record length and  $\sigma$  the standard deviation along a given axis. The results of this technique, together with other record characteristics are given in TABLE 4. Note that **all** vectors are resolved into **alongshore** (**positive toward 60°T**) and cross-shelf (**positive toward 150°T**) axes, and that **this definition of alongshore** is consistent with the orientation of the **peninsula, bathymetry**, and generally within about 10° of the individual records **principal axis**.

The strongest **alongshore** mean current was observed either *seaward* of the **50-m isobath (TP4, 6, and 9)** or west of Port **Moller (TP8)**, with mean speeds along this component of  $\sim 1$  to 6  $\text{cm s}^{-1}$  where the larger values occurred in the near-surface (12 to 19m below the surface) records. Statistically significant, but weaker ( $< 1$  to 3  $\text{cm s}^{-1}$ ) mean negative **alongshore flow** existed near-shore in the vicinity of Port **Moller (TP2A, E, and 7)**.

Table 4. - Current characteristics from TP moorings.

Mooring (depth ,m)	Instur. Depth (m)	Vector Speed (cm s <sup>-1</sup> )	Mean Dir (°T)	Principal Axis & % of Variance	Component Alongshore (cm s <sup>-1</sup> )	Means RMS cross-shelf (cm s <sup>-1</sup> )	KE of Components Alongshore (cm <sup>2</sup> s <sup>-2</sup> )	Cross-shelf (cm <sup>2</sup> s <sup>-2</sup> )
TP2A (32)	19N	3.7	200	70, 89	-2.8*1.4	2.4±0.6	12.6	1.9
	20	3.0	211	68, 69	-2.6*1.4	<b>1.4±0.8</b>	13.5	5.7
TP5 <b>(31)</b>	<b>19N</b>	2.6	194	57, 93	-1.8*1.8	1.9*0.5	30.6	2.3
	20	3.7	180	52, 83	<b>-1.8±1.9</b>	3.2*0.7	26.0	6.6
TP6 (69)	<b>19N</b>	2.1	038	50, 78	<b>2.0±1.0</b>	-0.8*0.4	12.0	3.8
	20	1.6	058	45, 68	<b>1.6±1.0</b>	<b>-0.1±0.4</b>	10.8	5.7
	55	1.2	108	50, 76	0.8±0.7	<b>0.9±0.2</b>	4.5	1.6
TP4	62N	<b>4.4</b>	013	48, 84	<b>3.0±1.5</b>	<b>-3.2±0.7</b>	18.0	4.3
TP2B (35)	<b>13N</b>	<b>1.0</b>	021	<b>80, 87</b>	<b>0.8±1.4</b>	-0.6*0.8	8.9	2.4
	25	<b>2.8</b>	176	63, 68	<b>-1.2±0.9</b>	2.5*0.5	4.4	1.7
TP7 (25)	12N	1.4	203	71, 96	<b>-1.1±1.4</b>	<b>0.8±0.5</b>	12.2	<b>1.8</b>
	15	2.1	210	53, 81	<b>-1.8±1.5</b>	<b>1.0±0.6</b>	9.8	<b>2.6</b>
TP8 (31)	12N	3.3	055	55, 95	3.2±2.4	-0.3*0.4	22.3	1.4
	21	1.8	145	46, 90	<b>0.2±1.9</b>	<b>1.8±0.7</b>	<b>13.8</b>	2.5
TP9 (89)	<b>14N</b>	6.1	040	32, 77	5.7*1.5	-2.1*1.9	13.4	8.4
	79	1.0	357	34, 83	0.5*1.3	<b>-0.9±0.8</b>	8.5	3.5

Where: **All** statistics are from 35h data, N represents **acoustic** current meter and **alongshore** and **cross-shelf** are **positive** 60° and 150° respectively.

Cross-shelf mean speeds were generally weaker and exhibited the tendency to be offshore in the upper water **column and** onshore closer to the bottom. This pattern was evident in the records from **TP2B**, where the cross-shelf component reversed sign over a 12 **m** vertical separation.

The characteristics of stronger **alongshore** mean flow was mirrored in the low frequency kinetic energy; **the alongshore** component was always greater than **the cross-shelf component**, generally by a factor of four. The relation between TP current record characteristics and those collected over the remainder of the southeastern Bering Sea **shelf** is discussed in Appendix **B**.

#### Vertical Structure:

In order to provide information illustrating vertical structure of currents over the middle shelf domain, moorings **with** surface flotation were **depi** eyed in August 1980 (**TP3A**) and in May 1981 (**TP3B**). The results are presented in Figures 31 and 32 as **35-hr** stick plots and in Figure 33 as **2.9 hr** **mean** speed, component speed and net current over the observation periods. During TP3A, stratification varied greatly, with the difference in sigma-t between lower and upper current meters ranging from 0 to 0.65, with an average **of ~0.5**); during **TP3B**, this index of stratification only varied from 0.25 to 0.44 with an average of -41.3. The **geostrophic** wind during the **two** observation periods was significantly different: during TP3A winds were towards the south for the first four days and then were weakly northward, while during **TP3B**, winds were strongly northward throughout most of the current record. Despite these differences in stratification and wind forcing, the shear in mean speed was similar, being  $2.8$  and  $1.9 \times 10^{-3} \text{ s}^{-1}$  during TP3A and B respectively. Further, the shear in **alongshore** speed was nearly identical below 20m, with

35.0 FILTER DATA

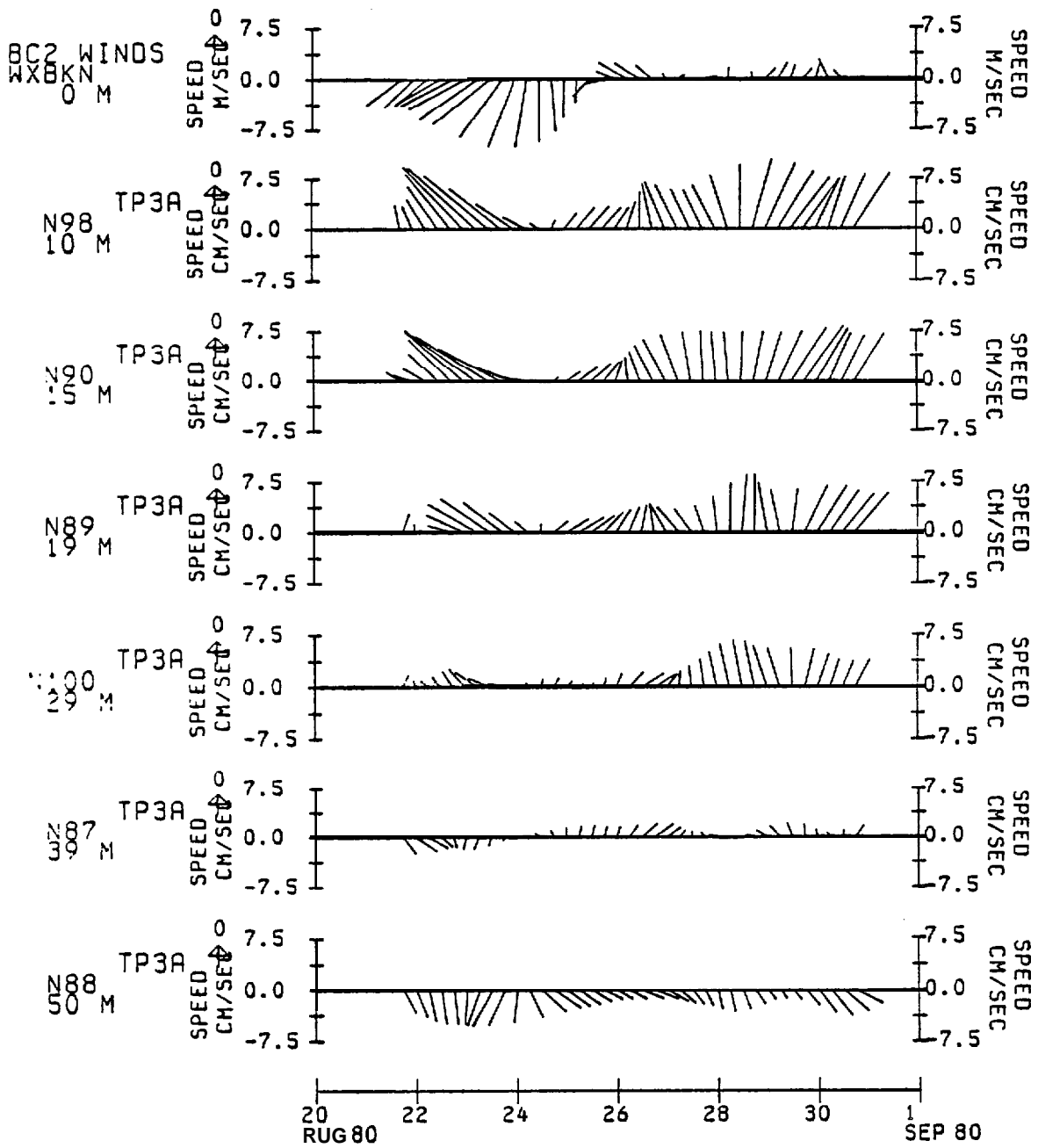
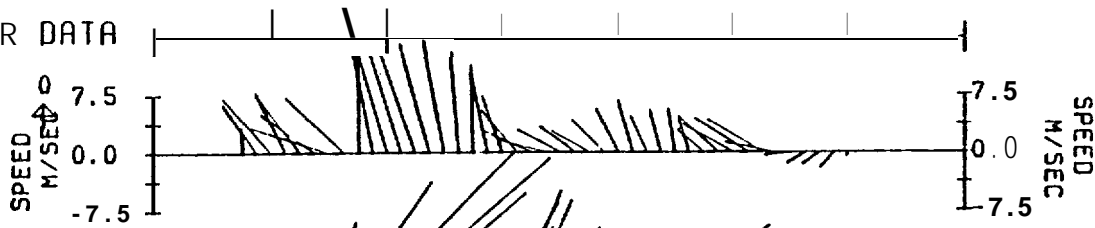


Figure 31. - Current records from TP3A presented as 6-hourly vectors.

35.0 FILTER DATA

BC2 WINDS  
WXBKN  
0 M



N98 TP3B  
4 M



N97 TP3B  
14 M



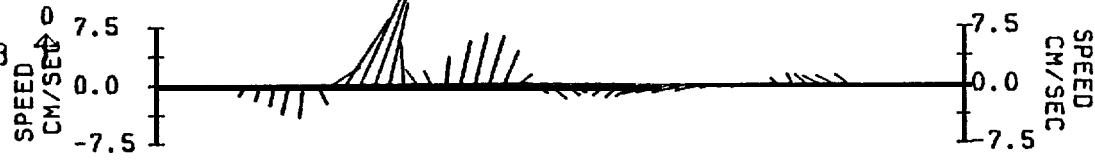
N87 TP3B  
19 M



N95 TP3B  
28 M



N96 TP3B  
49 M



16 MAY 81 18 20 22 24 26 28 30 MAY 81

Figure 32. - Current records from TP3B presented as 6-hourly vectors.

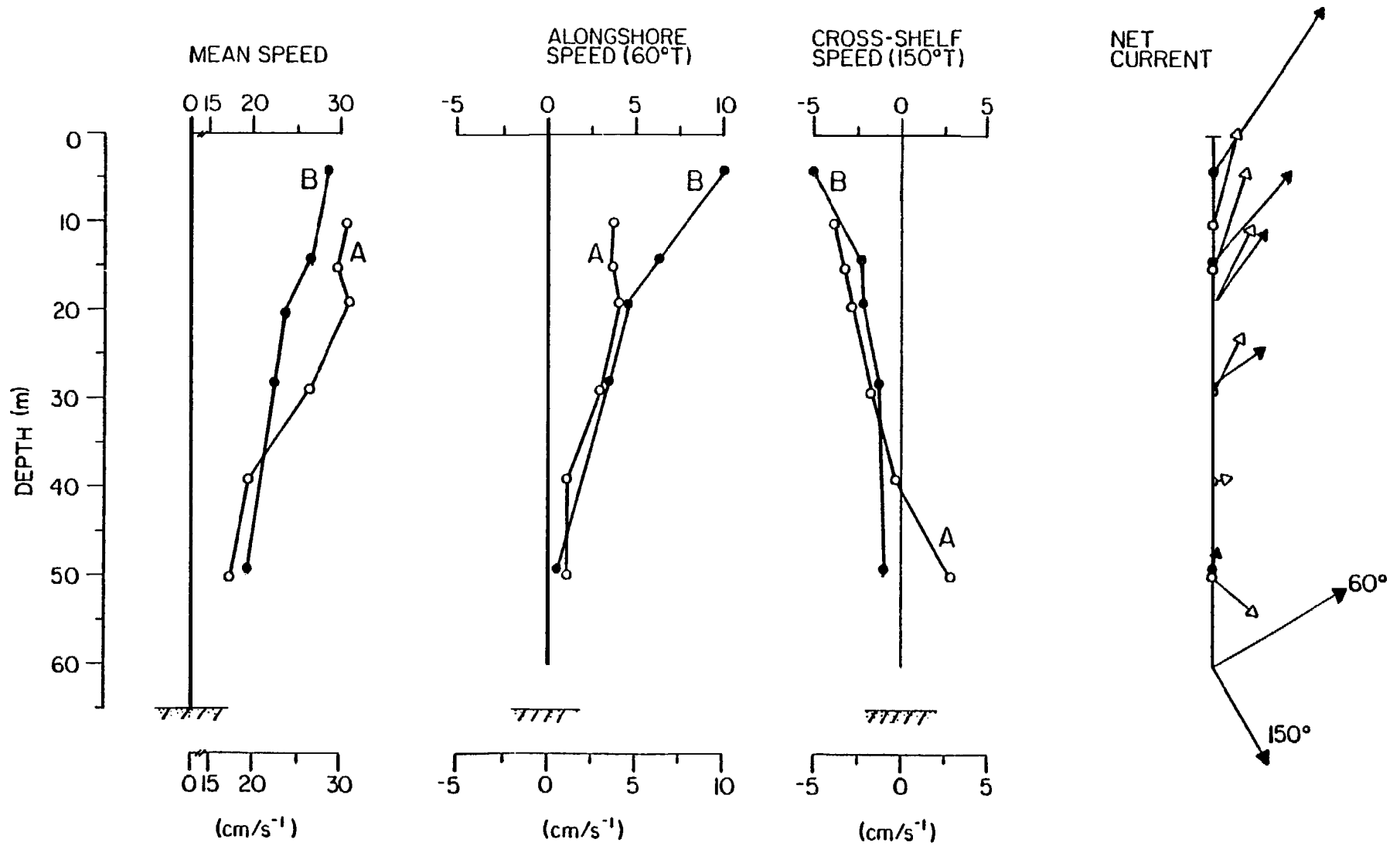


Figure 33. - Profiles of mean, alongshore, and cross-shelf speed and net current from TP3A and B.

the marked difference above this depth **likely** attributable to stronger and more consistent wind stress during **TP3B**. The cross-shelf speed profiles were also similar over *most* of the water column; however, during TP3A the profile indicated onshore flow *in* the bottom layer.

It is apparent that most of the shear resulted from wind stress (particularly during **TP3B**) and estimates of **baroclinic** shear would account for a 1 to 3 cm  $s^{-1}$  decrease of **alongshore** speed between the surface and **25db**. There is also a contribution to the shear from tidal currents, although the majority of this contribution would occur in the bottom boundary layer (about 3 to **15** m thick). Hourly alongshore speeds at four levels are shown in Figure 34. During this period winds were light (3 to 4m  $s^{-1}$ ), so that using a current response of 3% of the wind speed, the wind-induced shear in the upper mixed layer (about 25 m in depth) would be approximately 10cm S-I. Combining this estimate with reasonable values for **baroclinic** shear would account for most of the shear indicated between 10 and 29 m depth records, but not the shear of 20 to 25cm  $s^{-1}$  shown to exist during **floods** and ebbs between the 29 and 50 m records. Although *some* fraction, perhaps up to 50%, may be accounted for by tides, and the observation that the lower water column leads (by"about 15°) the surface is consistent with the tidal wave propagation, some of the observed shear **is** not accounted for by any of these mechanisms.

Wind: A comparison between **alongshore** and cross-shelf components of surface winds (herein called **BC2** winds) and those measured on Lagoon Point (near Port **Moller**) is shown in Figure 35. The **alongshore** components are markedly similar, with BC2 winds indicating somewhat greater speeds (record mean, 2.5  $ms^{-1}$  vs - 0.3  $ms^{-1}$  for **TPIA**). The cross-shelf winds are also similar, but **TPIA** winds were generally greater than those computed for **BC2** (record mean 1.1 ins-I vs  $\sim 0$  at **BC2**). Although there were differences in component speeds, the **alongshore**

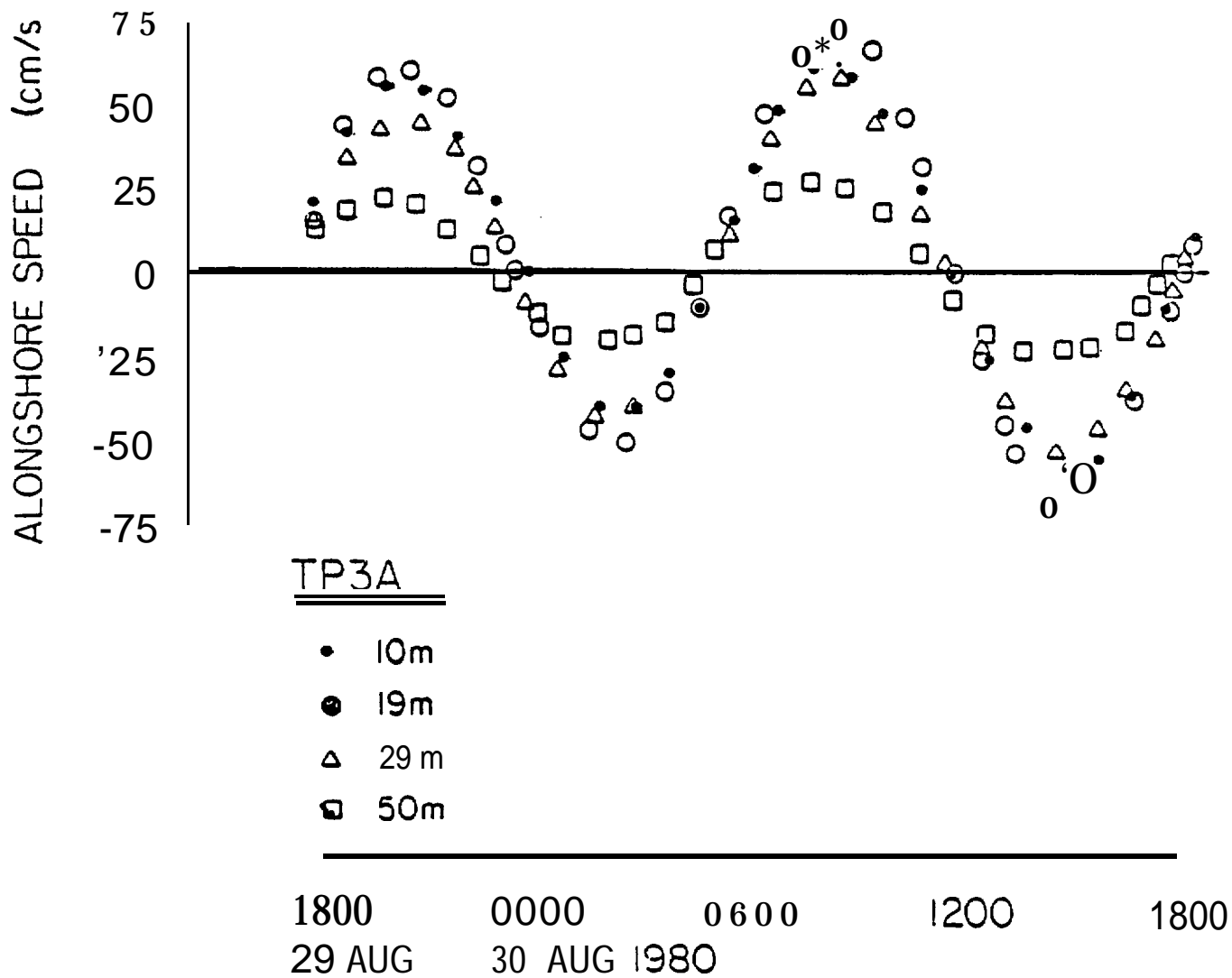


Figure 34. - Current speed at four depths from 2.9-hr data.

35. ° F LTER DAT<sup>e</sup>

530

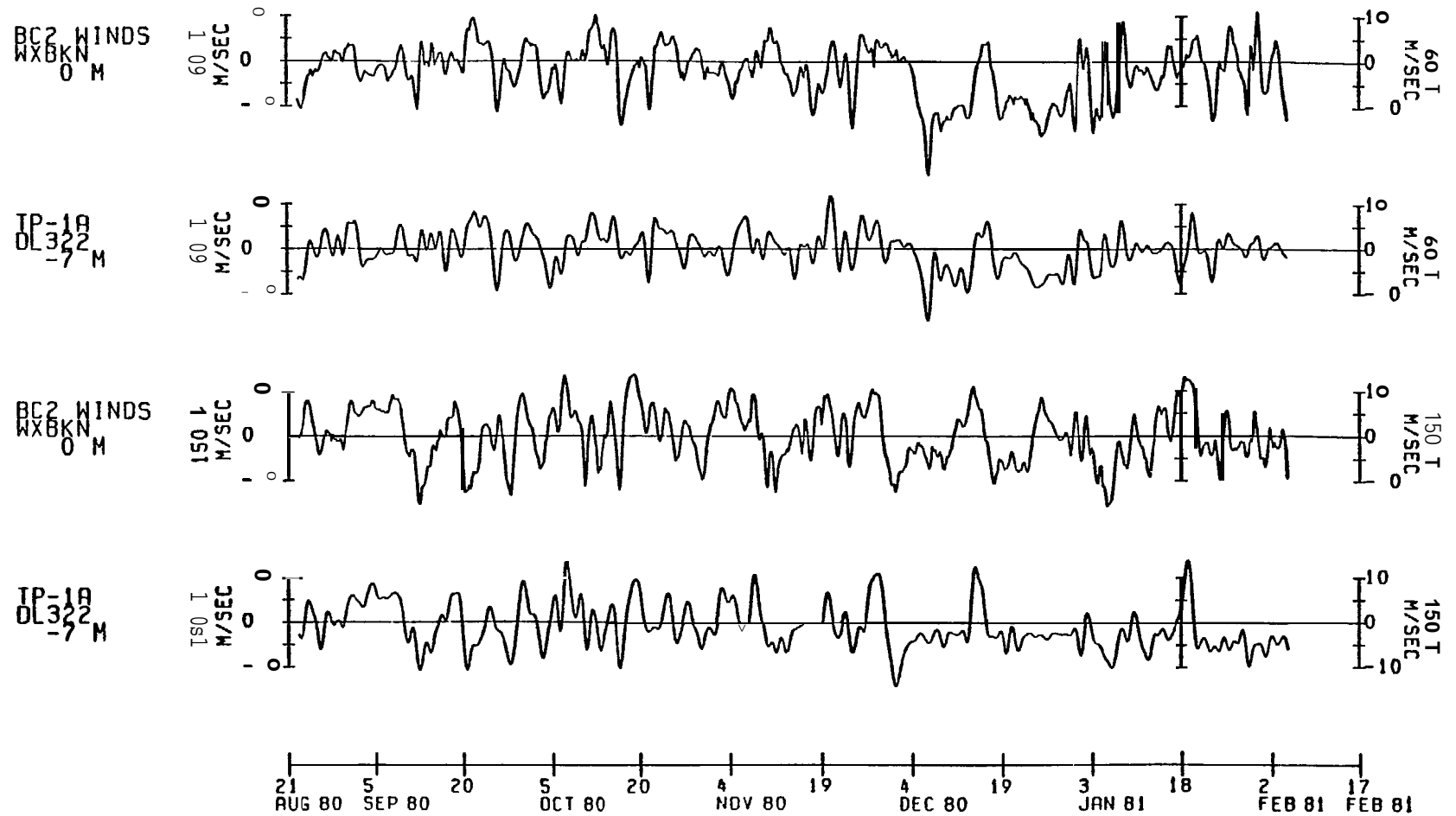


Figure 3 - Comparison of alongshore and cross-shelf components from surface BC2) and observed (TP1A) wind.

series were **highly coherent ( $K^2 > 0.6$ ) at all frequencies (figure 36A)**. There was, however, significantly **less** coherence squared at periods between 2.5 and 3.3 days in the cross-shelf series (figure 36B). While some of these differences may be attributed to the method of computing **geostrophic** winds from surface atmospheric pressure (see Section 3.3), the wind roses generated by the two time series (figure 37) indicated that there was about a 20% difference in the percentage **of wind observations** in the sectors between 270° to 330°, and 90° to 150°. Considering the local orography, some portion of the difference was likely due to pressure gradient winds along the orographic axis. **In general, this effect may be present wherever there are gaps in the mountain range along the Alaska Peninsula, particularly in the vicinity of Cold Bay** where the gap is both wide (about 20 km) and nearly flat.

#### 4.2.4 Salinity Time-Series

Moored current meter records provided some further insight regarding temporal changes in salinity (as computed from temperature, conductivity and pressure). In figure 38, 15-day averages of salinity are shown, where the individual points were **determined** by finding the differences between successive 15-day averages and replacing this value at the mid-point of a given averaging **interval**. **The relative change in mean salinity was greatest ( $\sim 2$ g kg<sup>-1</sup>) at TP2**, but the other series showed a similar trend of decreasing salinity over a period of about one month and this change was in October. Because the **advective** transport is both sluggish and **alongshore** toward the east, **Kvichak** River discharge was not a likely source of the less saline water. Instead, the less saline water likely was a **result** of addition from numerous **ungaged** streams and ground-water injection. This addition could result in the bands of relatively stratified **water** shown in Figure 160.

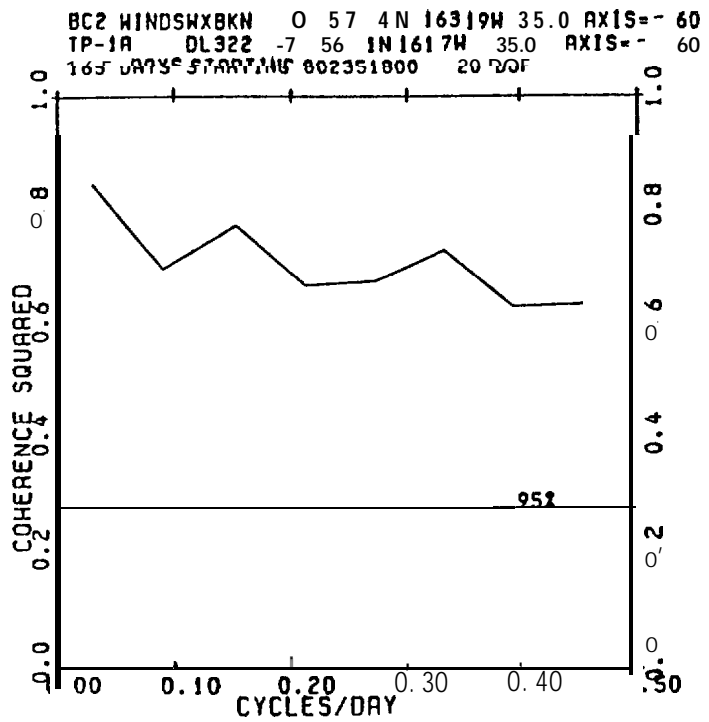
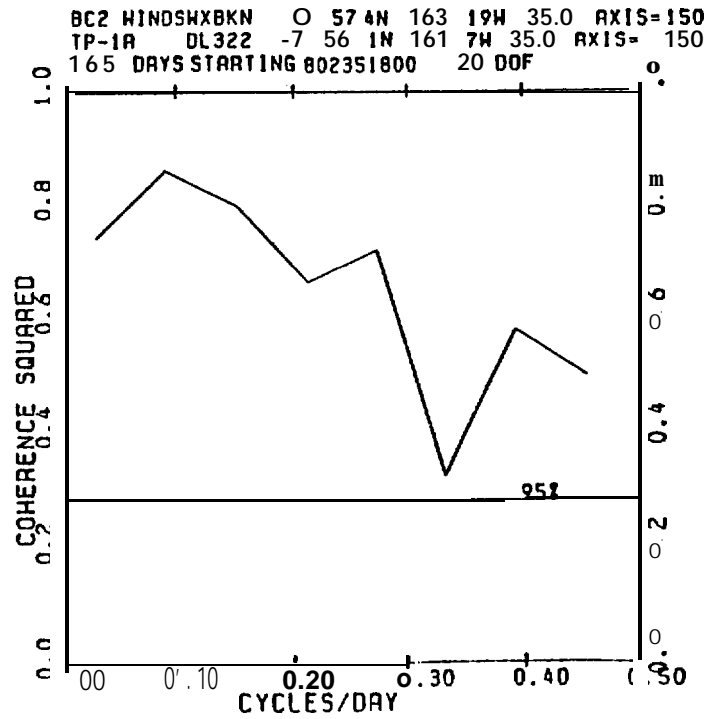


Figure 36. - Coherence squared estimates between surface and observed wind components.

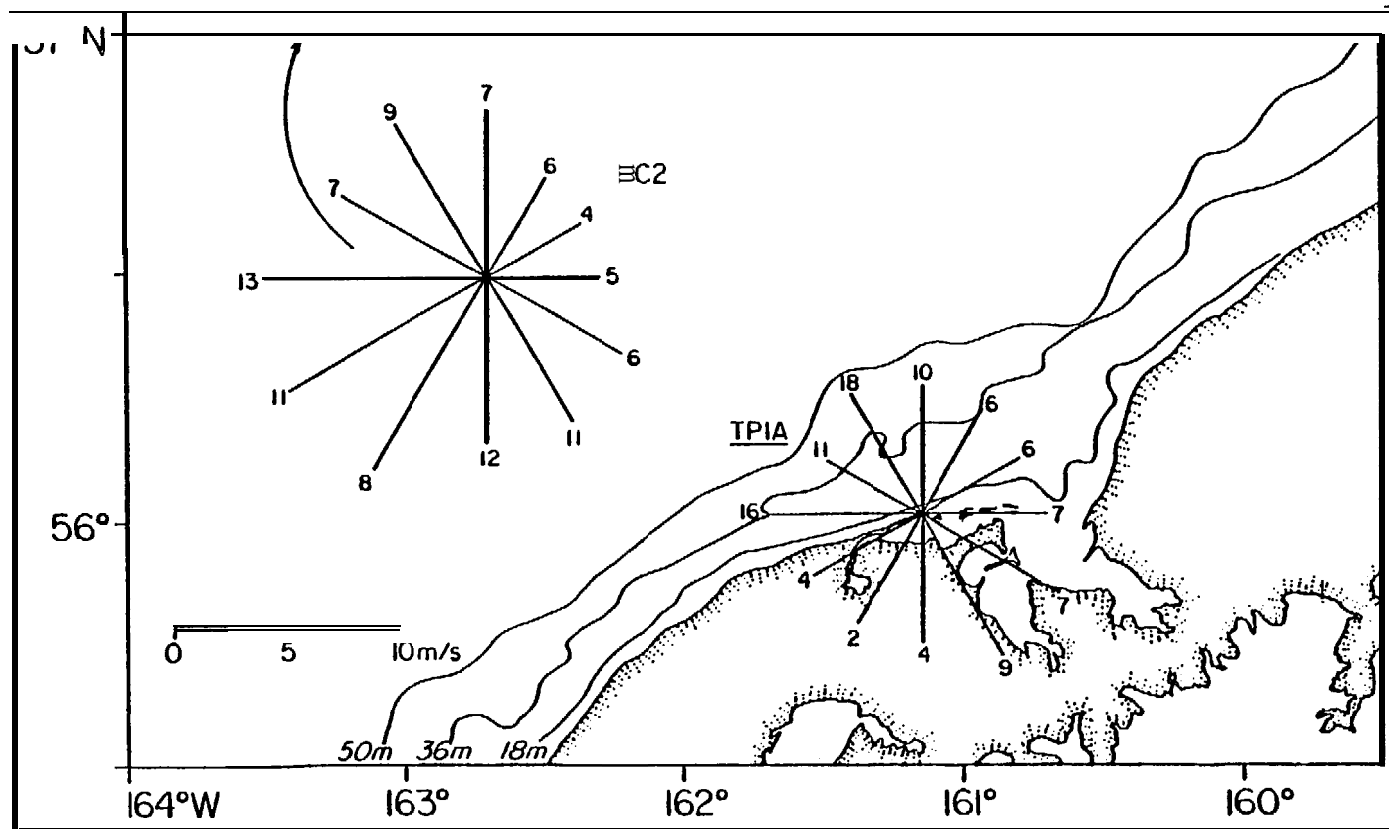


Figure 37. - Wind roses for ÆC2 and TP1A.

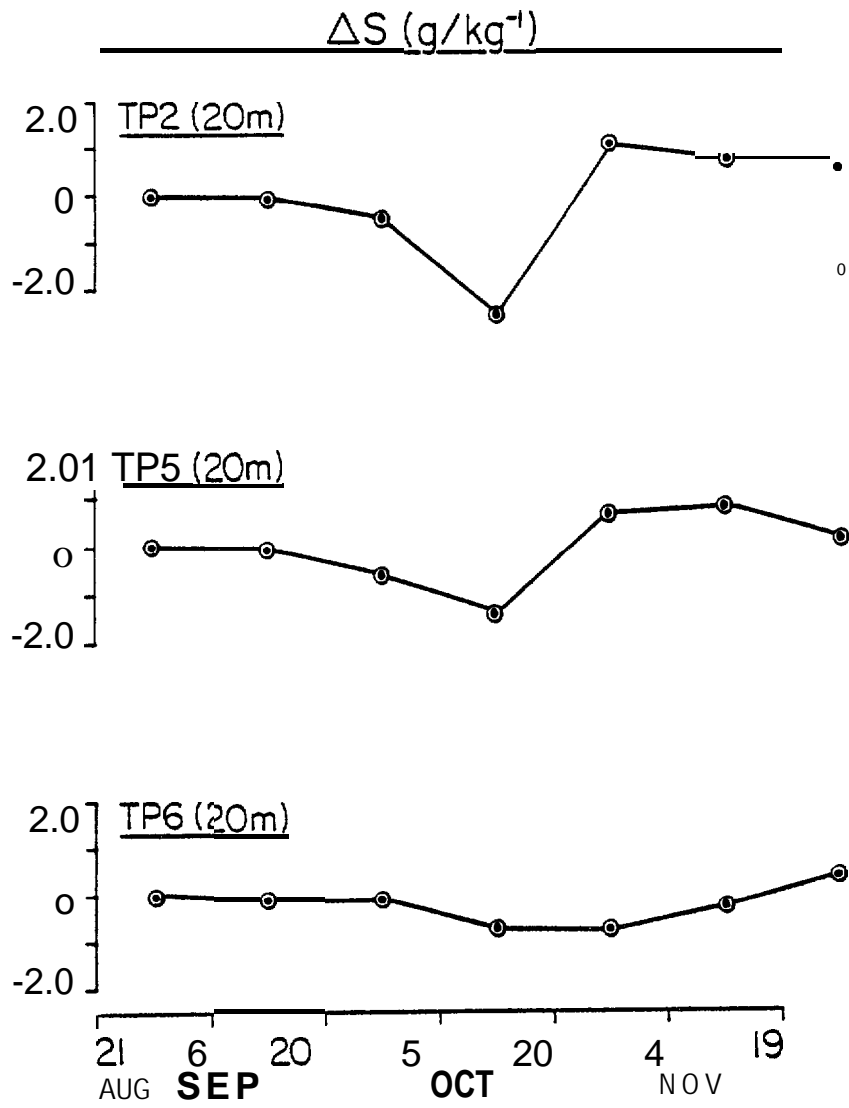


Figure 38. - Salinity time-series (15-day averages) from TP moorings.

## 5. SUMMARY AND CONCLUSIONS

The behavior of currents and bottom pressure observed between March and August 1980 has been described for Unimak Pass, Alaska. These data have been interpreted together with atmospheric pressure gradient, **geostrophic** wind, and CTD data. The following conclusions were reached:

(1) mean **flow** was from the **Gulf** of Alaska shelf westward through Unimak Pass, and reversals occurred in 18% of spring and 31% of summer **35-hr** filtered current observations, with mean flow during spring three times greater than in summer.

(2) currents at periods between 3 and 10 days in Unimak Pass were highly coherent with the bottom pressure difference along the strait, **which** provided the dominant forcing for fluctuations. At these periods most of the bottom pressure difference was related **to alongshore** winds which induced sea level changes along the Gulf of Alaska coast.

(3) Longer period (on the order of months) flow and **variability** was accounted **for by the presence of a southwestward** flowing coastal current. This feature appeared to be a westward extension of the **Kenai** Current.

(4) **Flow** of fresher coastal water through Unimak Pass resulted in formation of **a** front in the vicinity of Unimak Pass. This flow also may **influence baroclinic flow along the northern side of Alaskan Peninsula and provide some fraction of the northward transport through Bering Strait.**

**A characterization of hydrographic features and current behavior between August 1980 and June 1981 has also been described for the north Aleutian shelf** study area. These data were interpreted together with wind and river discharge data. The following conclusion were drawn:

1) In-general, waters over the continental shelf adjacent to the Alaska Peninsula adhere to the previously defined **hydrographic** domains (Kinder and Schumacher,

**1981a):** outer shelf domain (the small portion of the study area north of Unimak Island with depths  $\geq 80\text{m}$ ) waters were always stratified with upper and lower mixed layers separated by a column of weak stratification. Both temperature and salinity showed small seasonal ranges; middle shelf (depths greater than 50m and less than  $\sim 80\text{m}$ ) were typically two-layered during summer and well mixed from about October through March. An exception occurs when ice, primarily formed to the northeast, is transported over this domain and melts. Temperature and salinity ranged between  $\sim 10^\circ\text{C}$  and  $\sim 1.0\text{g kg}^{-1}$  respectively. The coastal domain (less than 50m) was generally mixed, however, the addition of freshwater as a "line source" (particularly between **Ports Moller and Heiden**) and from the **Kvichak** River, resulted in stratification (up to 3 sigma-t units) even though the water is shallow and tidal mixing energy strong. There was also a suggestion that melting ice could impact the local buoyancy/tidal mixing balance. Both temperature and salinity varied greatly, with  $\sim 14^\circ\text{C}$  and  $8\text{g kg}^{-1}$  changes respectively (where most of the salinity range was a result of Kvichak River addition).

2) **Hydrographic** data from February 1981 showed the impact of less saline Kenai current water upon coastal water along the Peninsula. This was most apparent in a reduction of mean salinity between Port **Moller** and Unimak Island between August 1980 and February **1981**. This lends support to a previous hypothesis that the **Kenai** Current was linked with flow around the perimeter of the southeastern Bering Sea shelf and continued northward toward Bering Strait (Schumacher, et.al., 1982).

3) Storms radically alter mean hydrographic domain characteristics. The enhanced turbulence can mix middle shelf water and increase SPM concentrations. These two factors could dominate vertical transport of oil, resulting in greater concentrations on the bottom in a shorter time than detrital rain.

4) Current records supported previous results (Kinder and Schumacher, 1981b; Schumacher and Kinder, 1983: see Appendix B) which infer a moderate ( $2$  to  $6 \text{ cm s}^{-1}$ ) **Eulerian** mean flow from the vicinity of Unimak Island, counter-clockwise around Bristol Bay, and thence northwest past **Nunivak** Island. A mechanism for long-term (order **months**) flow is the persistent cross-shelf density distribution, which resulted in **baroclinic** speeds of  $1$  to  $5 \text{ cm s}^{-1}$ , typically concentrated in a  $10$  to  $20 \text{ km}$  wide band in the vicinity of the  $50\text{-m}$  isobath. Scaling of **Eulerian** tidal residual flow suggested a weak contribution,  $<1.0 \text{ cm s}^{-1}$ , except where the tidal current was orthogonal to the  $50\text{-m}$  isobath off Port **Heiden** (Schumacher and Kinder, 1983, see Appendix B).

5) Although wind energy was evident in **alongshore** current pulses, mean winds during the current observations were weak and toward the west, in opposition to the observed mean flow. Cross-shelf current pulses were also evident, and the observed tendency **was** for offshore flow in the upper water column.

6) Comparison between surface and measured **winds indicated these series were highly coherent, particularly in the alongshore component.** At short periods ( $>2.5$  to  $3.3$  days), coherence was weak in the cross-shelf component and the **observations** showed that measured winds tended to be along the local orographic trend. Such down pressure gradient winds have been noted before (Schumacher and Pearson, 1981), and are **likely to be more significant at Cold Bay and in Unimak Pass.**

7) Substantial vertical shear in currents was observed during two mooring periods. The combination of **wind induced shear and geostrophic baroclinic** shear accounted for about one-half the observed values. The magnitude attributable to tides requires theoretical examination.

## 6. REFERENCES CITED

Allen, J. S. and P.K.Kundu, On the momentum, vorticity and mass balance on the Oregon shelf, J. Phys. Oceanogr., **8**, 13-27, 1978.

Bakun, A., Coastal upwelling indices, west coast of North America, 1946-71. Dept. of Commerce, Tech. Rep. NMFS SSRF-671, NOAA, Monterey, Calif., 1973.

Bowden, K.F., The flow of waters through the Straits of Dover related to wind and differences in sea level, Phil. Trans. R. Soc. London, Ser. A., 248, 517-551, 1956.

Brower, W.A., H.F. Diaz, A.S. Prechtel, H.W. Searby, and J.L. Wise, Climatic Atlas of the Outer Continental Shelf Waters and Coastal Regions of Alaska, vol. 1, Gulf of Alaska, Final Rep. RU-347, U.S. Dept. of Commerce/NOAA/ Alaska Outer Continental Shelf Environmental Assessment Program, Fairbanks, Alaska, 1977.

Chao, S.-Y., and L.J. Pietrafesa, The subtidal response of sea level to atmospheric forcing in the Carolina Capes, J. Phys. Oceanogr., **10**, 3.246-1255, 1.980.

Charnell, R.L., and G.A. Krancus, A processing system for Aanderaa current meter data, Tech. Memo. ERL PMEL-6, NOAA, Boulder, Colo., 1976.

Coachmen, L.K., and K. Aagaard, Reevaluation of water transports in the vicinity of Bering Strait, in The Eastern Bering Sea Shelf: Oceanography and Resources, vol. 1, edited by D.W. Hood and J.A. Calder, pp. 95-110, U.S. Dept. of Commerce/NOAA/OMPA, Washington, D.C., 1981.

Coachmen, L.K., and R.L. Charnell, Finestructure in outer Bristol Bay, Alaska, Deep Sea Res., **24**, 809-839, 1.977.

Coachmen, L.K., and R.L. Charnell, On lateral water mass interaction: A case study, Bristol Bay, Alaska, J. Phys. Oceanogr., **9**, 278-297, 1979.

Coachman, L.K., and J.J. Walsh, A diffusion model of cross-shelf exchange of nutrients in the southeastern Bering Sea, Deep Sea Res., **28**, 819-846, 1981.

Coachmen, L.K., K. Aagaard, and R.B. Tripp, Bering Strait, the Regional Oceanography, University of Washington Press, Seattle, 1975.

Coachmen, L.K., T.H. Kinder, J.D. Schumacher, and R.B. Tripp, Frontal systems of the southeastern Bering Sea shelf, in Stratified Flows, edited by T. Carstens and T. McClimans, pp. 917-933, TAPIR, Norway, 1980.

Defant, A., Physical Oceanography, vol. 1, Pergamon, New York, 1961.

Favorite, F., and D.M. Fisk, Drift bottle experiments in the North Pacific Ocean and Bering Sea--1957-60, 1962, 1966, and 1970, Data Rep. **67**, NOAA, NMFS, Seattle, Wash., 1971.

Favorite, F., **A.J. Dodimead**, and **K. Nasu**, Oceanography of the subarctic Pacific region, 1960-1971, Bull. 33, Int. N. Pacific Fish. Comm., Vancouver, Canada, **1976**.

**Fearnhead**, P.G., On the formation of fronts by tidal mixing around British Isles, Deep Sea Res., 22, 311-322, 1975.

Garrett, C., and B. **Petrie**, Dynamical aspects of Flow through the Strait of Belle Isle, J. Phys. Oceanogr., 11, 376-393, 1981.

Garrett, C., and B. **Toulany**, Variability of flow through the **Strait** of Belle Isle, J. Mar. Res., 39, 163-189, 1981.

**Gebhart**, B., and **J.C. Mollendorf**, A new density relation for pure and saline water, Deep Sea Res., 24, 831-848, **1977**.

Hattori, A., and **J.J. Goering**, **Nutrient** distributions and dynamics in the eastern Bering Sea, in The Eastern Bering Sea Shelf: Oceanography and Resources, vol. II, edited by **D.W. Hood** and **J.A. Calder**, pp. 975-992, U.S. Dept of Commerce/NOAA/OMPA, Washington, D.C., **1981**.

Hayes, S.P., Variability of current and bottom pressure across the continental shelf in the northeast Gulf of Alaska, J. Phys. Oceanogr., 9, 88-103, 1979.

Hughes, **F.W.**, **L.K. Coachman**, and **K. Aagaard**, Circulation, transport and water exchange in the western Bering Sea, in Oceanography of the Bering Sea, edited by **D.W. Hood** and **E.J. Kelley**, pp. 59-98, Institute of Marine Science, University of Alaska, Fairbanks, Alaska, 1974.

**Iverson**, R.L., **L.K. Coachman**, **R.T. Cooney**, **T.S. English**, **J.J. Goering**, **G.L. Hunt, Jr.**, **M.C. Macauley**, **C.P. McRoy**, **W.S. Reeburgh**, and **T.H. Whitledge**, **Ecological significance** of fronts in the southeastern Bering Sea, in Coastal Ecological, edited by **R.J. Livingston**, pp. 437-468, Plenum, **New York**, **1979**.

Kinder, T.J., and **L.K. Coachman**, The front overlaying the continental slope in the eastern Bering Sea, J. Geophys. Res., 83, 4551-4559, **1978**.

Kinder, T.J., and **J.D. Schumacher**, Circulation over the continental shelf of the southeastern Bering Sea, in The Eastern Bering Sea Shelf: Oceanography and Resources, vol. 1, edited by **D.W. Hood** and **J.A. Calder**, pp. 53-78, U.S. Department of Commerce/NOAA/OMPA, Washington, O.C., 1981a.

Kinder, T.J., and J.C). Schumacher, Hydrography over the continental shelf of the southeastern Bering Sea, in The Eastern Bering Sea Shelf: Oceanography and Resources, vol. I, edited by **D.W. Hood** and **J.D. Calder**, pp. 31-52, U.S. department of Commerce/NOAA/OMPA, Washington, D.C., **1981b**.

Kinder, T.H., **J.D. Schumacher**, **R.B. Tripp**, and **J.C. Haslett**, The evolution of the hydrographic structure over the continental shelf near Bristol Bay, Alaska, during summer **1976**, Tech. Rep. Ref: M78-16, Univ. of Washington, Seattle, 1978.

**Lagerloef, G. R.D. Muench, and J.D. Schumacher**, Low frequency variations in currents near the shelf break: Northeast Gulf of Alaska, J. Phys. Oceanogr., **11**, 627-638, 1981.

**Livingston, D., and T.C. Royer**, Observed surface winds at Middleton Island, Gulf of Alaska and their influence on the ocean circulation, J. Phys. Oceanogr., **10**, 753-764, 1980.

**Muench, R.D., and J.D. Schumacher**, Physical oceanographic and meteorological conditions on the northwest Gulf of Alaska, NOAA, Tech. Memo. ERL-PMEL-22, Boulder, Colo., 1980.

Overland, J.E., **Marine climatology** of the Bering Sea, in The Eastern Bering Sea Sea Shelf: Oceanography and Resources, vol. 1, edited by **D.W. Hood and J.D. Calder**, pp. 15-22, U.S. Dept. of Commerce/NOAA/OMPA, Washington, D.C., 1981b.

Overland, J.E., and **C.H. Pease**, **Cyclone** climatology of the Bering Sea and its relation to sea ice extent, Mo. Mea. Rev., **108**, 2015-2023, 1980.

Pearson, C.A., **H. Mofjeld**, and **R.B. Tripp**, Tides of the eastern Bering Sea shelf, in The Eastern Bering Sea Shelf: Oceanography and Resources, vol. 1, edited by **D.W. Hood and J.A. Calder**, pp. 53-85, U.S. Dept of Commerce/NOAA/OMPA, Washington, D.C., 1981b.

Pearson, C.A., **J.D. Schumacher**, and **R.D. Muench**, Effects of wave induced mooring noise on tidal and low frequency current observations, Deep Sea Res., **28A(10)**, 1223-1229, 1981.

Pease, C.H., **S.A. Schoenberg**, and **J.E. Overland**, A climatology of the Bering Sea and its relation to sea ice extent, NOAA Tech. Report, **ERL 419-PMEL 36**, 29 pp., 1982.

**Quadfasel, D.**, and **F. Schott**, Comparison of different methods of current measurements, Deut. Hydrogr. Zeit., **32**, 27-28, 1979.

Reed, R.K., Nontidal flow in the Aleutian Island passes, Deep Sea Res., **18**, 379-380, 1971.

Reed, R.K., and **J.D. Schumacher**, Sea level variations in relation to coastal flow around the Gulf of Alaska, J. Geophys. Res., **86**, 6543-6546, 1981.

Reed, R.K., **J.D. Schumacher**, and **C. Wright**, On coastal flow in the northeast Gulf of Alaska near Yakutat, Atmos. Ocean., **19**, 47-53, 1981.

**Royer, T.C.**, **Baroclinic** transport in the Gulf of Alaska, **II**, A fresh water driven coastal current, J. Mar. Res., **39**, 251-266, 1981.

**Royer, T.C.**, **D.V. Hansen**, and **D.J. Pashinski**, Coastal flow in the northern Gulf of Alaska as observed by dynamic topography and satellite-tracked drogued drift buoys, J. Phys. Oceanogr., **9**, 785-801, 1979.

Schumacher, J.D., **T.H. Kinder**, **D.J. Pashinski**, and **R.L. Charnell**, A structural front over the continental shelf of the eastern Bering Sea, J. Phys. Oceanogr., **9(1)**, 79-87, 1979.

Schumacher, J.D., and **R.K. Reed**, Coastal flow in the northwest Gulf of Alaska: The Kenai Current, J. Geophys. Res., 85, 6680-6688, 1980.

Schumacher, J.D., and **C.A. Pearson**, Bristol Bay Oceanographic processes, 5th Annual Report, RU549, U.S. Dept. of Commerce/NOAA/Alaska Outer **Continental Shelf Environmental** Assessment Program, Fairbanks, Alaska, 1980.

Schumacher, J.D., and **C.A. Pearson**, 6th Annual Report, RU549, U.S. Dept. of Commerce/NOAA/Alaska Outer Continental **Shelf Environmental** Assessment Program, Fairbanks, Alaska, 1980.

Schumacher, J.D., and **T.H. Kinder**, Dynamical characteristics of three low frequency current regimes **over the Bering Sea shelf**, submitted to J. Phys. Oceanogr., 1982.

Schumacher, J.D., **C.A. Pearson**, and **J.E. Overland**, On exchange of water between the Gulf of Alaska and the Bering Sea through Unimak Pass, J. Phys. Oceanogr., 87, 5785-5795, 1982.

**Seifert**, R., and D. Kane, Effects of seasonability and variability of **streamflow** on nearshore coastal areas, Final Rep. RU-111, (edited by **R.F. Carlson**), U.S. Dept. of Commerce/NOAA/Alaska **Outer Continental Shelf Environmental** Assessment Program, Fairbanks, Alaska, 1977.

**Takenouti**, A.Y., and K. Ohtani, Currents and water masses in the **Bering Sea**: A review of **Japanese** work, in Oceanography of the Bering Sea, edited by **D.W. Hood** and **E. Kelley**, pp. **39-75**, Occ. Pub. 2, Institute of Marine Science, University of **Alaska, Fairbanks**, 1974.

Thompson, W.F., and **R.V. VanCleve**, Life **history of the Pacific Halibut: (2) Distribution and early life history**, Rep. Inter. Fish Comm., **9**, 1936.

Webster, B.D., Ice edge probabilities for the Eastern Bering Sea, Tech. Memo., NWS, AR-26, NOAA, Anchorage, Alaska, 1979.

**Winant**, C.D., Coastal circulation and wind-induced currents, Ann. Rev. Fluid Mech., **12**, 271-302, 1980.

Wright, C., Observations in the Alaskan Stream during 1980, Tech. Memo. ERL PMEL-23, NOAA, Seattle, Wash., 1981.

APPENDIX A

FINAL DATA INVENTORY

James D. Schumacher and Thomas H. Kinder

Final Report, RU 549,  
**Transport** Processes in the North Aleutian Shelf

James D. Schumacher  
and  
Thomas H. Kinder

Appendix A: Final Data Inventory

Data acquisition for RU 549 (North Aleutian Shelf Transport Processes, NAST) began in March 1980 with the deployment of three moorings in the vicinity of Unimak Pass. This work was conducted under the direction of R. B. Tripp, University of Washington, from the RV Thompson. The remaining field work for the NAST experiment was accomplished during three cruises in 1980-81. These cruises are listed on the **Boujder** computer system (**R<sub>2</sub>D<sub>2</sub>**) by the following cruise identifiers: **RP4SU80AL4**, Aug.-Sept. 1980, ship *Surveyor*, Chief Scientist: Curl; **RP4SU81**, Jan.-Feb. 1981, ship *Surveyor*, Chief Scientist: Schumacher; and **RP4DI81A2**, May-June 1981, ship *Discoverer*, Chief Scientist: Pearson. Operations during these cruises included 514 CTD casts, and deployment and recovery of 15 moorings and one shore-based meteorological station maintained throughout the current observation period.

Since the completion of field operations for RU 549, two supplemental cruises were conducted in North Aleutian Shelf waters: **RP4D181AL6**, **Aug.-Sept. 1981**, ship *Discoverer*, Chief Scientist: Reed; **RP40C81AL3**, Sept.-Ott. 1981, ship *Oceanographer*, Chief Scientist: Schumacher. A total of 61 CTD casts were conducted during these cruises. The data have been processed and loaded on R<sub>2</sub>D<sub>2</sub>.

I. **Hydrographic Data:** Temperature and salinity data were collected during the NAST cruises using Plessey Model 9040 CTD Systems:

**NAST 1**, Aug 15-Sept 5 1980, **199** casts

**NAST 2**, Jan 30-Feb 17 1981, 153 casts

**NAST 3**, May 13-May 30 1981, 189 casts

The sampling interval was five times per second for simultaneous measurements of conductivity, temperature and depth. Data were recorded during the down cast using a lowering rate of 30 meters per minute. Nansen bottle samples were taken at approximately half of the stations to provide temperature and salinity calibration. The calibration corrections used for each cruise are:

**NAST 1, temp:-0.01°C**

**NAST 2, temp:-0.01°C**

**NAST 3, temp:+0.03°C**

**Salin:-0.04‰**

**salin:-0.05‰**

**salin:+0.09‰**

Data from monotonically increasing depth were despiked to eliminate excessive values and were averaged over one-meter intervals to produce temperature and salinity values from which density and geopotential anomaly were computed.

All of the CTD data have been processed and are available for use on R<sub>2</sub>D<sub>2</sub>.

**II. Time Series Observations:** Time series observations were made using the following equipment:

- B** - Neil Brown acoustic current meters
- RCM** - **Aanderaa RCM-4** current meters
- RCM/T** - **Aanderaa** current meters with transmissometer
- TG** - **Aanderaa** TG2 and TG3A bottom pressure gauges
- ST** - Sediment Traps
- TC** - Applied Microsystems temperature-conductivity sensors
- DL** - Digital data loggers
- MET** - Meteorological sensors (wind speed, direction, gust, and atmospheric temperature)

Taut wire moorings were used with an anchor and acoustic release at the bottom and a 450 kg buoyancy subsurface float about 2 meters above the upper current meter. Pressure gauges were located in a cage which was welded to the anchor. Wind sensors were located on a tower about 7 m above the ground. A compilation of observation period, position and instruments on a particular platform is given in Table A-1.

Current and pressure data were evaluated for quality, including **time** base accuracy and the presence of zero speeds. **Tidal constituents were determined from edited sample interval** time series. This is the **final** stage of our quality control procedures, i.e., the amplitude and phase of the dominant constituents are checked for relative and absolute consistency. The **one-hour-interval** time series available for use on **R<sub>2</sub>D<sub>2</sub>** are produced from the edited data using a **Lanczos** filter. These series, called 2.9-hr data, are filtered such that over 90% of the amplitude is passed at periods greater than 5 **hr, 50%** at 2.86 hr, and less than **0.5% at 2** hr.

Table A-2 is a list by master reference numbers of time series observations that are available on R<sub>2</sub>D<sub>2</sub>.

Table A-1. - Time-series observations.

Mooring	Deployed	Recovered	Lat	Long	Depth	Instruments
UP-1	22 Mar 1980	17 Aug 1980	54°33.7'N	165°23.9'W	84m	2 RCM, TG
UP-2	22 Mar 1980	16 Aug 1980	54°18.1'N	164°45.9'W	80m	2 RCM, TG
UP-3	21 Mar 1980	16 Aug 1980	54°09.6'N	164°00.4'W	69.5m	2 RCM, TG
TP-1A	19 Aug 1980	6 Feb 1981	56°00.7'N	161°06.8'W	-7m	MET, DL
TP-2A	1.9 Aug 1980	30 Jan 1981	56°07.1'N	161°17.6'W	32m	RCM/T, N, TG
TP-3A	18 Aug 1980	2 Sep 1980	56°24.1'N	161°39.6'W	65.4m	MET, 7N
TP-4A	1.9 Aug 1980	31 Jan 1981	56°31.2'N	160°09.3'W	68.5m	RCM/T, N, TG
TP-5A	22 Aug 1980	29 Jan 1981	56°31.2'N	160°18.1'W	31m	RCM/T, N, TG
TP-6A	22 Aug 1980	30 Jan 1981	56°46.5'N	160°18.1'W	59m	RCM, RCM/T, N, TG
TP-1B	7 Feb 1981	29 May 1981	56°00.7'N	161°06.8'W	-7	MET, DL
BBL	14 May 1981	30 May 1981	56°18.8'N	161°33.2'W	64m	3 RCM
TC	14 May 1981	31 May 1981	56°25.8'N	161°42.8'W	74m	12TC, DL
TP-2B	30 Jan 1981	29 May 1981	56°04.6'N	161°18.2'W	35m	N, RCM/T, TG, ST
TB-3B	14 May 1981	30 May 1981	56°19.1'N	161°32.5'W	65m	N, RCM/T, TG, ST
TP-7	31 Jan 1981	29 May 1981	56°02.0'N	161°13.1'W	25m	N, RCM/T, TG, ST
TP-8	2 Feb 1981	30 May 1981	55°51.8'N	162°02.4'W	31m	N, RCM/T, TG, ST
TP-9	1 Feb 1981	30 May 1981	56°29.7'N	161°42.3'W	89m	N, RCM/T, TG, ST

Table A-2. - **Time series** available on R2D2.

MRef	Mooring	Meter	Depth	Start	End	Comments
42	UP-1	<b>1811</b>	64	800821400	802292100	
43	UP-2	1.827	59	800821000	802291700	
<b>44</b>	UP-3	1815	47	800820400	802291300	
46	TP3A	<b>N99</b>	<b>5</b>	802320500	802461200	
47	"	<b>N98</b>	<b>10</b>	802320500	802461.200	
48	"	N90	<b>15</b>	802320500	802461.200	
49	"	N89	<b>19</b>	802320500	802461200	
<b>50</b>	"	<b>N100</b>	29	802320500	802461200	
51	"	N87	39	802320500	802461.200	
<b>52</b>	"	<b>N88</b>	50	802320500	802463.200	
<b>75</b>	UP-3	<b>TG121</b>	67	800820400	802291300	
76	UP-2	TG87	79	800821000	802291700	
78	TP-6	3293	20	802340800	810291800	
79	TP-5	2505	<b>20</b>	802341100	810291600	Transmissometer failed
<b>80</b>	<b>TP-2A</b>	2502	<b>20</b>	802323.200	810291400	Pressure channel = light attenuation
<b>81</b>	TP-6	2500	55	802340800	810291900	Pressure channel = light attenuation
82	<b>TP-2A</b>	N95	19	802321100	810301400	
83	TP-4	N96	62	802320700	810311800	
84	TP-5	N94	19	802341100	810291700	
85	TP-6	N97	<b>19</b>	802340800	810291900	
88	TP-4	<b>2501</b>	63	802320800	803150500	Pressure channel = light attenuation
89	TP-4	TG209	<b>66</b>	802320700	810211000	
90	TP-6	<b>TG120</b>	57	802340800	810292000	

Table A-2 (continued).

<b>MRef</b>	<b>Mooring</b>	<b>Meter</b>	<b>Depth</b>	<b>Start</b>	<b>End</b>	<b>Comments</b>
97	<b>TP-1A</b>	<b>DG322</b>	<b>-7</b>	802330200	810372200	
98	<b>UP-1</b>	TG85	<b>83</b>	800821400	802292100	
<b>99</b>	TP-2B	N88	13	810310500	811491400	
<b>100</b>	<b>TP-7A</b>	N89	<b>12</b>	810310800	83. 1493. 200	
<b>101</b>	TP-9A	N99	14	810320800	811501300	
102	<b>TP-8A</b>	N100	12	810340500	811471000	
<b>106</b>	<b>TP-3B</b>	N98	<b>4</b>	83. 3. 350000	811501700	
107	<b>TP-3B</b>	N97	<b>14</b>	83. 3. 350000	811501600	
108	<b>TP-3B</b>	<b>N87</b>	<b>19</b>	811350000	811501700	
109	TP-3B	N95	<b>2a</b>	811350000	811501700	
110	<b>TP-3B</b>	N96	<b>49</b>	811350000	83. 1501700	
111	<b>TP-2B</b>	2505	<b>25</b>	810310400	813. 291500	
<b>112</b>	TP-7	2500	<b>15</b>	810310700	811240900	
114	<b>TP-2A</b>	TG205	<b>30</b>	802321100	810190600	
115	<b>TP-2B</b>	2505	<b>25</b>	810310400	81. 3. 2910500	
116	TP-9	2502	<b>79</b>	810320800	811410400	
117	TP-8	<b>2501</b>	<b>21</b>	810340500	811491900	
118	TP-7	<b>TG121</b>	<b>24</b>	81. 0310700	811491400	
119	TP-8	TG87	<b>30</b>	810340500	811481200	
<b>120</b>	<b>TP-2B</b>	TG85	<b>34</b>	810310400	811491500	
121	TP-9	TG106	<b>88</b>	810320700	811501400	

**All hydrographic and Time series data will be submitted to NODC by September 1982.**

**Note:** In order to insure data acquisition, two current meters were located within 1 m of each other on UP-1, UP-2, and UP-3. When data from the two meters agreed (UP-1 and UP-3), only one data set was sent to Boulder. Redundant current meters proved to be useful in the case of UP-2 since one meter failed.

APPENDIX B

DYNAMICAL CHARACTERISTICS OF THREE LOW-FREQUENCY CURRENT REGIMES  
OVER THE BERING SEA SHELF

James D. Schumacher and Thomas H. Kinder

Final Report RU 549  
Transport Processes **in** the North Aleutian **Shelf**

Appendix B: Dynamical Characteristics of Three Low Frequency  
Current **Regimes** over the Bering Sea **Shelf**

James O. Schumacher

and

Thomas H. Kinder

ABSTRACT

**Using extensive direct** current measurements made **during the period 1975-1981**, we **describe** the general **circulation** over the southeastern **Bering** Sea and its differentiation by regimes related to depth and forcing mechanisms. Three regimes **are** present, delineated by water depth ( $z$ ): the coastal ( $z \leq 50$  m), the middle **shelf** ( $50 \leq z \leq 100$ ), and the outer shelf ( $z \geq 100$  m), and these are nearly coincident with previously described **hydrographic** domains. Statistically significant mean flow ( $\sim 1$  to  $10 \text{ cm s}^{-1}$ ) exists over the outer shelf, generally flowing towards the northwest but with a cross-isobath component. **Flow of similar magnitude (1 to  $6 \text{ cm s}^{-1}$ ) occurs in the coastal regime**, paralleling the 50-m isobath in a counterclockwise sense around the **shelf**. Mean flow in the middle shelf is insignificant. Kinetic energy at frequencies  $> 0.5 \text{ cpd}$  is greater over the outer shelf than **in the other two regimes**, suggesting that oceanic forcing is important there but **does not affect the remainder of the shelf**. Kinetic energy in the band from 0.5 to 0.1 cpd follows a **similar** pattern, reflecting the greater **number of storms over the** outer shelf.

Mean flow paralleling the 100- and 50-m **isobaths** appears **to be related to a combination of baroclinic pressure gradients (associated with frontal systems which separate the regimes) and interactions of tidal currents with bottom slopes located beneath the fronts**. Although winds **are** energetic, their highly variable behavior suggests they are not a primary driving force for mean flow.

## 1. Introduction

Beginning in 1975, closely spaced hydrographic stations and long-term, direct-current measurements were obtained over the southeastern Bering Sea continental shelf for the first time. We use these measurements, which were gathered by us and by others (see Acknowledgements), to delineate three low-frequency current regimes. These current regimes are nearly coincident with three hydrographic domains that are separated by relatively narrow transition zones or fronts. While some aspects of similar current regimes have been reported on other shelves, the great width (~500 km) of the Bering Sea shelf apparently permits a clearer separation of processes that are more compressed on narrower shelves.

Shelf dynamics typically are taken to extend from within about 10 km of the shore (the coastal boundary layer) to the vicinity of the shelf break (Csanady, 1976; Fischer, 1980). The seaward edge of the shelf regime is often taken coincident with a shelfbreak front, which, in turn, may be a manifestation of upwelling (e.g., Mooers, Collins and Smith, 1976), or be closely associated with a strong offshore boundary current (e.g., Mooers, Garvine, and Martin, 1979), or be independent of both upwelling and strong currents (e.g., Beardsley and Flagg, 1976; Flagg and Beardsley, 1978). Between the coastal boundary layer and the shelfbreak front, the hydrographic and current structures are often taken as uniform except for salinity in the presence of river runoff. Even when nonuniformities have been stressed, these differences have been smooth and usually do not allow a definition of separate zones or regimes. The concept of distinct dynamical regimes, which is clearly illustrated on the Bering shelf, may be useful in refining models and designing experiments on shelves where important dynamical differences are more subtle than in the Bering, but still present.

Following the preliminary results of Kinder and Schumacher (1981a), we a priori associate regimes with water depth ( $z$ ): **outer shelf ( $z \geq 100\text{m}$ )**, **middle shelf ( $100 > z > 50\text{ m}$ )** and **inner shelf ( $z \leq 50\text{m}$ )**. Flow in the regimes is delineated by characteristics of the vector mean- and low-frequency ( $\leq 0.5\text{ cpd}$ ) currents. The horizontal kinetic energy is examined using rotary spectral estimates in frequency ( $f$ ) bands corresponding to tidal energy ( $KE_T$ ), energy at frequencies related to meteorological forcing ( $KE_M$ :  $0.5 \leq f \leq 0.1\text{ cpd}$ ), kinetic energy of low-frequency events ( $KE_L$ :  $f \leq 0.5\text{ cpd}$ ), and the total fluctuating kinetic energy ( $KE'$ ). Although the tides ( $KE_T$ ) account for an average (using data from all three regimes) of 90% of the fluctuating kinetic energy and low-frequency fluctuations for only 6%, the low-frequency motions are not only of dynamical interest, but also have an influence on plankton and sediment distributions distinct from tidal currents. The observed flow characteristics are discussed in the context of 'first order' dynamics, which appear responsible for the observed sub-tidal flow features, and include baroclinic pressure gradients, tidal residual flow, response to wind, and effects due to oceanic (off-shelf) circulation.

## 2. Oceanographic Setting

The southeastern Bering shelf is bordered by the Alaska Peninsula, the Alaska mainland, and by a line running southwest from Nunivak Island to the Pribilof Islands, and thence following the shelfbreak southeastward to Unimak Pass (Fig. B-1). The shelf break occurs near the 200-m isobath, and this extremely broad ( $\sim 500\text{-km}$ ) shelf is unusually flat and featureless. Shelf waters receive an annual excess of precipitation over evaporation, and considerable freshwater runoff (notably from the Kuskokwim and Kvichak rivers) so that surface salinities decrease from 33 g/kg at the shelfbreak to less

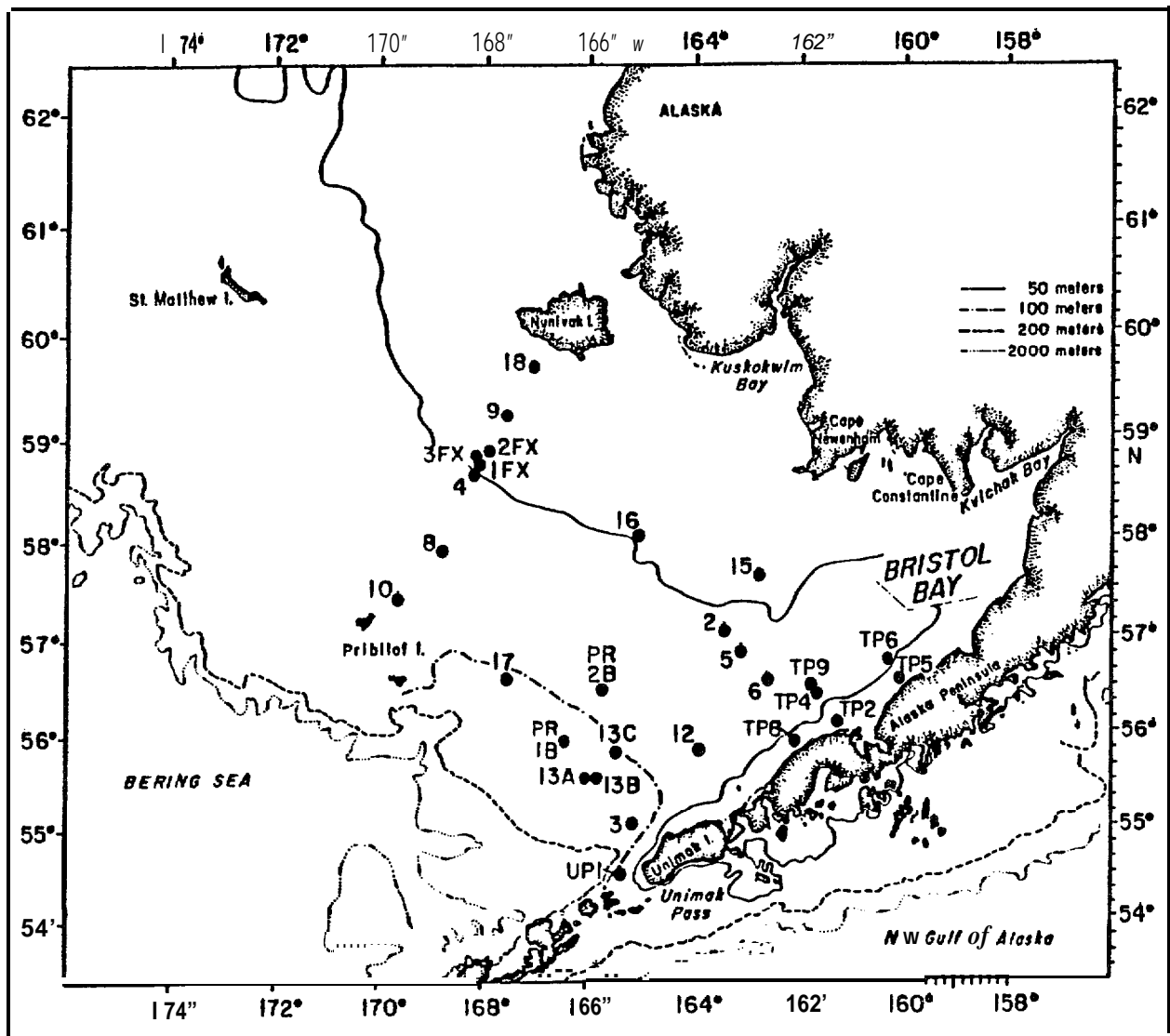


Figure B-1. - Geographic setting of the southeast Bering Sea with locations of current meter moorings. Most moorings had two current meters, one 10 m above the bottom and one 20 m below the surface. **Unless otherwise noted, e.g., the three FX moorings southwest of Nunivak Island, all moorings have a BC' prefix.**

than 31 g/kg nearshore. Ice cover is seasonal, varying from none in summer to greater than 80% coverage of 0.5- to 1.0-m thick ice during late winter in some years (Neibauer, 1980; Pease, 1980). Weather also varies with the season and is dominated by the progression of storms through the Bering (Overland, 1981; Overland and Pease, 1981). Winds during winter are generally stronger than during summer, winter storms (generally four to five per month) are more severe, and the mean winter wind is from the north. During summer, storms are weaker and less frequent, and the mean wind direction is from the south (Overland, 1980).

The shelf and oceanic domains are separated by a shelfbreak front (Kinder and Coachman, 1978), which is about 50 km wide (Fig. B-2). There is a weak westward-flowing boundary current parallel to the slope (the Bering Slope Current; Kinder, Coachman, and Gait, 1975), and eddies probably occur frequently seaward of the shelfbreak (Kinder, Schumacher, and Hansen, 1980). Farther inshore is a front, approximately parallel to the 80/100-m isobaths, which separates the three-layered stratification of the outer shelf domain from the two-layered stratification of the middle shelf domain (Coachman and Charney, 1979). Inshore of this front, a third front parallels the 50-m isobath and separates the middle shelf from the unstratified waters of the coastal domain (Schumacher et al., 1979). Kinder and Schumacher (1981a) summarized the hydrographic structure across the shelf and Coachman et al. (1980) discussed the system of fronts. The frontal system is most clearly defined during summer, but it can be distinguished throughout the year using appropriate parameters.

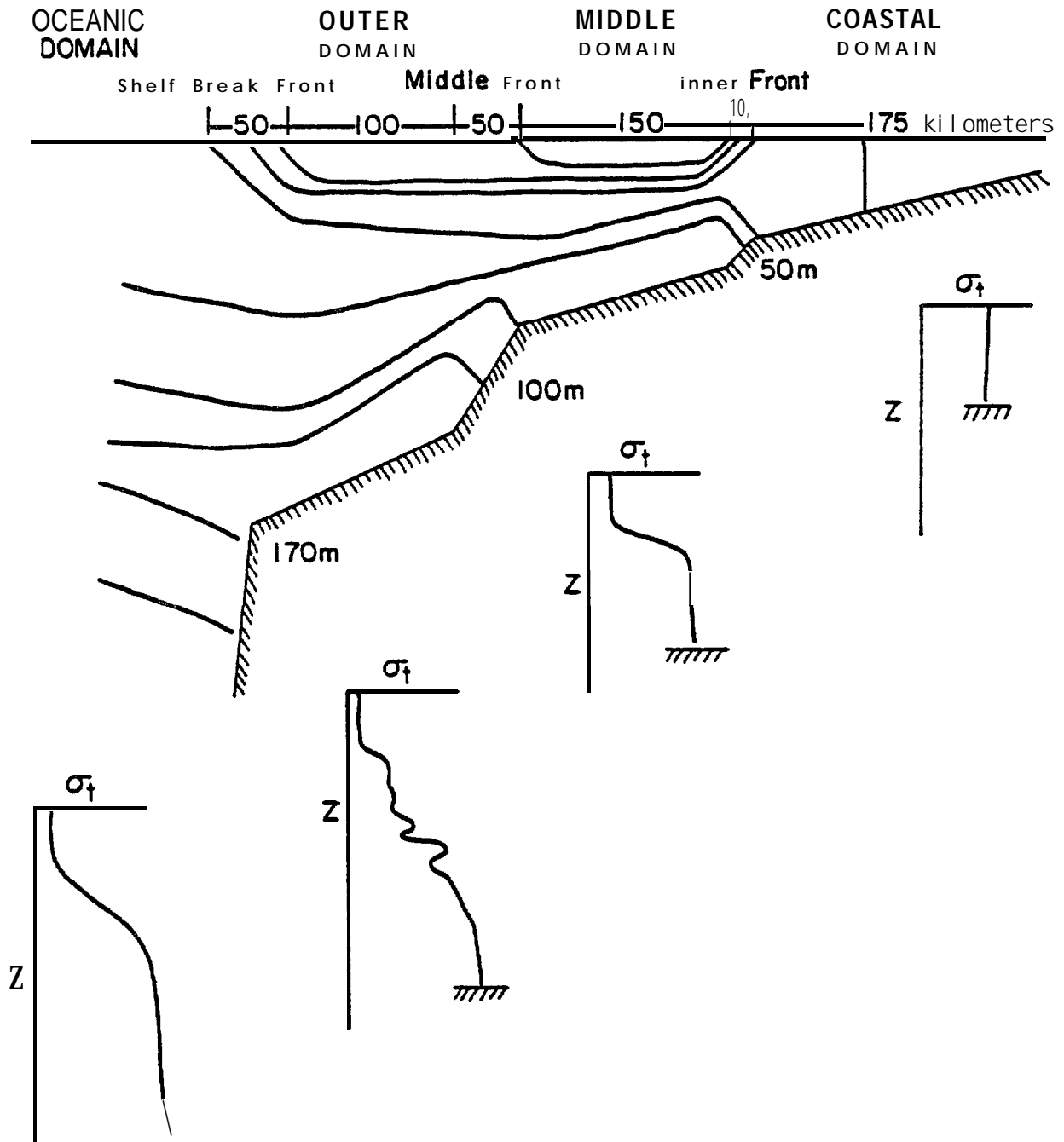


Figure B-2. - A schematic of the cross-shelf density structure illustrating the system of hydrographic domains separated by fronts. Vertical profiles are shown beneath each domain. This picture is representative of periods when there is positive buoyancy input at the surface, i.e., during summer or near melting ice.

### 3. Methods

Most of the measurements were made using **RCM-4 Aanderaa** recording current meters on taut-wire moorings. Typical instrument placement was 20 m **below** the surface and 10 m above the bottom. The subsurface flotation was usually at 18-m depth, and exerted about **1000 lb** ( $1 \text{ lb} = 4.45\text{N}$ ) buoyancy. Sampling intervals varied between 10 and 60 minutes. We estimate that directions were accurate to  $\pm 5^\circ$  and speeds to  $\pm 1 \text{ cm/see}$ , exclusive of **rotor** pumping or mooring motion.

It is known that mechanical current meters such as the **RCM-4** may give erroneous speeds because of effects from either mooring motion or **high-frequency** water motion (see **Quadfasel** and Schott, 1979, for several references.) **Pearson, Schumacher, and Muench** (1981) examined the performance of moorings like ours on the Alaskan shelves, and they found that speed differences at tidal frequencies were  $\leq 10\%$  when data from windy seasons were compared with data from calm seasons. Extrapolating their results to lower frequencies, we believe that **the effects of mooring motion and rotor pumping were minor and that errors were probably limited to a few percent increase of the speeds of** the low-frequency current (which these flows were often strongest during windy periods).

At some locations along the Alaska Peninsula, Neil Brown acoustical current (ACM) meters were used to avoid biological fouling problems that had been encountered with RCM-4 current meters. We used ten-minute averages of the original one-minute sample intervals. Accuracy is similar to that of the **Aanderaa** meters, but **rotor pumping** does not occur.

Fifty-seven current meter time series records acquired during 1975-1981 were used in this study (Table B-1). Usable record lengths varied from 36 to 246 days, the average record length was about 100 days, and the total **current-** record years was about 20. A 35-hour low-pass filter was used to separate

Table B-1. - Summary of current data. The letters indicate consecutive observation periods.

MOORING	1976	1977	1978	1979	1980	1981	
COASTAL	BC9		B C				
	BC15	A	G				
	BC16		A				
	BC18		A				
	FX1				1-10		
	FX2						
	FX3						
	TP5						
	TP2						A B
	TP8						
MIDDLE SHELF	BC2	A	C D E				
	BC4	A B	G D				
	BC5						
	BC6						
	BC8						
	BC10						
	TP4						
	TP6						
	TP9						
	UPI						
PR2B							
OUTER	BC3	A	B C				
	BC13	A	B C				
	BC17						
	PRI B						

● UPPER  
○ LOWER

sub-tidal frequencies; the data processing is described in detail in **Charnell and Krancus** (1976).

#### 4. Mean Flow

The vector mean velocity for each of the **35-hr filtered current records** is given in Table B-2. We employed a method similar to Allen and **Kundu** (1978) to define an independent time scale ( $\tau$ ), estimated as the area under the **autocorrelation** function for a particular record. The time scale  $\tau$  was then used to provide a root-mean-square error estimate E, given by

$$E = \pm \sigma / (T/\tau)^{1/2}$$

where T is the record length and  $\sigma$  the standard deviation along the vector mean **axis**. As a level of confidence in the vector mean **flow**, we used **twice** the root-mean-square error **estimate which is analogous to** a 95% level of **significance**.

The current regimes were apparent in the distribution of **mean velocity** (Table B-2, Fig. B-3). Vector mean speeds were highest in the outer shelf regime at  $3 \text{ cm s}^{-1}$  ( $>4 \text{ cm s}^{-1}$  if **BC3C** at 20 m is included), and all but one (10/11) record mean was significant. In the **middle** shelf regime the vector mean speed was c  $1 \text{ cm s}^{-1}$ . Away from the inner front (**BC2**, **BC5**, **BC6**, **BC8**, **BC10**, and **PR2B**) fewer than half (5/12) of the record means were significant. Close to the front (**BC4**, **TP4**, **TP6**, and **TP9**), most (13/16) of the record means were significant. In the coastal regime the vector mean speed was  $\sim 2 \text{ cm s}^{-1}$ , and most (15/18) of the record means were significant.

The outer shelf regime had the strongest **mean, followed by the coastal and the middle shelf regimes**. Mean flow was significant in the outer shelf and coastal regimes, but in the middle shelf regime it was significant only near **the** front. The distinctions between regimes would probably be heightened if attempts to obtain current meter records near the shelf break had not been

Table B-2. - Characteristics of observed currents.

Mooring: Depth Series (meter depth)	Mean Velocity $\pm 2$ RMS (cm s <sup>-1</sup> : 'T)	Kinetic Energy Error	Energy (cm*s <sup>-2</sup> )			Distribution	
			KE	KE'	KE <sub>T</sub>	KE <sub>L</sub>	KE <sub>M</sub>
<b>COASTAL</b>							
BC9: 41 m							
B(23)	4.6±1.8 : 305	11	424	349	<b>2</b>	41	
B(33)	3.0*1.4 : 311	5*	189	154	<b>2</b>	19	
C(23)	1.0±1.1 : 313		341	335	6	4	
C(33)	1.0±0.7 : 278	*	234	223	6	5	
BC15: 49m							
A(20)	2.4±0.6 : 270	3	<b>482</b>	477	5	<b>3</b>	
C(20)	2.3*0.6 : 271	3*	<b>489</b>	479	<b>6</b>	<b>4</b>	
L-(34)	1.0±0.6 : 302		307	300	<b>4</b>	3	
BC16: 48m							
(20)	0.9±1.0 : 307	*	410	397	5	<b>5</b>	
(37)	0.3*0.4 : 009	*	255	237	3	<b>2</b>	
BC18: 31m							
(20)	1.1±0.4 : 010	*	341	337	15	8	
FX1: 48m							
(38)	1.8±0.8 : 292	2	240	228	6	4	
FX2: 43m							
(20)	2.1*1.2 : 307	2	526	510	9	6	
FX3: 46m							
(14)	2.3±1.4 : 316	<b>3</b>	547	526	12	9	
(36)	1.8±1.2 : 293	<b>2</b>	<b>246</b>	237	8	5	
TP5: 31m							
(20)N	2.5±1.2 : 194	3	756	684	35	25	
TP2: 32m							
A(20)N	3.0±1.3 : 211	4	627	576	<b>19</b>	14	
B(20)N	1.0±0.7 : 021	*	647	628	10	5	
TP8: 31m							
(12)N	3.3±1.8 : 055	5	739	706	<b>22</b>	10	

Table B-2 (continued).

Mooring: Depth Series (meter depth)	Mean Velocity $\pm 2$ RMS Error ( $\text{cm s}^{-1}$ : °T)	Kinetic Energy ( $\text{cm}^2 \text{s}^{-2}$ ) Distribution				
		KE	KE'	KE <sub>T</sub>	KE <sub>EL</sub>	KE <sub>M</sub>
<b>MIDDLE SHELF</b>						
<b>BC2: 66m</b>						
A(20)	0.3±1.6 : 272	*	188	158	17	13
B(55)	1.2±0.8 : 089	*	199	184	10	7
C(20)	0.8±0.6 : 320	*	174	161	4	3
D(21)	0.8±1.0 : 077	*	284	253	19	13
E(20)	0.6±0.6 : 217	*	219	183	3	2
E(55)	0.2±0.4 : 261	*	162	148	2	1
<b>BC4: 56m</b>						
A(30)	2.5±2.2 : 272	3	432	390	34	27
A(47)	0.6±2.0 : 298	*	267	228	24	20
B(30)	1.9±0.7 : 286	2	337	298	20	15
C(25)	2.5*1.2 : 314	3	426	413	4	3
C(52)	1.1*0.9 : 295	3	221	215	3	3
D(20)	3.6±1.6 : 304	7	521	391	33	25
D(48)	2.9±1.4 : 305	4	187	148	24	18
E(20)	1.3*1.4 : 301	*	428	417	7	4
E(48)	0.8±1.0 : 284	*	194	190	3	2
G(18)	3.8*1.2 : 295	7	452	431	11	4
G(46)	2.1±1.2 : 302	2	158	150	6	1
<b>BC5: 70m</b> (50)	0.1±0.6 : 023	*	199	193	3	1
<b>BC6: 76m</b> (50)	1.0*0.4 : 041	*	224	221	3	2
<b>TP4: 69m</b> (63)	4.5±1.4 : 013	10	362	330	22	12
<b>TP6: 59m</b> (20)	1.6±0.8 : 058	1	643	606	16	12
(54)	1.2±0.4 : 108	*	324	311	6	4
<b>BC8: 73m</b> (54)	0.3±0.7 : 325	*	275	272	2	1
<b>BC10: 66m</b> (49)	1.0±1.3 : 171	2	232	227	3	1
<b>TP9: 89m</b> N(14)	6.1±2.4 : 040	17	455	423	21	12
<b>UP1: 84m</b> (64)	5.8±4.4 : 311	17	786	710	50	12
<b>PR2B: 89m</b> (30)	1.3±0.9 : 096	*	214	199	7	4
(60)	0.7±0.9 : 128	*	185	168	6	4

Table B-2 (continued).

Mooring: Depth Series (meter depth)	Mean Velocity $\pm 2$ RMS -1 Error (cm s <sup>-1</sup> )	Kinetic Energy (cm <sup>2</sup> s <sup>-2</sup> ) Distribution				
		$\overline{KE}$	KE''	KE <sub>T</sub>	KE <sub>L</sub>	KE <sub>M</sub>
OUTER SHELF						
<b>BC3: 115m</b>						
A(20)	4.1*3.8 : 015	8	544	384	112	46
B(105)	1.1±1.0 : 335	*	217	192		8
C(20)	16.7±6.2 : 011	140	512	352	1::	62
C(100)	6.3±1.8 : 358	20	257	212	28	19
<b>BC13: 120m</b>						
A(100)	1.8±1.4 : 343	2	109	97	8	4
B(100)	1.9*1.6: 329	2	187	171	4	2
C(96)	4.4±2.0 : 317	14	151	120	15	8
C(22)	5.3±2.8 : 333	10	304	205	75	37
<b>BC17: 104m</b> (96)	3.2±1.6 : 292	5	196	171	17	9
<b>PR1B: 124m</b> (33) (93)	1.6*2.5 : 300 2.4*1.4 : 320	<b>1</b> <b>3</b>	179 172	131 151	34 11	12 5

Where: the RMS error is defined in the text; the letter assigned to a given mooring was a sequential identification; an \* indicates that the kinetic energy of the vector mean ( $\overline{KE} = \frac{1}{2} \overline{u^2}$ ) was  $< 1.0 \text{ cm}^2 \text{ s}^{-2}$ ; the remaining KE estimates are derived from  $\frac{1}{2}$  (sum of the rotary variance) in the respective frequency bands. An n after the meter depth represents an acoustic current meter.

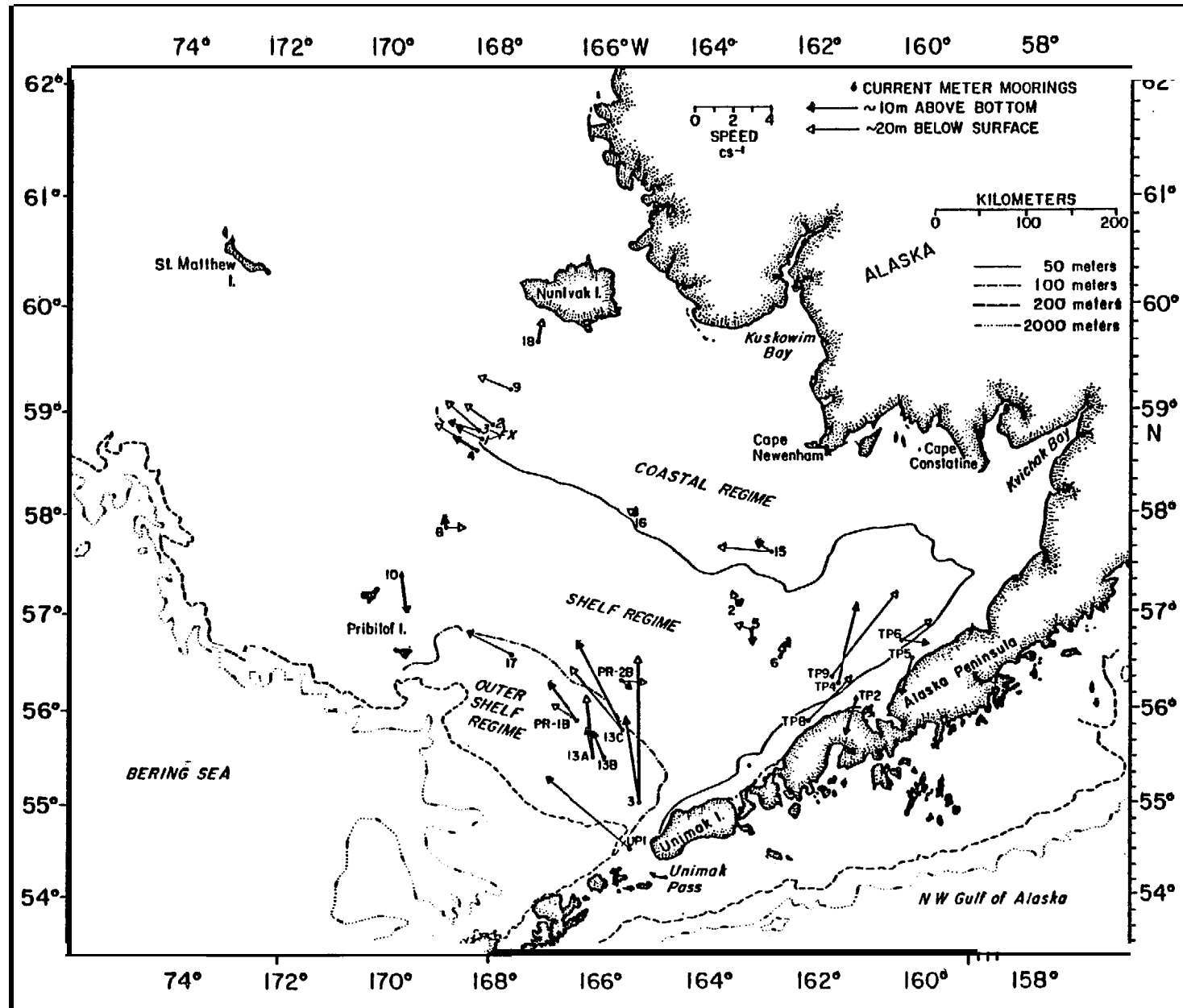


Figure B-3. - Mean flow based on all records at each mooring site. Table B-1 shows record lengths.

hampered by the intensive **bottom trawl** fishery in that area. This absence of current meter data can be partly remedied by considering **at Lagrangian** measurements. Data from shallow drogued (**~17m**) drifters, deployed over the outer shelf and **middle domains and tracked by satellite**, confirm current regime characteristics inferred **from moored data**. **Six drifters, deployed in** summer 1977 over the **outer shelf and** slope, indicated vector mean speeds **over** the outer shelf of 4 to  $10 \text{ cm s}^{-1}$  directed towards the northwest (Coachman and **Charnell**, 1979; Kinder, Schumacher, and Hansen, 1980). Two of these **i**nstruments drifted into middle shelf waters near the **Pribilof** Islands, and during this time their vector mean speeds were  $\sim 1.0 \text{ cm s}^{-1}$ . **Three** drifters launched in June 1976 (in the middle shelf domain between **BC2** and **BC6**) indicated vector mean speeds  $< 1 \text{ cm s}^{-1}$  towards the northeast over a 100-day period (Kinder and Schumacher, **1981b**).

Vector mean flow over the outer shelf and coastal regimes generally had **larger** along-isobath than cross-isobath components. For most of the outer shelf regime, **isobaths** are aligned such that **315°T** and **045°T** can be taken as along-shelf and cross-shelf axes. Resolving all outer shelf vector mean currents along these axes yields mean along-shelf currents of 4.1 and  $2.6 \text{ cm s}^{-1}$  at the upper and lower observation levels with cross-shelf components of 3.1 and  $0.9 \text{ cm s}^{-1}$  at the same levels. For the coastal regime, we used the orientation of the 50-m isobath to define the along- and across-isobath currents. Along the Alaska Peninsula **060°T** is the along-shelf direction, **270°T** applies in the vicinity of **BC15**, and **315°T** is used between Cape Newenham and Nunivak Island. The cross-isobath component is directed toward the middle shelf regime. Resolving significant vector mean currents from coastal and nearby middle shelf moorings along these axes yielded along-isobath currents of 2.8 and  $1.6 \text{ cm s}^{-1}$  at upper and **lower** levels and cross-isobath components of  $0.5$  and  $0.1 \text{ cm s}^{-1}$ , respectively.

## 5. Low-Frequency Currents

To illustrate the time-dependent nature of the low-frequency currents, progressive vector diagrams (**PVD's**) characteristic of the behavior in each of the regimes are shown in Fig. B-4. Each PVD was constructed from 100 days of current observations collected during winter and summer in each of the three current regimes. (Note that the length scales are different for each record). The **outer shelf records had excursions of ~500 km in 100 days, maximum 5-day velocities of 20 to 30 cm s<sup>-1</sup>, numerous low-frequency events of variable speed and direction, and periods of very weak flow.** The examples of middle shelf regime flow show net 100-day excursions of **150 km** (for **BC-2D** during winter] but only 4 km **at BC-5**, with maximum 5-day velocities of 4 to 8 cm s<sup>-1</sup>. We note **that about one-half of the net excursion at BC-2D occurred during one 10-day period of eastward flow.** No persistent mean-flow or low-frequency fluctuations appear in either record. The **PVD's** from the **coastal regime indicate currents with the most persistent directions, although 5-day excursions included some reversals and periods of no net flow. Maximum excursions of 25 and 85 km with speeds of 6 and 20 cm s<sup>-1</sup> were observed for BC 15 and 9, respectively.** Thus, subtidal currents in the outer shelf and coastal waters were a resultant of low-frequency pulses superimposed on a significant mean flow component. Pulses in the coastal regime tended to **be along the mean flow axis and of short duration (≤10 days), whereas in the outer shelf regime pulses had components both along and orthogonal to the vector mean (i.e., the isobaths) and were persistent over longer periods.** In the middle shelf regime a super-position of pulses of variable direction led to very weak (**~1 cm s<sup>-1</sup>**), statistically insignificant, vector mean **flows.**

A further dynamical characterization of the flow field within the three regimes is made by determining the frequency distribution of horizontal

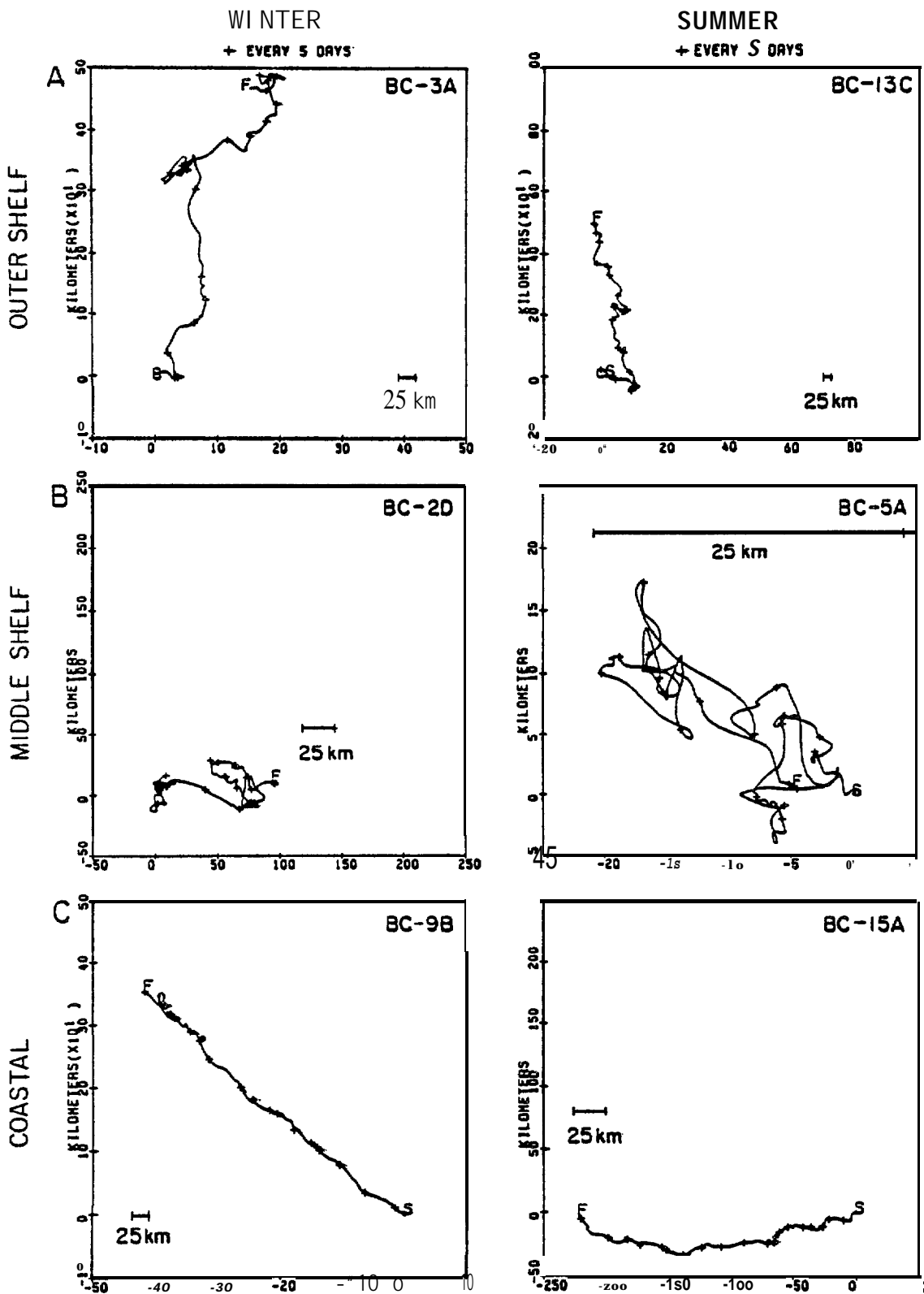


Figure B-4. - Progressive vector diagrams for winter and summer conditions in the outer, middle, and coastal regimes. A 25-km scale parallel to the east-west axis is shown on each PVD since scales are different. (S signifies the start and F the finish of each plot.)

**kinetic energy per unit mass** (KE; Table B-1). Rotary spectra were calculated from the 2.9 and **35-hr**, low-pass-filtered current records. Spectra of the first series were used to determine kinetic **energy in semidiurnal** and diurnal tidal frequency bands ( $KE_T$ ) and, by summing over all **bands, the total fluctuating kinetic energy** ( $KE'$ ). Spectra of the second current series **provided estimates of low-frequency** ( $f < 0.5$  cpd) kinetic energy ( $KE_L$ ). We assigned that subset of low-frequency energy between 0.5 and 0.1 cpd to kinetic **energy related to meteorological forcing** ( $KE_M$ ). This band encompasses important meteorological forcing in the Bering Sea (see Section 6, below), although other mechanisms also can function at these frequencies.

We present  $KE_L$ ,  $KE_M$  and [ $KE_L - KE_M$ ] versus water depth for each current record (Fig. B-5). The highest energy levels were observed over the outer shelf, with moderately high levels in the coastal regime. All records except **UP1** from the coastal **or middle shelf** regimes with  $KE_L > 20 \text{ cm}^2 \text{ s}^{-2}$  had a substantial portion of their observation period during winter. A similar trend of energy versus depth of water was found at meteorological frequencies;  $KE_M$  levels were generally **higher in the outer shelf regime, low in the middle shelf regime, and some records (from winter) in the coastal regime** showed moderately high levels. The difference between  $KE_L$  and  $KE_M$  (Fig. **B-5c**) indicates that records **with non-meteorological, low-frequency energy**  $> 10 \text{ cm}^2 \text{ s}^{-2}$  were either from the **outer shelf regime or from moorings located near the coast**.

Mean kinetic energy over all records in each regime confirmed that the outer shelf regime is more energetic at subtidal frequencies (Table B-3).

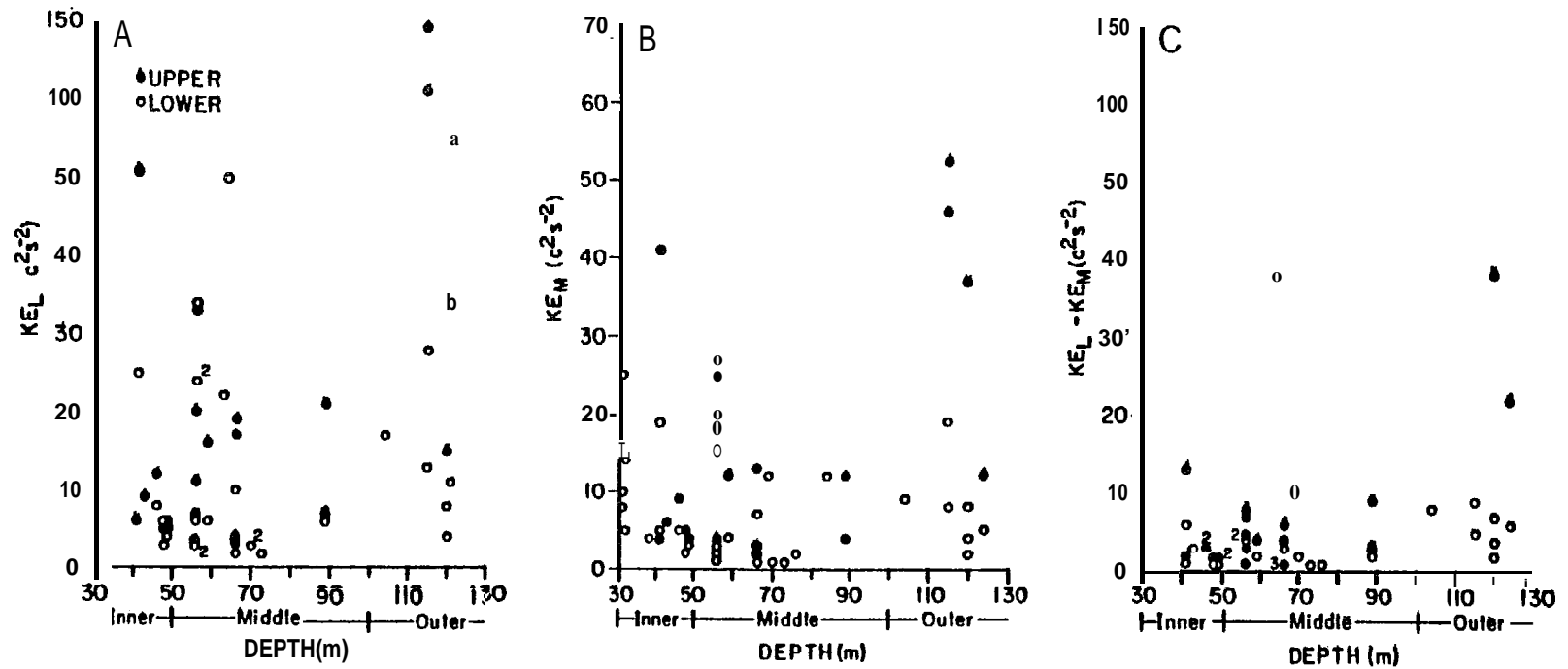


Figure B-5. - Estimates from all records of (A)  $KE_L$  (total low frequency energy), (B)  $KE_M$  (kinetic energy between 0.5 and 1.0 cpd), and (C)  $KE_L - KE_M$  versus mooring depth. Note that the record which indicates energy greater than  $20 cm^2 s^{-2}$  in the middle regime is from UP1, in Unimak Pass. (For A and C the vertical scale changes units after  $50 cm^2 s^{-2}$ ; the small numbers represent repeated values.)

Table B-3. - Mean values of kinetic energy.

Regime	Number of Records	$KE_T \pm \text{St. D.}$	$KE_L \pm \text{St. D.}$	$KE_M \pm \text{St. D.}$	$KE_L / KE_T$ (% $\pm$ St. D.)	$KE_M / KE_L$ (% $\pm$ St. D.)
Outer	11	199*91	41 $\pm$ 48	19 $\pm$ 20	13 $\pm$ 8	50 $\pm$ 9
Middle	28	289*145	12 $\pm$ 10	8 $\pm$ 8	4 $\pm$ 3	64 $\pm$ 17
Coastal	18	410*170	14*13	10*10	4 $\pm$ 4	69 $\pm$ 13

All units are  $\text{cm}^2 \text{s}^{-2}$ . The **ratios** were calculated by determining each record's ratio and then **forming** a mean value; all values were rounded to the nearest integer.

We tested the hypothesis that the difference between any pair of the mean percent of  $KE_L$  was not **equal** to zero at the **95% level** of confidence using a two-sample "t-test" (**Freund, 1971**). The results indicate that a statistically significant difference existed between outer shelf and either middle **shelf** or coastal regime **values** of percent of  $KE_L$ , but that estimates from the latter two regimes were not significantly different.

Examination of  $KE_L$  values supports the concept **of** a distinction only between outer **shelf and both of the two shoreward regimes**. The lack of a significant difference between energy **levels** in the middle shelf and coastal regimes suggests that the dominant forcing mechanism for **low** frequency flow in these regimes is similar. In both regimes,  $KE_M$  accounted for approximately 'We-thirds' of 'EL' compared to **one-half** in the outer shelf regime. (The **difference between the mean** percent of  $KE_M$  over the outer shelf and that **applicable to either middle shelf** or coastal regime records is statistically **non-zero**.)

Bristol Bay weather is dominated by storms that migrate through the area; thus winds tend **to** rotate around the compass (Overland, **1981**; Overland and Pease, **1981**). Such rotation is reflected in current response as **loops** with **2-** to 5-day time scales in the **PVDS** **eras** **rotating vectors** (**Fig. B-6**). The **exact nature of the current** response varies with the translation velocity and intensity of the storm and with pre-storm characteristics of the current and mass field. **As an example, we present in Fig. B-6 the current response to a typical March** cyclone during a period when there are records from all three regimes. The **track** of the **low-pressure** center (Mariner's Weather Log, 1977) indicated that it was located at **~ 52°N, 170°W** on **24 March** 0000 GMT, and that by **1200** it had crossed the Aleutian **chain and was located north of Unimak** Island (**55.5°N, 164°W**). On the following day (0000 GMT, 25 March), the center had crossed the Alaska Peninsula and was located **at ~58°N, 155°W**. This storm passed close to **BC-13** and **BC-2** and continued approximately 100 km south of **BC-9**. The strong winds associated with this storm blew first toward the **northwest and then veered to southeastward as the storm passed a given location. North of the center, winds were initially more westward, then shifted to eastward.** The change in current direction reflected rotating wind **vectors** and the storm's influence was apparent for about 3 days. We thus interpret many of the **2- to 10-day** loops in the PVDS (like those in Fig. B-4) to be storm responses.

## **6. Seasonal Variations of Meteorological and Oceanographic Characteristics**

Before examination of **seasonal characteristics in the current records, we** establish general climatology' **ical** conditions and the associated wind conditions in the study area. Overland and Pease (1981) have produced maps of storm counts

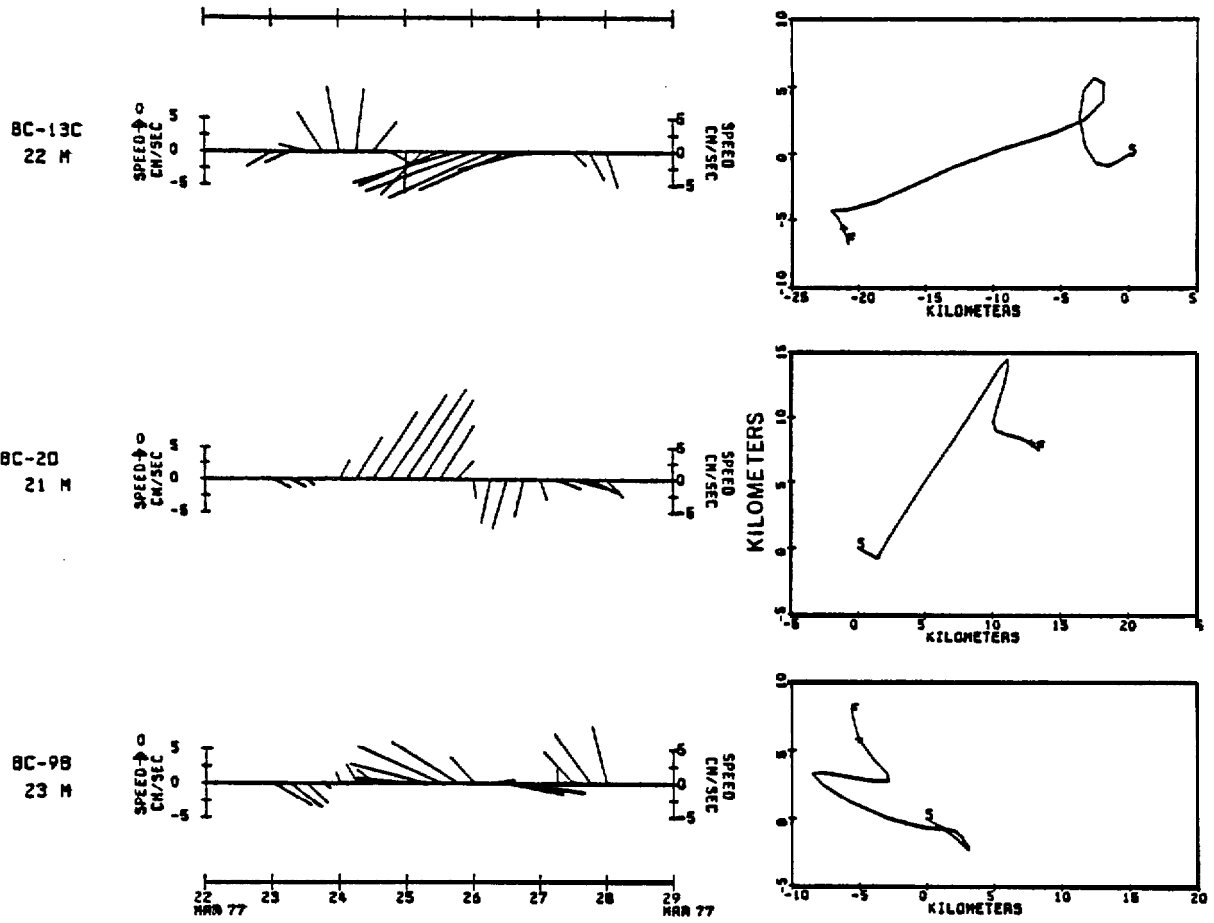


Figure B-6. - An example of current response depicted as 6-hr vectors and PVDS to a storm which transverse the outer, middle, and coastal regimes.

from October through March by **2°- latitude** by 40-Longitude squares for 23 years of observations (see their Figure 2). The postmarked feature of **these maps relevant** to the study area is that there are significantly more storms **over the outer shelf and adjacent basin than over the middle shelf**. For example, during the 23 Novembers there were more than 60 storms over the former outer shelf less than 30 over most of the middle shelf. There is also a tendency for more storms along the Alaska Peninsula (40) than over the middle shelf (30). **Using a climatic atlas (Brower et al., 1977)**, we can extend the results of Overland and Pease to include April through September. Scalar mean winds over the outer shelf regime are greater than those over the **middle shelf and coastal regimes for April, May, and September** (by 28, 25, and 12 percent), respectively. During June, July and August there is little difference throughout the study area.

**Geostrophic** winds were computed by Fleet Numerical Weather Central (Bakun, 1973) from a 3°- latitude by 3°- longitude model grid and interpolated to a surface **position near mooring EC-2** for the **6-yr. period September 1975 to September 1980**. The resulting speeds are plotted in Fig. B-7 where the values are the average of the six monthly means for both speed and variance of speed. Using the six-year mean wind speed ( $7.4 \times 1.7 \text{ ms}^{-1}$ ) and mean **variance** ( $14.1 \times 4.2 \text{ m}^2 \text{ s}^{-2}$ ) as guidelines, 'summer' is defined as June through August and 'winter' as October through March, with the remainder being transitional. With these definitions of summer and winter, we present current characteristics from representative current record segments from **each of the regimes** (Table B-4).

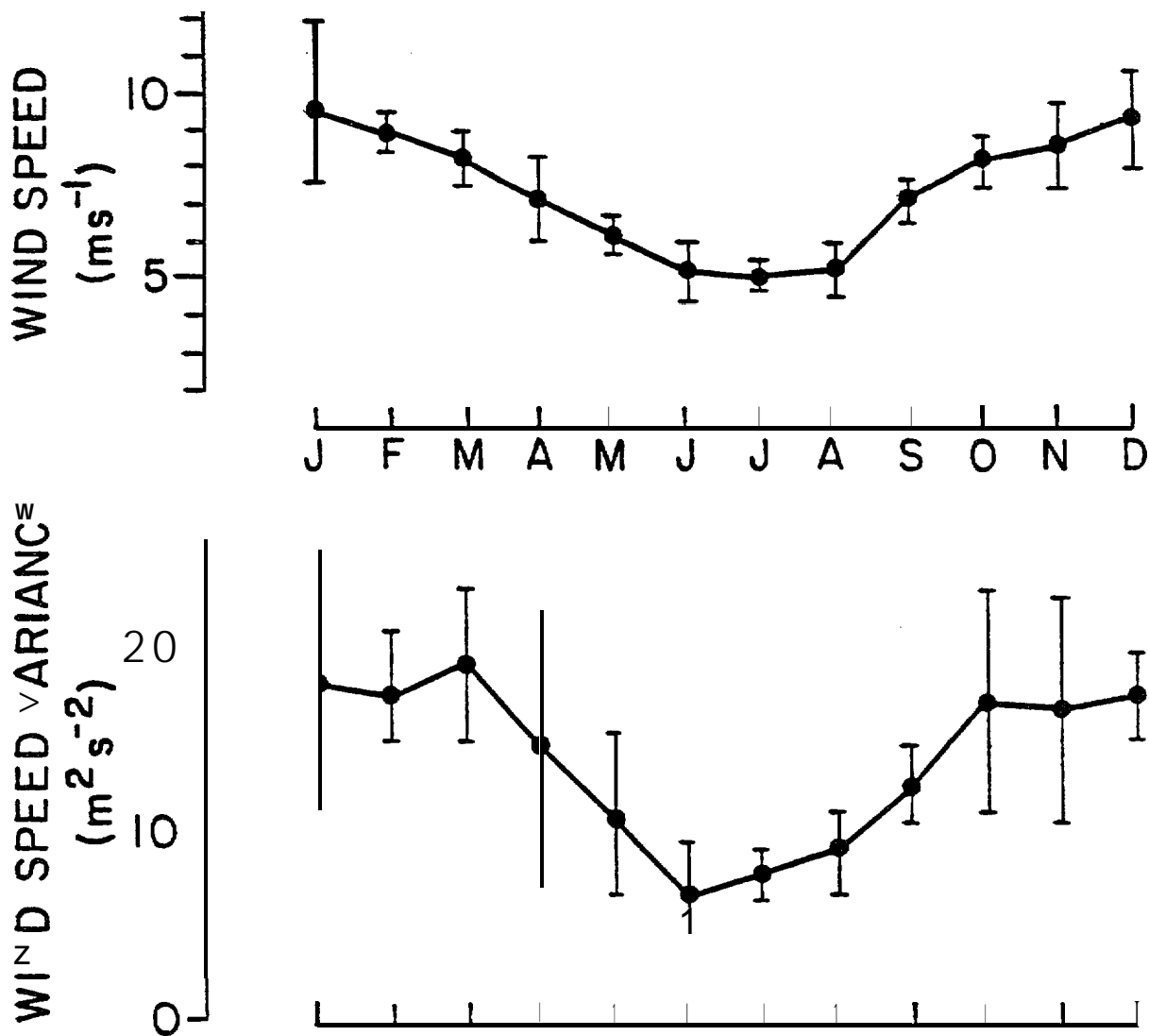


Figure B-7. - Mean and variance of wind speed from monthly averages of surface geostrophic wind between September 1975 and September 1980. The error bars represent the standard deviation for each value.

Table B-4. - Seasonal characteristics of currents.

Mooring (instru. )	Segment Length (days)	Vector (cm s <sup>-1</sup> : °T)	Mean (T)	KE <sub>L</sub> (cm <sup>2</sup> s <sup>-2</sup> )	KE <sub>M</sub> (cm <sup>2</sup> s <sup>-2</sup> )	Mooring	Vector (cm s <sup>-1</sup> : °T)	Mean (T)	KE <sub>L</sub> (cm <sup>2</sup> s <sup>-2</sup> )	KE <sub>M</sub> (cm <sup>2</sup> s <sup>-2</sup> )
		WINTER			SUMMER					
				COASTAL						
BC9B(23)	92	6.2:310	60	45	BC9C(23)	1.0:303	6	4		
(33)	92	4.0:317	24	20	(33)	1.0:275	6	4		
TP5 (20)	38	4.0:178	37	21	TP5(20)	2.3:171	14	11		
				MIDDLE SHELF						
BC2B(50)	92	1.8:081	72	9	BC2E(50)	0.2:232	2	1		
D(21)	92	1.1:085	19	12	BC2E(20)	0.4:197	2	1		
BC4D(20)	54	3.1:315	33	24	BG4G(18)	2.1:296	11	5		
O(48)	40	2.6:314	11	6	E(49)	0.9:284	3	2		
B(30)	50	3.9:335	23	16	C(25)	2.5:346	4	3		
PR2B(30)	45	2.1:107	14	7	PR2B(30)	0.7:025	4	2		
(60)	45	1.1:148	12	5	(60)	0.4:034	3	2		
				OUTER SHELF						
BC3A (20)	92	5.6:018	123	47	BC3C (20)	15.6:008	123	48		
BC13C(96)	36	3.0:318	14	4	BC13B(100)	1.9:329	5	1		
PR1B (33)	60	1.7:353	34	12	PR1B (33)	3.9:262	18	5		
(93)	60	1.4:346	12	5	(93)	2.9:316	7	4		

Within the coastal regime, winter currents were more energetic in kinetic energy of the vector mean flow,  $KE_L$  and  $KE_M$ ; energies increased above the summer values by about 2 to 38 times, 3 to 10, and 2 to 11 times in the respective bands. The magnitude of vector mean speeds also showed substantial increases, but direction varied by less than 45°. The middle shelf regime also exhibited a substantial increase in kinetic energy from summer to winter with changes in  $KE_L$  and  $KE_M$  ranging from about 3 to 10 times and 2 to 12 times, respectively; the seasonal change in vector mean speed at BC4 was similar to that observed in coastal records. There were, however, substantial changes in direction at both BC2 and PR2B. Over the outer shelf the seasonal

change in kinetic energy was less than observed in the other **two regimes**, and **furthermore**, **outer shelf** vector mean speeds were greater in summer. **(We note that for these records, the average  $KE_T$**  in a given regime varied between seasons by **less than 18% with** the largest seasonal changes occurring in the **coastal and middle shelf** regimes. Here,  **$KE_T$  was** generally less in winter than in summer. Because this reduction was accompanied by changes in phase, **it** has been **suggested** (Pearson, **Mofjeld, and Tripp, 1981**) **that ice cover alters the** propagation characteristics of the tidal waves on the shelf.) These comparisons are consistent with the proposition that meteorological forcing of low-frequency currents is important in all three regimes, but dominant only in the coastal and middle shelf regimes. In the outer shelf regime, the lack of seasonal **correlation between current and wind strengths**, and the large values of  $K_L - K_M$  strongly suggest a **non-meteorological** cause.

#### 7. Causes of the Mean Circulation

The mean circulation of the southeastern Bering Sea shelf is now well defined (Fig. B-3). There is a low-speed current (1-5 cm S-I) in the coastal regime, perhaps more concentrated in the vicinity of the 50-m isobath and inner front, which flows northeast along the Alaska Peninsula, around Bristol Bay, and then northwest past Nunivak Island. Water to maintain this circulation is from the southeast corner of the basin and from the Alaskan shelf south of the peninsula via Unimak Pass (Schumacher, Pearson, and Overland, 1982), reinforced by freshwater that accumulates inshore of the inner front.

There is no significant mean circulation within the middle shelf regime.

In the outer shelf regime there is a low-speed northwesterly drift (1-10 cm  $s^{-1}$ ) toward the **Pribilof** Islands, which is perhaps more concentrated near the 100-m isobath and **middle front**. **Water to** maintain this circulation flows

also from the southeastern corner of the basin with a **possible** contribution from Unimak Pass.

The tendency for mean flows in both outer and coastal regimes to parallel **isobaths** suggests that they are at least in part driven by cross-shelf variations in the mass field. Although inferring currents from dynamic calculations in shelf seas is tenuous, on the southeastern Bering Sea shelf approximate agreement with direct measurements is observed. Dynamic topographies for the outer **shelf** regime (Kinder, 1977; Kinder et al., 1978; Coachman and Charnel, 1979) indicate a northwestward **baroclinic** flow of  $\sim 5 \text{ cm s}^{-1}$ , in agreement with the measured mean flows. **Baroclinic geostrophic** currents and measured mean flow along the 50-m isobath from Cape **Newenham to Nunivak** Island also agree (Schumacher et al., 1979). Further, the freshwater flux into the coastal domain has a **long** residence time so that during winter when the  **$\sim 10$ -km-wide** inner front often vanishes, horizontal pressure gradients still exist between the coastal and middle shelf domains (Kinder and Schumacher, 1981b). We used **hydrographic** data collected through the ice in February 1978 to compute **geostrophic** speeds of 3 to 4  $\text{cm s}^{-1}$  toward the northwest in the vicinity of **BC-4**. Dynamic topographies previously computed over the middle regime suggested either very weak flow towards the southeast (Kinder, 1977; Kinder et al., 1978) or spatially complex and weak flow (Reed, 1978). In Fig. B-8 we present a composite of dynamic relief, based on data collected on six cruises during summer in 1975, 1976, 1980, and 1981. Dynamic height contours are shown only for synoptic data (over the outer shelf), and the differences in dynamic heights across a particular section are presented for sections not occupied on the same cruise. In general, calculated **geostrophic** flow in the outer and coastal regimes approximates the observed vector mean currents, and the weak and variable dynamic height differences of the middle shelf agree with the negligible mean currents directly observed in this regime.

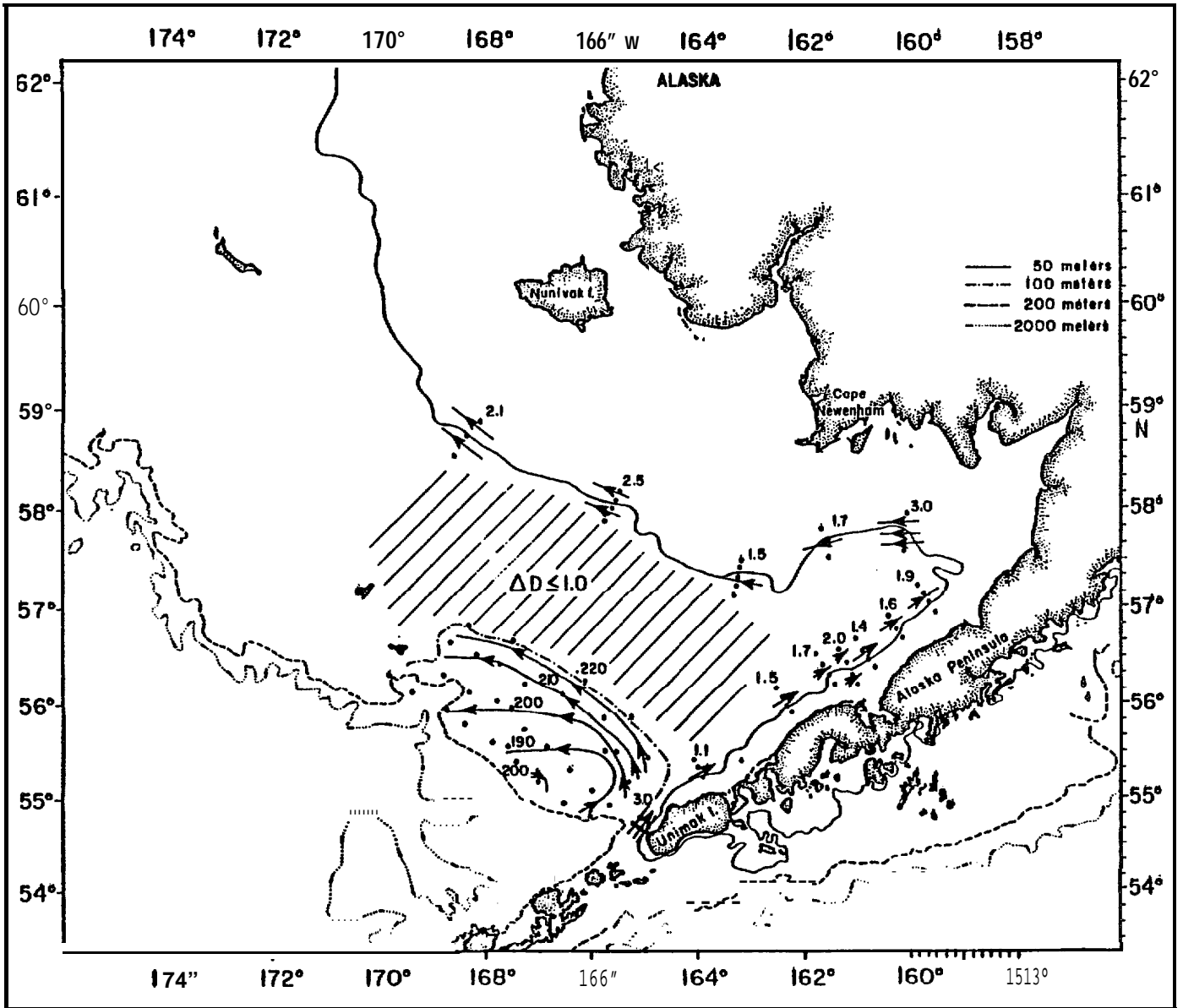


Figure B-8. - A compilation of hydrographic data from six cruises during summer conditions presented as dynamic relief contours (0/80 dbar) for the outer shelf and dynamic height (0/40 dbar) difference along sections normal to the inner front. The dots represent CTD station locations and the contour interval is 1 dyn cm. The shaded portion of the middle shelf regime shows that  $\Delta D \leq 1$  dyn cm (0/40 dbar) throughout this area for the six cruises.

There are other mechanisms that might contribute to driving mean flow, including various interactions of tidal currents with the topography. The **largest tidal amplitudes are found along the Alaska Peninsula where the nearly rectilinear  $M_2$  tide has an amplitude of  $\sim 35 \text{ cm s}^{-1}$  (Pearson, Mofjeld, and Tripp, 1981).** The  $M_2$  constituent contributes 53, 67 and 75 percent of  $KE_T$  in the inner, middle, and outer shelf regimes, respectively, and thus is a possible source for generating residual flow.

**Residual current can be generated by the interaction of oscillating velocity with either sea surface height or mean depth. Longuet-Higgins (1969) described in theoretical terms the former mechanism.** This mode of interaction generates a Stokes drift whose velocity is scaled by  $\bar{\eta} \bar{u} / h$ , where  $\eta$  is the perturbation about mean sea level ( $h$ ) and  $u$  is the tidal velocity. Throughout most of the study area  $\bar{\eta} \approx 0.5 \text{ m}$ ,  $h \approx 55 \text{ m}$  and  $\bar{u} \approx 20 \text{ cm s}^{-1}$  so that the depth-averaged Stokes velocity is less than  $1.0 \text{ cm s}^{-1}$ , but along the Alaska Peninsula and in inner Bristol Bay where tidal heights and speeds are maximum, Stokes **velocities could be as large as  $5 \text{ cm s}^{-1}$ .** Thus, this mode of interaction between tides and topography may be important in the shallow coastal regime, but not over the entire shelf.

The interaction of oscillating tidal currents with mean depth and changes in depth was examined by Robinson (1981), and Loder (1980) presented convincing evidence that this mechanism results in significant mean flow around **Georges Bank**. This mechanism requires changes in mean depth normal to the tidal flow. Over the **study** region, strong tidal currents flow normal to the **isobaths** only in **the** coastal regime away from the Alaska Peninsula (Pearson, **Mofjeld**, and Tripp, 1981, Figure 8-13). Over **most of** the shelf (away from the Peninsula) **the bottom** slope is extremely small (less than  $10^{-4}$ ) except in the vicinity of the middle and inner fronts where the slope is about  $0.5 \times 10^{-3}$ . Even where

mean velocity is statistically significant, it is small so that following **Loder** (1980) we assumed weak nonlinearity so that the depth-averaged Eulerian velocity is approximated by his equation (29):

$$\bar{V} \sim - \frac{H_d U_d^2 f dH/dx}{2\omega^2 H^2} \frac{3Hd - 2}{H}$$

where  $H_d$  is the depth on the deep side of the bathymetric feature,  $U_d$  is the cross-isobath tidal velocity at frequency  $\omega$ ,  $H$  is the depth at the location of interest and  $f$  is the local **Coriolis** parameter. Using observed values, we estimate along-isobath speeds of about 2 to 4 cm s<sup>-1</sup> in the vicinity of the inner and middle fronts. **Robinson** (1980) also provided equations for magnitude estimates which have the form  $v \sim 0.11\Delta h/h$  and  $v \sim 0.225\Delta h/h$  for the middle and inner front regions. The maximum change in depth is  $\sim 10\%$  and 5% for the two regions and therefore this approach for scaling residual tidal speeds gives magnitudes of about 1 cm s<sup>-1</sup>. These estimates of along-isobath velocities generated by tidal interaction with bathymetry are consistent with our observations of vector mean flow, so that such interactions may be important in the two regions noted above.

## 8. Causes of Low-Frequency Fluctuations.

That portion of the  $KE'$  associated with periods greater than 10 days (i. e.,  $KE'_L - KE'_M$ ) was most evident in current records from the outer shelf (cf. Figures 4A and 5C). **Csanady** (1978) and **Beardsley** and **Winant** (1979) suggest that interaction between oceanic circulation seaward of the shelf and shelf bathymetry can produce mean and low frequency shelf currents. **Lagerloef**, **Muench**, and **Schumacher** (1981) show that in the Gulf of Alaska a current component existed at periods greater than 10 days and was stronger than the

seasonal signal. Smith and **Petrie (1982)** suggest that over the **Scotian shelf** topographic **Rossby** waves resulted in enhanced kinetic energy at oceanic forcing periods (10 to 90 days) and **alongshelf** current pulses. Flow over the basin adjacent to the present study area includes **mesoscale** features that can persist for months (**Kinder, Schumacher, and Hansen, 1980**). The interaction of such **features and** possibly Rossby waves (**Kinder, Coachman, and Gait, 1975**) with shoaling shelf bathymetry could result in the observed kinetic energy at time scales between those of storm and seasonal forcing.

The observed spatial and seasonal wind behavior was manifested in current kinetic **energy**: winter being more energetic and energy levels being greater over the outer shelf. The spatial change in fluctuating wind energy may drive the **convergence between the outer and the middle shelf regimes** that is implied from the lack of mean flow in the latter regime. Coachman (1982) reported a **convergence of  $\sim 3 \text{ cm s}^{-1}$**  from one month's records collected at the same locations as **PR 1B** and **PR 2B** and suggests that this may be due either to atmospherically forced 'sloshing' of water on the outer shelf or to fluctuations in the oceanic forcing. Because the climate is dominated by storms, vector **mean winds** tend to be weak. Direct observations of wind on St. **Paul** Island indicate that the strongest monthly mean was only  **$\sim 3.4 \text{ in s}^{-1}$**  toward the southwest (**Brewer et al., 1977**). Thus, winds **likely** contribute little to mean **current** generation in any of the regimes. Further, since most of the outer and middle **shelf waters** are farther than a **Rossby** radius from the coast, they respond by **following** the rotating winds.

## 9. summary

Using rotary spectral and standard statistical techniques, we analyzed an accumulation of ~20 years of current records from twenty-five locations on the vast southeastern Bering Sea shelf. The results permit a general characterization of mean and low-frequency current and kinetic energy regimes that exist in these three zones differentiated by depth and hydrography--coastal, middle shelf, and outer shelf.

**Coastal:** This regime is bounded by the coastal boundary layer and by the 50-m isobath or inner front. **Vector mean** flow parallel to the 50-m isobath is **statistically significant**. Speeds paralleling this feature are generally **between 1 and 6 cm s<sup>-1</sup>**, with the higher values during winter. **The coastal current was observed from the vicinity of Unimak Pass, along the Alaska Peninsula to the vicinity of Nunivak Island. Although kinetic energy in this regime is dominated by tides (~96%), significant energy at meteorological frequencies can be clearly distinguished as current pulses. Because vector mean winds are weak, we believe wind-driven circulation contributes little to the observed mean flow; instead, a combination of baroclinic geostrophic current and current generated as a result of interaction between tides and shoaling bathymetry are the primary forcing mechanisms.**

**Middle Shelf:** This regime is bounded by the **50-m** and 100-m **isobaths**, and hence by the inner and middle **fronts**. **Vector mean flow within this regime is not significant except near its boundaries, where it parallels isobaths.** As is the case with the coastal regime, **kinetic energy in this regime is mostly at tidal frequencies. Kinetic energy at meteorological frequencies is only slightly less than in the coastal regime, but the lack of coastal boundaries precludes large changes in sea level and resultant rectification of current pulses,so** that currents respond to the wind as rotating vectors.

Outer shelf: This regime lies between the 100-m isobath and the shelf break or **the middle and shelf break fronts**. **Vector mean flow is statistically significant, with along- (toward the northwest) and across- (toward the northeast) isobath** speeds generally between 1 to 10  $\text{cm s}^{-1}$  and <1 to 5  $\text{cm s}^{-1}$ , respectively. In this regime,  $\text{KE}_T$  accounts for about 60% of the fluctuating kinetic energy, and both  $\text{KE}_M$  and energy at oceanic forcing frequencies are greater here than in the other regimes. Estimates of both baroclinic geostrophic speeds and those generated by tidal interaction with shoaling bathymetry (under the middle front) are similar in magnitude and direction to the observed flow along **isobaths**. The cross-shelf flow may be a response to wind forcing at higher frequencies. The kinetic energy at oceanic forcing frequencies, however, is of equal magnitude to that in the meteorological forcing frequency (cf., Table B-3).

Although this analysis provides a picture of the general circulation over the southeastern Bering Sea and its differentiation by regimes related to depth and forcing mechanisms, many questions still remain regarding the dynamics responsible for observed features. In particular, why is the low-frequency energy, which is abundant over the outer shelf, not propagated into the middle shelf? Further, no measurements are available to relate pressure and current fields in the Bering Slope current, whose flow **field** has been interpreted as planetary waves interacting with the slope (Kinder, Coachman, and Gait, 1975), with those over the outer shelf.

## ACKNOWLEDGMENTS

We acknowledge the aid of a large number of persons, not only in the preparation of this paper but in carrying out the field work and data processing which have led to its existence. Most of the current **meter data** were obtained during a project on which we were co-investigators with L. K. Coachman and the late R. L. **Charnell**. In particular, we thank Dr. Coachman for both useful discussions and current meter data from the PROBES moorings.

This study was supported in part by the Bureau of Land Management through interagency agreement with the National Oceanic and Atmospheric Administration, under which a **multiyear** program responding to needs of petroleum development of the Alaskan continental shelf has been managed by the Outer Continental Shelf Environmental **Assessment** Program (OCSEAP) Office, Juneau, Alaska.

REFERENCES CITED

- Allen, **J.S.** and **P.K. Kundu**, 1978. On the momentum, **vorticity** and mass balance on the Oregon Shelf. **J. Phys. Oceanogr.** , **8**: 13-27.
- Bakun**, A., 1973. Coastal **upwelling** indices, west coast of North America, 1946-71. U.S. Dept. of Commerce, **Tech Report NMFS S5RF-671**. NOAA Seattle, **WA**.
- Beardsley, R.C.** and **C.N. Flagg**. 1976. The water structure, mean currents, and **shelf-water/slope-water** front on the New **England** continental shelf. Mere. Soc. Roy. **Sci. Liège**. Ser 6. **10**:209-225.
- Beardsley, R.C.** and **C.D. Winant**, 1979. Mean circulation in the mid-Atlantic bight. **J. Phys. Oceanogr.** , **9**: 612-619.
- Brewer, W.A., **H.F. Diaz**, **A.S. Prechtel**, **H.W. Searby** and **J.L. Wise**, . 1977. Climatic Atlas of the Outer Continental Shelf Waters and Coastal Regions of **Alaska**, Vol 1, U.S. Dept. of Commerce/NOAA, Arctic **Envir. Info.** and Data **Center Anchorage, AK**: 443 pp.
- Charnell, R.L.** and **G.A. Krancus**. 1976. A processing system for Aanderaa Current Meter Data. NOAA Tech. Memo. ERL PMEL-6, 50 pp.
- Coachman, **L.K.** and **R.L. Charnell**. 1979. On lateral water mass interaction - a case study, Bristol Bay, Alaska. **J. Phys. Oceanogr.** **9**(2): 278-297.
- Coachman, L.K., **T.H. Kinder**, **J.D. Schumacher**, and **R.B. Tripp**. 1980. Frontal systems of the southeastern Bering Sea Shelf. In: Stratified Flows, 2nd Int. Assoc. Hydraulic Res. Symposium, **Trondheim, June 1980** Carstens and **T. McClimans**, Eds., **TAPIR Publishers, Norway**: pp. 917-933. "
- Coachman, L. K., 1982. Flow convergence over a broad, **flat** continental shelf. In press, Continental Shelf Res. , Vol 1.
- Csanady, **G.T.** 1976. Mean Circulation in Shallow Seas. **J. Geophys. Res.** **81**(30): 5389-5399.
- Csanady**, G.T., 1978. The arrested topographic wave. **J. Phys. Oceanogr.** , **5**: 231-244.
- Fischer, H.B.** 1980. Mixing Processes on the Atlantic Continental Shelf, Cape Cod to Cape Hatteras. **Limnol. Oceanogr.** 25(1) : 114-125.
- Flagg, C.N.** and **R.C. Beardsley**. 1978. On the stability of the shelf water/slope water front south of New England. **J. Geophys. Res.** **83**(C9) : 4623-4631.
- Freund, J.R., 1971. Mathematical Statistics, Prentice-Hall, Inc. **Englewood Cliffs, NJ**: 463 pp.
- Kinder, T.H., 1977. The **hydrographic** structure over the continental shelf near Bristol Bay, Alaska, June 1976. Univ. Wash, Dept. **Oceanogr.** Technical Report (Ref. **M77-3**): 61 pp.

- Kinder, T.H. and L.K. Coachman. 1978. The front overlaying **the** Continental slope in the eastern Bering Sea. J. Geophys. Res. **83(C9):4551-4559.**
- Kinder, T.H. and J.D. Schumacher. 1981a. Circulation over the continental shelf of **the** southeastern Bering Sea. In: The Eastern Bering Sea Shelf, Oceanography and Resources, Vol I, D.W. Hood and J.A. Calder, editors, U. S. Dept. Commerce/NOAA/OMPA: 31-52.
- Kinder, T.H. and J.D. Schumacher. 1981b. Hydrographic structure over the continental shelf of the southeastern Bering Sea. In: The Eastern Bering Sea Shelf, Oceanography and Resources, Vol. I, D. W. Hood and J. A. Calder, editors, U. S. Dept. Commerce/NOAA/OMPA: 31-52.
- Kinder, T.H., L.K. Coachman and J.A. Gait. 1975. The Bering Slope current system. J. Phys. Oceanogr. **5(2):231-244.**
- Kinder, T.H., J.D. Schumacher, and D.V. Hansen. 1980. Observation of a **baroclinic** eddy: An example of **mesoscale** variability in the Bering Sea. J. Phys. Oceanogr. **10(8):1228-1245.**
- Kinder, T.H., J.D. Schumacher, R.B. Tripp and J.C. Haslett. 1978. The evolution of the **hydrographic** structure over the continental shelf near Bristol Bay, Alaska, during summer 1976. Univ. Wash., Dept. **Oceanogr. Technical Report (Ref: M78-16):** 72 pp.
- Lagerloef, S.E., R.D. Muench and J.D. Schumacher, 1981. Very low frequency variations in currents near the northeast Gulf of Alaska shelf break. J. Phys. Oceanogr. , **11(5):627-638.**
- Loder, J.W. 1980. Topographic rectification of tidal currents on the sides of Georges Bank. J. Phys. Oceanogr. , **10:1399-1415.**
- Lonquet-Higgins, M.S. 1969. On the transport of mass by time-varying ocean currents. Deep-Sea Res. , **16**, 431-447.
- Mooers, C.N.K., C.A. Collins, and R.L. Smith. 1976. The dynamic structure of the frontal zone in the coastal **upwelling** region off Oregon. J. Phys. Oceanogr. **6(1):3-21.**
- Mooers, C.N.K., R.W. Garvine, and W.W. Martin. 1979. **Summertime synoptic variability of the Middle Atlantic shelf** water/slope water front. J. Geophys. Res. **84(C8):4837-4854.**
- Niebauer, J.H. 1980. Sea ice and temperature variability in the eastern Bering Sea and its relation to atmospheric fluctuations. J. Geophys. Res. **85(C12):7507-7515.**
- Overland, J.E. 1981. Marine climatology of the Bering Sea. In The Eastern Bering Sea Shelf, Oceanography and Resources, Vol I, D.W. Hood and J.A. Calder, editors, U. S. Dept. Commerce/NOAA/OMPA: 15-22.
- Overland, J.E. and C.H. Pease, 1981. Cyclone climatology of the Bering Sea and its relation to sea ice extent. Monthly Weather Review, **110(1):5-13.**

- Pearson, C.A., H. Mofjeld, and R.B. Tripp. 1981.** Tides of the eastern Bering Sea shelf. In: The Eastern Bering Sea Shelf, Oceanography and Resources, Vol. 1, D.W. Hood and J.A. Calder, eds. U.S. Dept. Commerce/NOAA/OMPA: 53-85.
- Pearson, C. A. , **J.D. Schumacher**, and R. II. **Muench. 1981.** Effects of wave-induced mooring noise on tidal and **low-frequency** current observations. Deep-Sea Res. , **28A(10):1223-1229.**
- Pease, C.H. , 1980. Eastern Bering **Sea** ice processes. Monthly Weather Review, **108**: 2015-2023.
- Quadfasel, D.** and F. **Schott.** 1979. Comparison of different methods of current measurement. Dt. hydrogr. Z. **32(1):27-38.**
- Reed, R.K. , 1978. The **heat budget** of a region in the eastern Bering Sea, summer 1976. J. Geophys Res. , **83**: 3636-3645.
- Robinson, I. S. **1981.** Tidal **vorticity** and residual circulation. Deep-Sea Res. , **28A:195-212.**
- Schumacher, J.D. , **T.H. Kinder**, **D.J. Pashinski**, and **R.L. Charnell. 1979.** A structural front over the continental shelf of the eastern **Bering** Sea. J. Phys. Oceanogr. **9(1): 79-87.**
- Schumacher, J.D., **C.A. Pearson** and **J.E. Overland**, 1982. On exchange of water between the Gulf of Alaska and the Bering **Sea** through Unimak Pass. J. Geophys. Res. , **87(C8): 5785-5795.**
- Semtner, A.J. and Y. Mintz**, 1977. Numerical simulation of the Gulf Stream and mid-ocean eddies. J. Phys. Oceanogr. , **7**: 208-230.
- Smith, **P.C.** and **B.D. Petrie**, 1982. Low-frequency circulation at the edge of the **Scotian** shelf. J. Phys. Oceanogr. **12:28-46.**